國立交通大學

生物科技學系

博士論文

「固定化酵素動力參數量測平台」之模型建構與計算

A Systematic and Standardized Approach

to

Modeling and Measuring Immobilized Enzyme Kinetics

研究生：李政哲

指導教授：楊裕雄 博士

中華民國 九十八年 七月

「固定化酵素動力參數量測平台」之模型建構與計算

A Systematic and Standardized Approach to Modeling and Measuring Immobilized Enzyme Kinetics

研 究 生： 李政哲　　Student： Cheng-Che Lee

指導教授： 楊裕雄　　Advisor： Yuh-Shyong Yang

國立交通大學

生物科技學系

博 士 論 文

A Thesis

Submitted to Department of Biological Science and Technology

College of Biological Science and Technology

National Chiao Tung University

in Partial Fulfillment of the Requirements

for the Degree of

Doctor of Philosophy

in

Biological Science and Technology

June 2009

Hsinchu, Taiwan, Republic of China

中華民國九十八年七月

「固定化酵素動力參數量測平台」之模型建構與計算

研究生：李政哲　　指導教授：楊裕雄 博士

國立交通大學生物科技學院生物科技學系博士班

摘　　要

有效整合 top-down 與 bottom up 製程技術於前瞻跨領域「奈米生醫電子」至為關鍵；其中如何評估局部固定化在元件無機介面上生物分子的工作性能就顯得十分重要，這些生物分子可以是 DNA、RNA、蛋白質(特別是具有辨識與催化的酵素分子)。在先期測試中施以掃描電壓於固定化酵素，雖然其活性調控的現象可以被清楚地觀測到，然而卻無法量測固定化酵素動力參數的即時改變趨勢。因此，本研究團隊在執行 94 年度奈米國家型科技計畫學術卓越計畫—「生化感測與仿生調控功能的奈米結構與生物分子混成系統之研究」時，也規劃了生物調控器的研究子題；因應評估將酵素嵌入標準積體電路和微機電系統的平面化技術，我們著手開發了一套可靠合理的即時偵測與分析固定化酵素動力的量測平台。

在本研究中固定化於二氧化矽基材表面的酵素共有三株，它們分別是老鼠酚亞硫酸基轉移酵素(E.C.2.8.2.1)、醯亞胺水解酵素(E.C.3.5.2.2)、假絲酵母菌脂肪分解酵素(E.C.3.1.1.3)。兩項主要的貢獻與理論特徵是：(1)針對符合 Michaelis-Menten 動力學模式的酵素催化反應並考量質量傳送效應，以系統化、標準化建立表面反應限制的模型用以量測固定化於平面基材的酵素視動力參數值 K^*_m 和 V^*_{max}；(2)根據上述數學模型建構標準流程化的實驗操作方式，並對 Michaelis-Menten 參數估算提出新的線性圖解法，其斜率即為視參數 K^*_m 值，且縱座標與橫座標分別具有直觀的物理意義—縱軸表示在兩個極端基質濃度下反應產率的差值，橫軸在低基質濃度下則近似於基質濃度；此圖解法亦有利於數值分析求解。

我們以流道高度 167 微米的微流體反應器為實驗平台，成功地量測了老鼠酚亞硫酸基轉移酵素與假絲酵母菌脂肪分解酵素固定化在二氧化矽基材的及時視動力參數值 K^*_m 和 V^*_{max}；同時本研究也針對固定化酵素失活與基質溶解度限制的實務問題，提出對應的解決方法。整套量測系統將使我們有能力觀察到電訊號調控固定化酵素活性的動力參數改變的量值，進而研究相應的調控機制。

A Systematic and Standardized Approach to Modeling and Measuring Immobilized Enzyme Kinetics

Student: Cheng-Che Lee Advisor: Dr. Yuh-Shyong Yang

Department of Biological Science and Technology

National Chiao Tung University

Hsinchu, Taiwan, Republic of China

Abstract

How to efficiently combine top-down and bottom-up approaches has become essential in the interdisciplinary field of nano-bio-electronics. It is also important to be able to evaluate the performance of working bio-molecules, like DNA, RNA, proteins (especially for enzymes), immobilized and localized onto the surface of inorganic devices. Although a response of modulated activity was clearly observed via applying a voltage scan onto immobilized enzymes in previous pilot testing, there was no available scheme used to characterize the intrinsic properties of the immobilized enzymes and the corresponding effect of in-situ stresses for further analyzing the modulated mechanism. For developing " An Artificial-Bio Hybrid Nano-System Capable of Sensing and Regulation," a reliable and reasonable analysis of immobilized enzyme *in situ* became a crucial step to embed enzyme onto the planar technology of standard IC and MEMS for the bioregulator subprogram, which belonged to National Research Program for Nanoscience and Technology in the period 2005-2008.

In this study, we have successfully immobilized three enzymes, rat-phenol-sulfotransferase (rat-PST, E.C. 2.8.2.1), D-hydantoinase (E.C. 3.5.2.2), and *Candida rugosa* lipase (CRL, E.C. 3.1.1.3) onto the silicon dioxide surface. The main contributions and theoretical characteristics should be: (1) A surface reaction limited model, based on systematic and standardized approach, mathematically derived from mass transfer dynamics and Michaelis-Menten equation for measuring apparent K^*_m and V^*_{max} of immobilized enzyme on planar surface was developed. (2) A new linear plot proposed with a slope K^*_m, of which axes containing straightforward, meaningful parameter groups - the difference in reaction yield between two extreme substrate levels (y-axis) versus the reaction conversion fraction (x-axis), is simple to apply either graphically or numerically.

The K^*_m and V^*_{max} of rat-PST and CRL immobilized on silicon oxide surface were successfully determined in situ. The issues of enzyme inactivation during activity assays and limit of substrate solubility were both concerned in developing measurement approach in this study. Based on this platform, we will be able to make quantitative analysis of electric signal regulation on enzyme activity, and to study its related fundamental mechanisms.

Acknowledgment

還記得陳之藩先生在〈謝天〉這篇文章裡說道：「因為需要感謝的人太多了，就感謝天吧！」對我而言，生命的成長卻更像演化的縮影，任何「成就」都是一連串阻力、助力、有意、無意地在時空中交錯醞釀而成，匆匆六年的博士班時光使我學會了「敬畏天」。

在這段訓練過程中，首先要感謝楊裕雄教授創造一個資源豐富、前瞻與基礎研究兼顧的跨領域學習環境，營造一個可以相互腦力激盪，又可以動手操作的實驗家天堂；在這裡我曾和學弟漢平、坤霖一起體會一即使實驗屢次失敗也可以很興奮，很開心！他是我的指導教授，一個雖不會對學生施以強壓，其領導的研究生也常能不眠地工作的成功實驗室負責人。

又在研究的結尾也是出發點的此刻，能獲得台灣「半導體之父」張俊彥院士的親自鼓勵與賞識，彷彿在研究路上打了一劑強心針，由衷感謝這位令我尊敬的長者。其次也要感謝黃調元教授、林鴻志教授、柯富祥教授，有了他們的愛才惜才與殷殷指導，才能在混成元件與仿生感控系統的理念建構上，使初生之犢的我能持續保持旺盛的戰鬥力，不知天高地厚地一路過關斬將，帶著豐碩的戰利品衝刺到終點。又呂平江教授、徐琅教授、盧向成教授及高健薰組長，您們對我論文的意見和用心，除了讓我的論文更紮實、完整，同時也啟發我下一階段可以嘗試的研究方向。

六年也是漫長的，家人是最實在的依靠。謝謝爸爸、媽媽、太太得歆毫無怨言的支持，還有現在兩歲十個月的女兒澄昀經常帶給我們單純快樂的幸福感。除了做研究，喜歡教書其實是我重回校園的主因；有一個學期我以類似讀書會的方式強迫向學弟妹推銷所謂「生物電子」的課程，感謝淵仁、程允、秉鈞、漢平和文穎幾乎風雨無阻，給足了面子。我也抽空陸續輔導明暄、張辰、見陽、詠嫣、芳璿、羿伶、芳謙與芳諭的數、理、化，我總嘗試在每次 2~3 小時亦師亦友的互動學習中，擺脫升學這種低層次的枷鎖，希望年輕學子能體會與欣賞數學與自然科學的優美架構；然而也得感謝這些聰慧高中生的大哉問，使我能重新以初學者的角度看問題，這對研究工作本身是正面的，因為這常常能使我回到問題的基本面上去。

這頁 A4 的「致謝」看似人名的堆砌，其實正是一段我不想遺忘的記憶…李奇翰學長、郁吟、慈安、俊榮、羿蓉、靜玟、偉迪、青辰、佩綺、陸宜、音汝、酵素暨蛋白質實驗室的所有同學、朋友、學弟妹，還有一群「新事」課輔的原住民小朋友 — 謝謝大家！

Contents

Chapter 1 Introduction

1.1 Background

Owing to the large surface to volume ratio, the conductance of a semiconductor nanowire (or a nanotube) is significantly affected by the surface charge. Many research groups have exploited in this property to develop highly sensitive biosensors. However, essentially all nanowire technologies reported in literatures so far are still having difficulty to efficiently reproduce the biosensors' performance with nanowire FET devices. This issue limits its expanded purpose in research, not to mention its potential application, especially for detecting a complex system at bioreaction level.

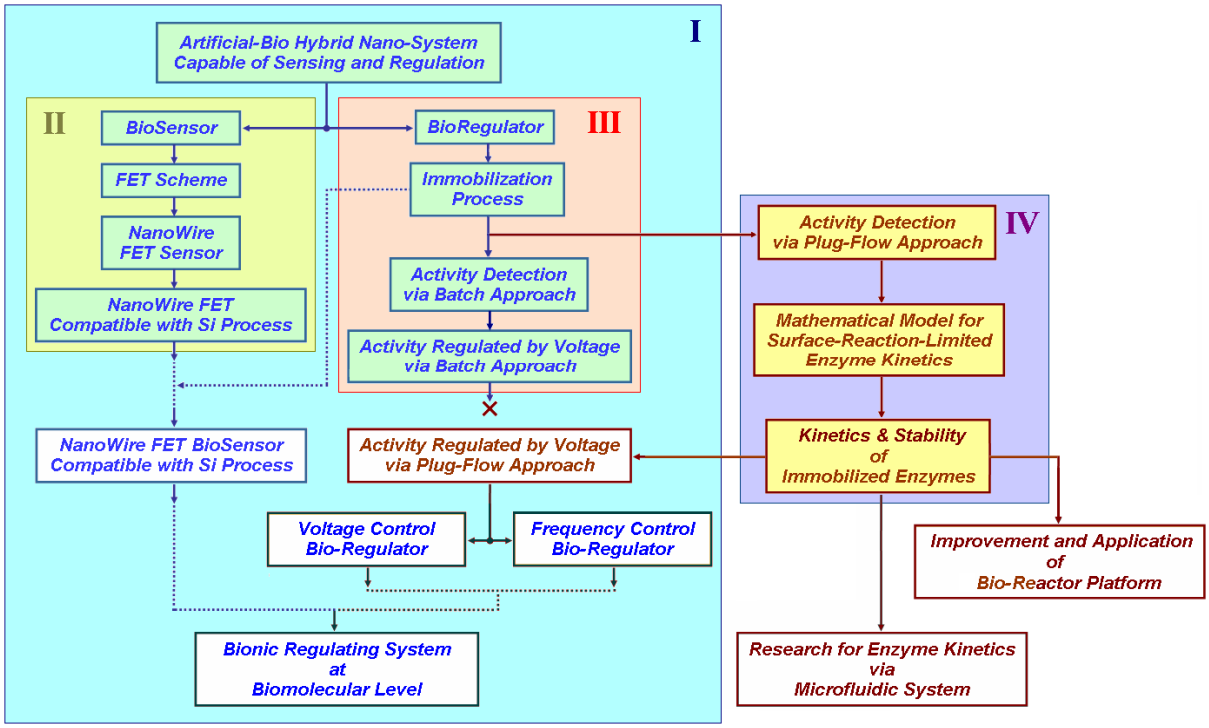

Figure 1. Research flowchart: Block I is the research flowchart for the project "An Artificial-Bio Hybrid Nano-System Capable of Sensing and Regulation;" Block II shows the stage of research and development for "Nanowire FET Compatible with Si process;" Block III represents the technology development of enzyme immobilization and research of "Activity

Regulated by Voltage via Batch Approach;" Block IV is the progression, "How to systematic and standardized extract the kinetics of immobilized enzyme."

On the other hand, there are also still few researches on developing bioregulating systems at biocatalytic level directly controlled by electric signals, therefore we try to do it and further combine with biosensor as a bionic system. The three principal goals of this project: 1) to develop a highly sensitive and selective nano-biosensor, of which the scheme must be highly reproducible and compatible with low-cost Si process, 2) to develop a novel bioactivity regulator, which uses a locally-intensified electric field or oscillated electric field to induce the conformational change or to match the turnover frequency of enzymes immobilized on a silicon-based material, and therefore regulates their activities, 3) to construct a bionic system at bioreaction level by integrating the above-mentioned nano-biosensor and bioregulator developed in this project.

In order to meet these goals, it clearly needs three subprograms, which closely support each other in the different researching phases. The strategies, included in these subprograms, are a) to develop a nanowire biosensor with novel and reliable processes, b) to integrate enzyme engineering and SAMs technology for biosensing and bioregulation, c) to construct a bionic system with a cascade of bioreactions on the nano-electronic devices, and d) to integrate and assemble the biosensing, bioregulating, and NEMS technologies into a multi-functioned bionic platform. Figure 1 is the research flowchart, which clearly shows the research strategy and progression. There were preliminary results published in previous studies,[1-4] and Block IV in Figure 1 was the major research topic of this thesis.[5] The executive summaries of the subprograms are illustrated as follows:

Subprogram 1: Reproducible, reliable and high-sensitivity nanowire devices for biosensing and bioregulating

Development of highly sensitive nanowire (NW) devices with reproducible and reliable performance is essential for this project. In this subprogram, a novel approach is proposed for the preparation of Si nanowires and the associated device fabrication. In this approach, the Si NWs are formed on the sidewall of a step structure after deposition and etching steps. Accompanied with the patterning of source/drain regions that are formed in a self-aligned manner during the aforementioned etching step, the Si NWs are then employed as the channel portion of a field-effect transistor device. The overall process sequence is very simple and compatible with low-cost Si manufacturing processes and tools, while the feature size of the Si NWs can be well controlled. It is thus very suitable and promising for mass production of future bio-sensing products.

One of the potential issues for the approach is probably the crystallinity of the Si NWs that could be the noise source, and contribute to the leakage current. In line with this, several re-crystallization techniques, such as metal-induced lateral crystallization (MILC) and excimer laser annealing (ELA), will be employed to enlarge the grain size. With these advanced methods, quasi-single-crystal Si NWs are expected, which could dramatically improve the sensitivity of the fabricated device. In addition to modifying the material and electrical properties of NWs, we further propose a new concept to enhance the sensitivity of the devices. This is realized by a side-gate design that could modulate the Vth of poly-Si NWs to an appropriate value by applying a voltage to the side-gate. The channel doping step normally used to adjust the Vth of NW required in conventional NW device fabrication could thus be skipped.

The fabricated devices will be used for biosensing purpose by examining the surface bio-reactions on the NW and their effects on the electrical characteristics of the test samples. New

test structure design with a locally-intensified electric filed will also be studied for bioactivity regulation. By combining the biosensors and the bio-regulators, a multi-functioned bionic system could be constructed.

Subprogram 2: Highly sensitive detection for trace specific biomolecules and a novel bioregulator controlled by a locally-intensified electric field

Based on the innovative and reliable scheme of silicon nanowire devices, developed in the subprogram 1, this subprogram plans to develop three key applications. The related goals are: (1) a highly sensitive and selective biosensor instrumental for medical diagnosis at detecting range to pM, (2) a revolutionary bioregulator, of which the local conformational states of biomolecules are changed by a locally-intensified electric field, and (3) a multi-functioned bionic system, at bioreaction level, for research and application by integrating the biosensor and the bioregulator technologies mentioned above.

For constructing a highly sensitive biosensor, the spatially controlled monolayer-immobilization of biomolecules on device surfaces is one of the important challenges in this subprogram, and it will strongly affect the sensitivity of biosensors and the commanding of regulators. The nano-tech group, responsible for the subprogram 3, will provide its support to tackle this issue. The bio-research group, in charge of this subprogram, attempts to use this biosensor in medical diagnosis to detect and identify the trace-but-crucial bio-molecules, like beta-endorphin (10~30 pM), neuropeptide Y (29.2+ 3.6 pM), and cholecystokinin (5.2+0.9 pM), etc.

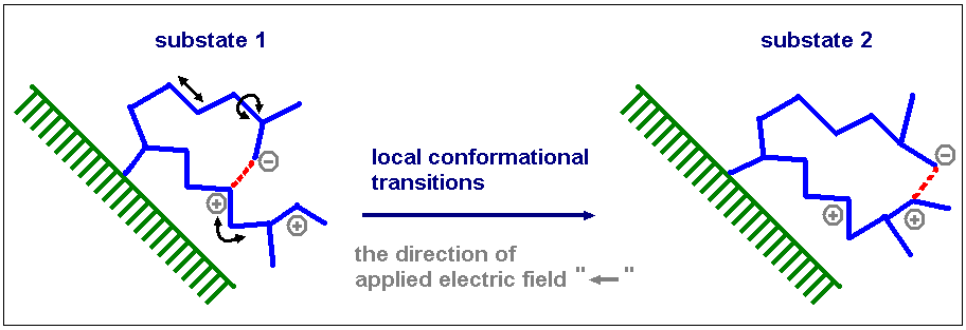

Figure 2 The local conformation of immobilized biomolecule, under an electric field, is changed from substate 1 to substate 2. (The conformational transitions among substates are achieved through changing the covalent bond lengths, angles, and dihedral angles.)

Next, based on a similar technology to that of the biosensor, this subprogram will further design and construct a novel bioregulator, through which the local conformation of biomolecules is changed from one substate to another substate by adjusting the intensity or modulating the frequency of electric field. If the biomolecule belongs to a kind of enzyme, then its bio-activity should be regulated. Figure 2 schematically shows the operation principle of this bioregulator. Besides the potential value for biomedical applications, the bio-research group will use this bioregulator scheme as a new skill for studying (a) the allosteric interaction, (b) the disulfide bond formation effected by the enzyme conformation at different substates, and (c) the ion concentration effect of specific metal on the enzymatic catalysis. The locally-intensified electric field will be used to induce the conformational change of the first two cases, and change the local concentration surrounding the enzyme in the last case. Using the bioregulator scheme and by intentionally mutating some selected amino acids away from active site, this subprogram tries to study the phenomena of intra-molecular variations and the effect of local ion concentration on enzymes.

At the third research phase, the goal of this program is to construct a multi-functioned bionic system, which is capable of sensitively detecting and specifically commanding a cascade of bioreactions. For this goal, the bio-research group will be responsible for

designing the related bioreactions and studying the dynamic model in this cascade of bioreactions.

Subprogram 3: Interface study and system integration between nanoelectronic devices and biomolecules

The subprogram is aimed to study the interface and system integration for the other two subprograms. In the interface study of bionic system, we will immobilize the $Si(OR)_3(CH2)_nR'$ molecules (R: CH_3, C_2H_5; R': $-NH_2$, -SH, -COOH) onto the surface of nanowire to offer the functional groups for further versatile biomolecular reactions of sensing and regulation. The influencing parameters such as the assembling temperature, liquid or gas assembling, vacuum or atmospheric environment, surface cleanliness, and molecule structure will be studied in details. The effect of monolayer/multilayer, packed molecule density and surface clean recipe on the electrical properties of these devices for enzyme sensing and regulation will also be carefully evaluated. Prior to system integration, the suitable immobilization method will be established and standardized for the fabrication of sensor and regulation.

In regard to the integration of electrical devices and fluidic channels, we will focus on investigating the structure fabrication, heterogeneous surface bonding, flowing system design and channel surface treatment. The baby system is achieved after optimization of the above parameters. Then, we will study the biomolecular reaction, immobilization, electrical detection, washing, re-immobilization, detection and so on under 37^{o}C. The system will be applied to control and regulate the biomolecular reaction once the reliability of the system has passed the initial test. The potential barriers are (1) signal interference from micro/nano scale

bubbles, defect particles and memory effect, and (2) poor sensitivity from low immobilization efficiency, assembling molecular instability and contaminated element diffusion into the sensing gate. Figure 3 depicts the bionic system; a normal-regulated biochemical pathway regulated as shown in Figure 3(a), and a pathway of an irregular mechanism regulated by the bionic system as shown in Figure 3(b). In this example, the normal bio-system is able to recognize specific species, A, B, C, D, and α, and catalyze two reactions $E_{A\rightarrow B}$ and $E_{C\rightarrow D}$. If a defective enzyme $E_{C\rightarrow D}$ leads to a block of certain bio-reaction C→D, then A, B, or α could be accumulated to abounding level. Based on the knowledge obtained from various conditions leads the researchers rather clearly realize this mechanism, the bionic system would be designed and applied to mend the defect, a deficiency of enzyme $E_{C\rightarrow D}$, that may be caused by a mutation. As shown in Figure 3(b), the sensing device determines the species α (or A, B), consequentially releases an electronic signal informing the artificial bioregulator to modulate the activity of enzyme $E_{C\rightarrow D}$ immobilized on the regulating device. Analogous instances occurring in organism are possibly achieved by the bionic system.

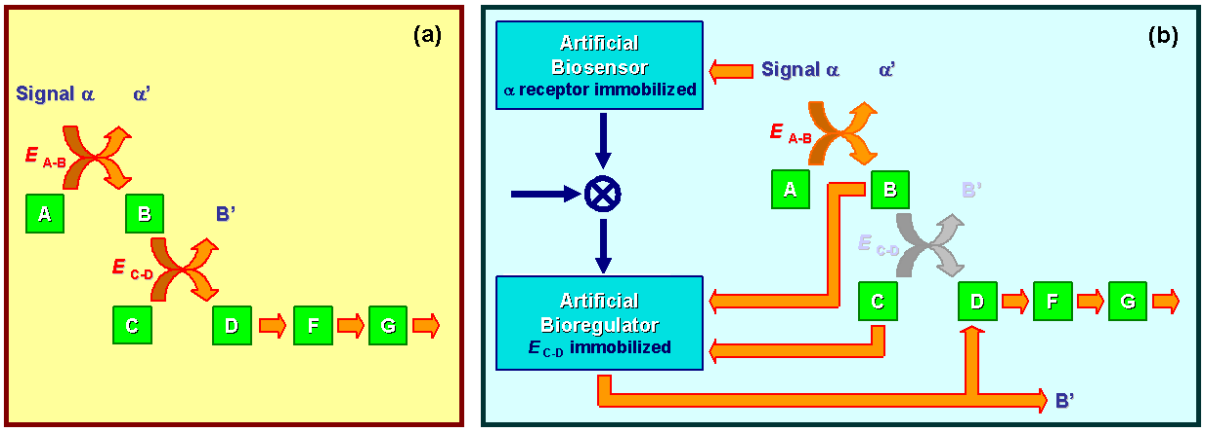

Figure 3 Schematic diagram of a bionic system showing a regular mechanism as left Figure and a $E_{C\rightarrow D}$ deficient irregular pathway mended by the bionic system, as shown at right. The dark-blue line and orange line represent electric signal and bio-molecular paths, respectively.

1.2 Reproducible, Reliable and High-sensitivity Nanowire Devices for Biosensing and Bioregulating

1.2.1 Perspective and background

Minimization of silicon electronics is being actively pursued. One-dimensional structures, such as nanowires (NWs), have great potential for testing and understanding fundamental concepts about the roles of dimensionality and size in electrical properties, and could be the ideal building block for nanoelectronics,[6] because they can function both as devices and as the interconnect wires that access them. Owing to the inherent high surface-to-volume ratio feature, NWs can suppress short-channel effects encountered in nano-scale MOSFETs[7] and provide high surface sensitivity for sensing devices. Many possible applications of Si NWs have been exploited, including nano CMOS,[7, 8] memory devices,[9] NW TFTs,[10] and biosensors.[11]

Preparation of Si NWs could be categorized into two types, namely, top-down and bottom-up, described as follows:

(I) Top-down: This approach uses advanced lithography techniques, such as deep UV,[12] e-beam[13] or nanoimprint,[14, 15] to generate the NW patterns, followed by an etching step to obtain the NW structures. These techniques are well developed and mature for mass-production purpose. Nevertheless, very expensive equipments and cutting-edge techniques are required. Conventional photolithography processes (e.g., G-line and I-line steppers), though relatively cheap for manufacturing, are not capable of patterning NWs directly. Some special skills such as thermal flow, chemical shrink, and spacer patterning[15] have been proposed to help generate the nano-scale patterns using these conventional lithography tools.

(II) Bottom-up: This approach typically utilizes deposition methods to prepare the NWs, and synthesize the NWs on a substrate. Afterwards, these NWs were harvested and dispersed into a solution. Depositing the harvested NWs onto another oxidized substrate and making

electrical contacts to the NWs, will complete the device structure. Many deposition methods have been developed nowadays which include laser ablation catalyst growth,[16] chemical deposition catalyst growth[17] and oxide-assisted catalyst-free method.[18] The first two methods are carried out with metal nanocluster catalyst as the energetically favored sites for absorption of gas-phase reactants, and then the cluster supersaturates and grows a wire-like structure of the materials. The process is based on vapor-liquid-solid (VLS) mechanism. Nanometer-diameter catalyst clusters define the size of wires produced by VLS growth, in which bulk quantities of single crystalline NWs can be obtained. The approach can also be applied to prepare NWs of other materials in addition to Si, such as III-V compounds and II-VI compounds.[19] However, metal contamination is a potential concern in this approach. Oxide-assisted catalyst-free method is conducted without metal nanocluster catalyst, and thus is free from metal contamination. Nevertheless, there could be plenty of defects in the wires, and hence it is not applicable to electronic devices. In addition, these aforementioned methods usually suffer from the poor control of structural parameters such as NW's diameter, length, and orientation.

Methods used to assemble and align the NWs prepared by "bottom-up" approach include electric-field-directed assembly,[20] microfluidic channel[21] and Langmuir-Blodgett (LB) technique.[11] Electric field method is via interaction between electric field of two parallel electrodes and polarity of NWs, and therefore directs the wires. Although electric fields enable more control over assembly, this method is limited by electrostatic interference between nearby electrodes as separations below micrometer level and requirement of extensive lithography to fabricate the electrodes. Fluidic channel method is to align wires by flowing NWs suspension inside a PDMS mold, and could obtain layer-by-layer assembly of multiple crossed NW arrays. However, the size of fluidic channels may limit alignment of NWs. LB method could assemble a large-area anisotropic NWs by compression process, but

it is restricted to preparation of one monolayer. Overall, for practical applications, more refinement is needed to improve the reproducibility and controllability of the above methods.

In a brief, most of the proposed schemes for device fabrication based on "bottom-up" nanostructures are plagued by complex integration that lacks reproducible transfer and positioning of NWs and reliable ohmic contacts. Moreover, the control of doping concentrations in self-assembled semiconducting NWs remains a challenge, and it's difficult for high-density integration. On the other hand, the top-down approaches usually require expensive lithography apparatus and materials that dramatically increase the fabrication cost. To circumvent these shortcomings, we propose to develop a new method for preparation and fabrication of Si NWs devices in this subprogram.

1.2.2 Specific aims and research approaches

We propose a new approach that could potentially resolve the shortcomings mentioned above. Our approach, albeit based on "top-down" approach, involves only mature and low-cost process skills. Since it could be easily realized using state-of-the-art IC processing, this new scheme is thus very suitable and promising for future practical manufacturing.

The main process steps and the structure of the proposed poly-Si NWs are shown in Figure 4 and 5. The fabrication flow is briefly described as follows: First two dielectric layers (dielectric 1 and dielectric 2) were deposited on a Si substrate, followed by lithographic and etching steps performed on dielectric 2 to form a step structure on the surface. An a-Si layer was then deposited by a low-pressure (LP) CVD system. After the Si layer deposition, source/drain (S/D) implant was performed with low implant-energy (Figure 4 (a)), so that most implanted dopants are located near the top surface of the Si layer. S/D photoresist patterns were then formed on the substrate using g-line or an I-line stepper (Figure 5 (a)). A

reactive plasma etch step was subsequently used to remove the Si layer. The sidewall Si NW channels were formed in this step in a self-aligned manner (Figure 4 (b) and Figure 5 (b)). Note that the implanted dopants in places other than S/D regions will be removed during the etch step because of the very shallow projected range just mentioned. After this step, an annealing step was performed to active the S/D dopants and to transform the a-Si layer into poly-Si.

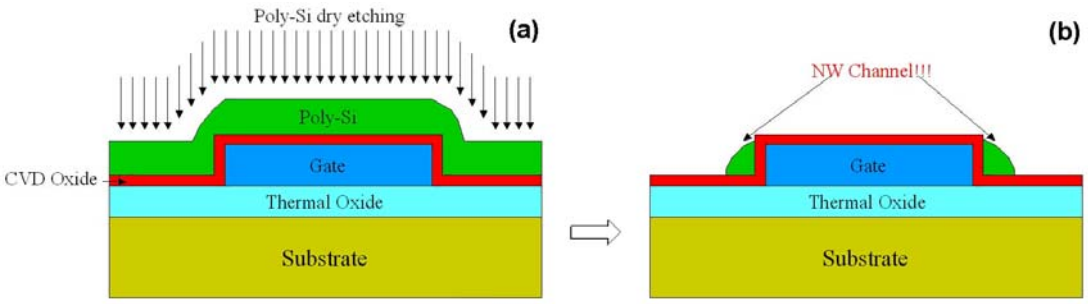

Figure 4 Cross-sectional views (along the A-B direction in Figure 4 (a)) of the device structure after S/D implant (a) and NW etching (b)

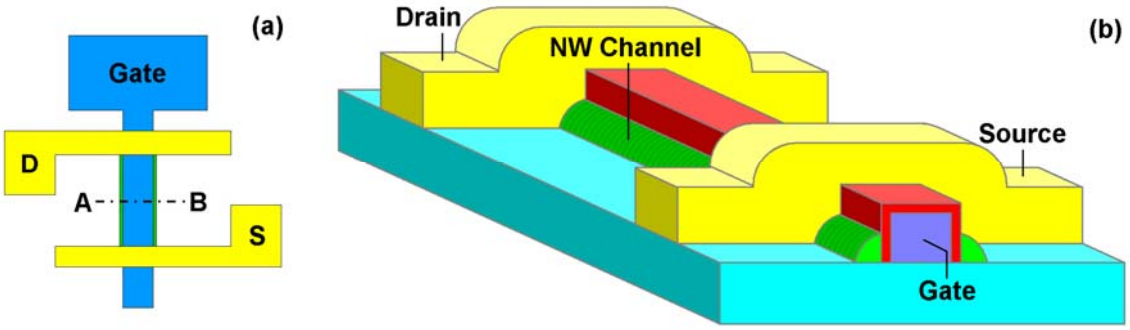

Figure 5 (a) Top-view layout, and (b)stereo-view of the fabricated poly-SiNW FETs

Advantages of this approach include: (1) feature size of NWs is related to the thickness of deposited film and could be well controlled; (2) NWs can be positioned accurately; (3) formation of NW channel, source and drain simultaneously, (4) no metal contamination concerns; (5) S/D to channel contacts are reliable through the use of implant process; (6) both p- and n-channel devices are easily fabricated, and thus CMOS integration is easy to achieve.

One of the potential issues for the proposed approach is probably the structural defects contained in the channel layer of the device which could be the noise source and contribute to the leakage current. Two strategies are adopted to cope with the issue:

(I) Promotion of the crystallinity of the NWs

Many studies have shown that metal-induced lateral crystallization (MILC)[22, 23] and excimer laser annealing (ELA)[24] can dramatically improve crystallinity of the Si layer and enlarge grain size to about one micrometer. MILC employs metal as precursor to lead amorphous Si to re-crystallize at lower temperatures because of lower energy barrier of recrystallization resulting from the reaction between metal and Si. Excimer laser can provide sufficient energy for amorphous Si to recrystallize, and hence the recrystallization could proceed at a lower temperature. In this subprogram both methods will be investigated to develop a practical recrystallization skill for improving the crystallinity of the NWs.

(II) Structure modification

In addition to the structure mentioned in Figure 4 and 5, (denoted as "Type I" in Figure 6), two alternative types of devices will also be studied in this subprogram, as shown in Figure 6 (denoted as "Type II" and "Type III"). All these types use the substrate as the bottom control gate during operation. The modified Type II scheme possesses an additional "side-gate" which could be used to set the Vth to an appropriate value for sensing. With this design, the channel doping step for Vth adjustment could be skipped. In addition, the side-gate bias could also potentially screen part of the channel defects and improve the device sensing performance. Type III is to increase the NW sensing surface area by removing the dielectric 2. The sensitivity is consequently raised due to higher NW surface to volume ratio.

In addition to the completion of high-sensitivity biosensor devices, our research team plans to further exploit the proposed SiNW fabrication method by designing a locally-intensified electrical field to analyze the relationship between biological molecular activity and its structure. The schematic is as illustrated in Figure 7. In the loading window area, the upper π -

shaped poly-Si electrode (light blue color) and the lower SiNW electrode (green color) with immobilized biological molecules will form a locally-intensified electrical field, with the electric field being intensified on the narrow SiNW.

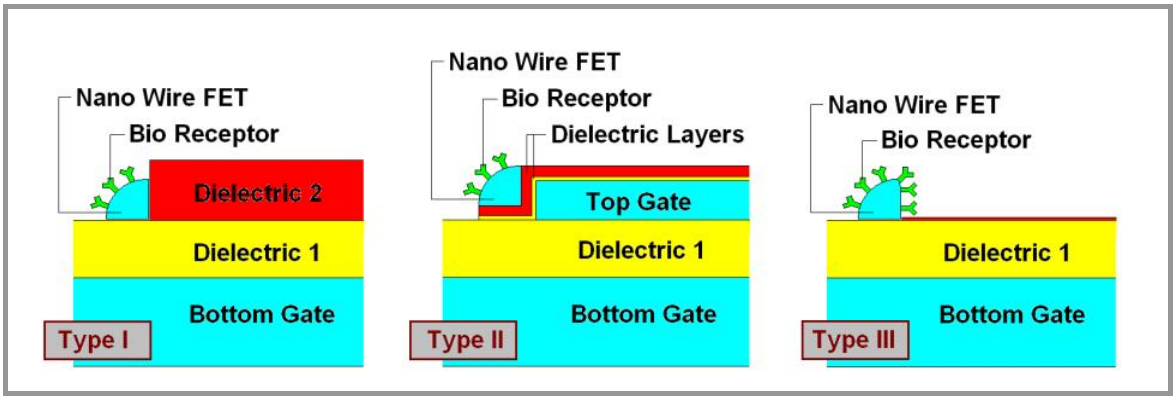

Figure 6 Three types of poly-SiNW FETs for biosensing

By utilizing the electric field to induce the conformational change of the enzyme already immobilized on the SiNW, we can further quantitatively regulate its bioactivity to obtain the information regarding field-regulated enzyme activity. In this way, we can establish a theoretical model and provide a microscopic view regarding the sequence mutation on the conformation and activity of enzyme. This scheme can open a brand new frontier in the research of bio-protein engineering.

Overall, a novel technique for fabrication of SiNWs and FETs that is superior to conventional “top-down” and “bottom-up” methods is proposed. Table 1 highlights the major advantages of the proposed scheme. This technique is manufacturable and economic, and is capable of providing a reliable high-performance poly-SiNW FET not only for biosensors but also for investigating nano-scale semiconductor physics. It is also compatible with the low-temperature poly-Si (LTPS) technologies, and could be integrated on low-cost and flexible substrates (such as glass or plastic), making the fabrication of system-on-panel (SOP) for biologic sensing and regulating purpose possible. In short, we believe our proposed technique

of SiNWs fabrication indeed represents a breakthrough development, and will be crucial for supplying cheap and credible biosensing chips.

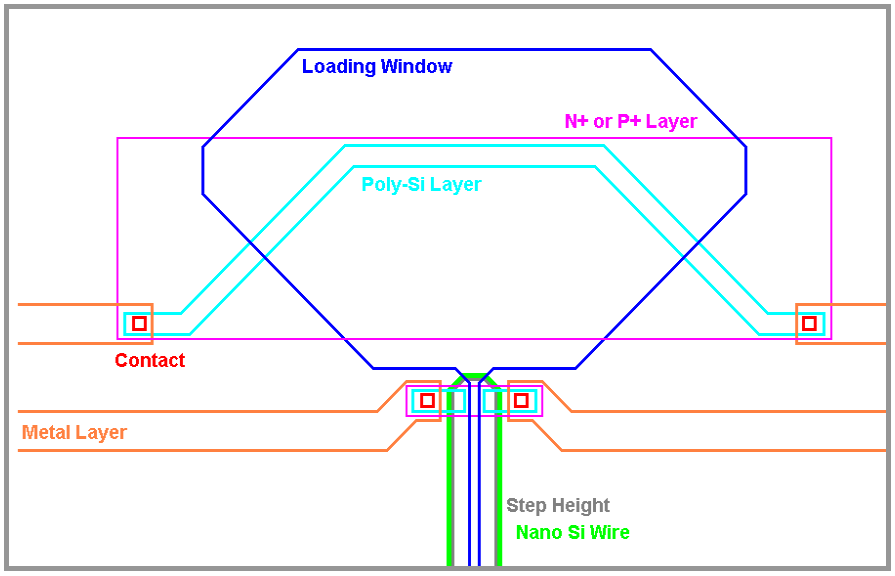

Figure 7 The bioregulator device layout designed to establish a locally-intensified electric field. It shows both the π–shaped poly-Si electrode (light blue) and the poly-SiNW (bright green) with the immobilized enzymes – sulfotransferases.

Table 1 Comparison of SiNWs formation among top-down,[12, 13, 15] bottom-up [10, 16, 17, 20, 21] and our approach.[23, 25-28]

Characteristics / Process & Scheme	Size of NWs	Alignment of NWs	Sensitivity	Cost & Process
Top-down	Good control	Good control	Can be high	Expensive, high techniques & complicated
Bottom-up	Rely on nanocluster and growth time	Not easy to control	Can be high	Medium, but complex integration
Our Approach	Good control	Good control	Can be improved by recrystallization & V_{th}-*set to modify*	Cheap & simplified; reliable & reproducible

1.3 Highly Sensitive Detection for Trace Specific Biomolecules and a Novel Bioregulator Controlled by a Locally-intensified Electric Field

1.3.1 Perspective and background

Bioelectronics, a novel interdisciplinary research field, involves the integration of biomolecules with electronic transducers, such as electrochemical (EC) and field-effect transistors (FET). The application of biomolecules, such as enzymes, antigen-antibodies, or DNA, on the electronic transducers dominates the characteristics of the biomolecules-transducer interface and enables the electronic transduction of biorecognition or biocatalytic events to occur on the transducer. A couple of interesting instances include, but not limited to, a variety of biosensors, biofuel cells, and bionic utilities, such as electronic noses and tongues. Nowadays, biosensor is a relatively well-organized device that is designed and fabricated by assembling the biorecognition matrices with diverse transducers.

The employment of semiconductor-based devices, such as ion-sensitive field-effect transistors (ISFETs) and enzyme-based field-effect transistors (ENFETs), as transduction elements for biocatalytic transformations and biological recognition events is a crucial and successful subject in bioelectronics and analysis. Enzyme-based field-effect transistors (ENFETs) are based on the biocatalytic reaction, specifically between immobilized enzyme and substrate occurring on the functionalized gate surface of a well-prepared ISFET, altering the charge at the gate surface and yielding an electronic signal dependent on the substrate concentration. The sensing performance of the ENFET is generally affected by the integration method of the enzyme and the ISFET device. Several investigations reported in literatures have illustrated enzyme-immobilized in thick-film manners, including the immobilization of the desired enzymes in thick polymer films (e.g., polyvinylchloride, polyacrylamide hydrogels, or polyurethane) and membrane (e.g., Nafion or polyvinylpyridine)

covered crosslinked enzyme matrices on the ISFET devices. This type of sensors, nevertheless, demonstrated a high diffusion resistance of the substrates through the polymer membranes, leading to a long response time and a moderate sensitivity. An alternative configuration organizing monolayer (or multilayer) enzyme-based ISFET, therefore, was developed and substantially improved the response time and sensitivity.

Apart from the modification of the biocatalytic matrices, the performance of a FET-based device could be enhanced by a re-construction of the FET element. A promising approach is toward a reduction of gate-dimension resulting in a highly sensitive device. Nano-dimensioned gate materials such as nanotubes or nanowires[11, 29] have been illustrated in recent reports; nevertheless, these studies suffer from the limitations of reproducibility, reliability, and stability. The present project proposes a novel fabrication process that reproducibly and reliably produced a silicon nanowire and the associated FET device.

It is well understood that the conformation of the biomolecules shall be altered by the surrounding physical parameters such as temperature and pH, sequentially resulting in the change of function or biocatalytic activity. Previous researches have controlled and optimized the biocatalytic properties and functions by altering temperature, pH, concentration of cofactor, etc. These regulation methods are usually executed in batch manner, difficult to perform precisely and locally. In contrast, a few methods handling the distribution, mobility, conformation, and conjunction of biomolecules by electronic and magnetic forces are currently being investigated and are interesting. These methods demonstrated numbers of advantages over the traditional manners particularly in the ability to regulate biomolecules in a confined area. Furthermore, with respect to the viewpoint of application, the electric field is preferable over the magnetic field, as the facilities of forming a magnetic field are relatively complicated that hampers the approach toward the miniaturization. On the other hand, both fabrications of a miniaturized electronic contact and signal conduction across the interface between biomolecules and electronic transducer are quite simple and doubtlessly

accomplishable by the current technology. Study associated with the regulation and coordination of biomolecules, their corresponding functions, and diverse properties by electric field is a core issue in the field of bioelectronics and is crucial.

1.3.2 Specific aims and research approaches

Many trace but important elements, of which the concentrations range from nM to pM, are well known to participate in the variously crucial homeostatic objectives in human beings. For example, neuropeptide Y (NPY; 29.2+3.6 pM) and cholecystokinin (CCK; 5.2+0.9 pM) are some of the important peptides which play vital biological roles in various degenerative disorders (Qureshi et al., 2000). Those neuropeptides are widely distribution throughout the brain and are believed to participate in several physiological and pathophysiological processes, including pain sensation, memory, neuroendocrine functions, and regulation of release of monoamine transmitters.

Furthermore, the infinitesimal absence of those minor elements could lead to enormous effects on series of physiological reactions, so how to develop a rapid, highly sensitive, reliable, and low-cost detecting system is an imperative issue in the biosensor research field insofar.

At first research phase of this subprogram, the goal is just to research and develop a highly sensitive biosensor for detecting specific trace biomolecules, especially for the continuous measurement of disintegrated rate of disparate drugs in serum and accurate detection of those microelements for the physiological disorders. We will first use avidin-biotin matching system to check and improve the performance of the Si nanowire device developed by the subprogram 1, and examine the transport function of microfluidic channel made by the

subprogram 3. In the initial research period, we will immobilize biotin on the Si nanowire, which is locally and selectively modified by a monolayer of APTES in advance.

Besides bioelectronics, having been focusing on the study of the enzymes - *sulfotransferases* (STs) for many years, our recent research also has aimed at the vital relationship between sulfotransferase and neuroscience, and the intratissue distribution of sulfotransferases. After having mastered the spacially-immobilized and mon olayer-modified technologies for the previous Si nanodevices, we plan to use these technologies to detect those biomolecules involved in a cascade of bioreactions catalyzed by well-known sulfotransferases in our laboratory. This approach not only provides the advanced improvement and the technology spreading for the biosensor developed in this project, but also warms up the following research phases.

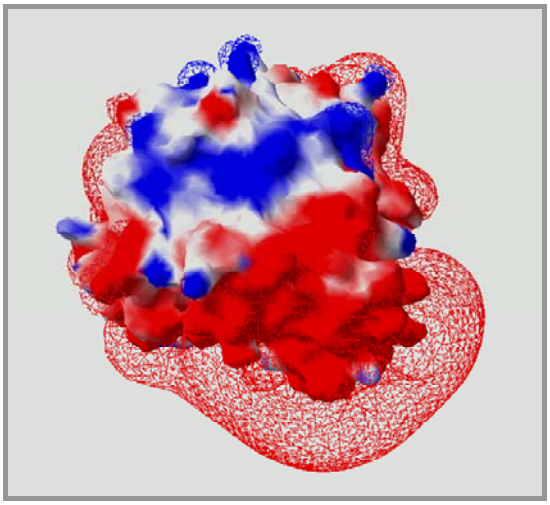

Figure 8 The structure of hSULT1A1 (or hSULT1A3) shows the simulated electrostatic potential. The red meshes and blue ones stand for locally negative and positive charge distributions, respectively.

To research and develop a novel bioregulator controlled by a locally-intensified electric field is the core subject at the second research phase. The enzymes – STs will be immobilized on the bioregulator device developed by the subprogram 1. The structures of STs are

consisting of PAPS binding site which conserved among STs and the related substrate binding site. The regulation of STs can be achieved by redox of flexible loop,[30] metal ion effect,[31] cofactor/substrate catalysis,[32] and so on.

The electrostatic potentials of STs are positive around PAPS binding site and are negative near the surface sandwiched PAPS binding site. Figure 8 shows the structure and the simulated electrostatic potential distribution for STs (hSULT1A1 or hSULT1A3); the red meshes and blue ones stand for locally negative and positive charge distributions, respectively. It is apparently that STs are polar biomolecules, at least for some specific zones. The conformations of STs immobilized on the developed bioregulator device should be evidently effected under an applied electric field, so the related catalysis could be modulated. It had been reported that Mn^{2+} ion efficiently stimulates the specific activity of dopa/tyrosine sulfotransferase to several hundred folds.[33] It is a rational inference that if we can change the local metal ion concentration around the immobilized enzymes, in about hundred-nanometer range, then we can modulate the activity. This project also plans to practice this regulating mechanism not by changing the overall concentration, but just the local concentration around the immobilized enzymes. This subprogram attempts to study and utilize these conformational variations, which modulate the activity of enzymes STs, to develop an artificial bioregulator controlled by a locally-intensified electric field. Three applicable regulating mechanisms and the related bioreactions are proposed and will be designed, respectively. These mechanisms could be classified as: (a) conformational change of polar enzymes induced by electric field, (b) turnover rate modulated by frequency of electric field, (c) allosteric effect due to conformational change enhanced by electric field, and (d) allosteric effect due to ion concentration variations controlled by electric field. Figure 9 schematically shows the operation mechanisms of the proposed bioregulator in this project, and Table 2 briefly illustrates the corresponding operation conditions to the different mechanisms.

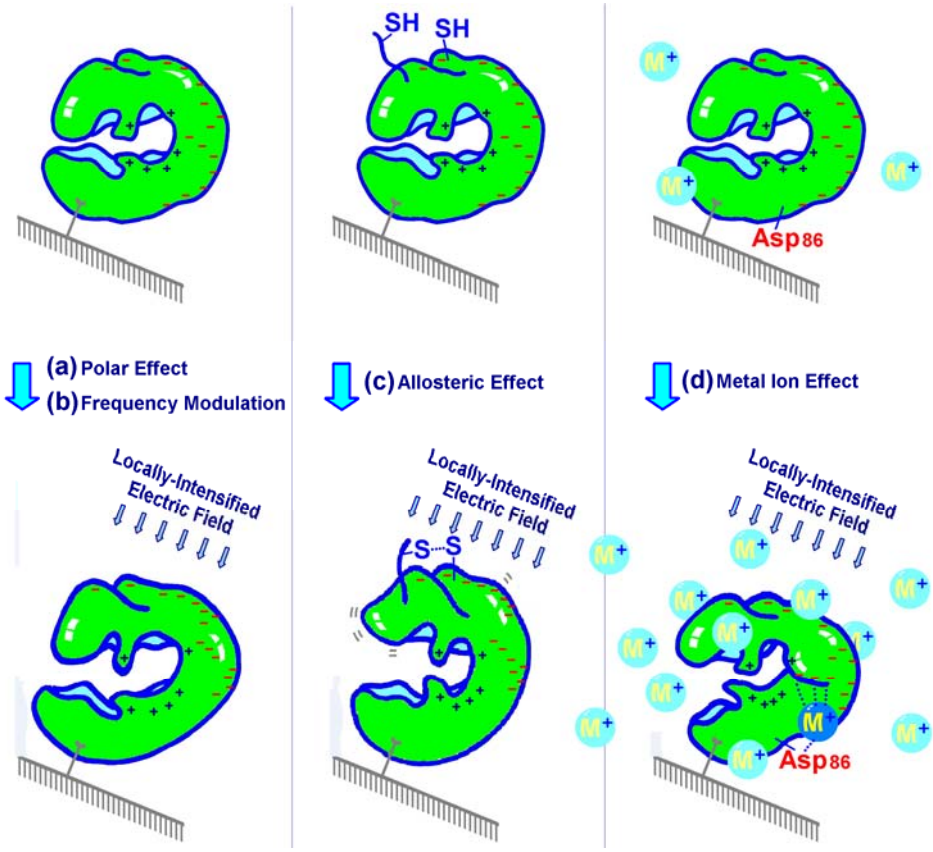

Figure 9 Three applicable regulating mechanisms induced by a locally-intensified electric field are schematically shown. The working enzymes (the deformable green ones) on the bioregulator are immobilized on SiNWs (the inclined planes) in this project. The conformational changes of working polar enzymes under the applied electric field, are mainly caused by (a) only the polar issue, (b) turnover modulated by matching frequency of electric field, (c) the allosteric effect enhanced by the relative position change (between two cysteines; the formation of disulfide bond leads to an allosteric effect.), and (d) allosteric effect induced by the concentration change of metal ion. (light blue balls; the deeper blue one is captured by Asp86, and then an allosteric effect is induced.)

In both of the mechanisms (a) and (c), the conformational changes are induced by locally-intensified electric fields; while in the mechanism (c), this conformational change enhances an intra-molecular bond formation, which could further changes and stabilizes the conformation.

Clearly, this proposed bioregulator is operated by a locally-intensified electric field around the immobilized enzymes, so it could sensitively and efficiently regulate a biochemical reaction under a mild condition, like in vivo. Even in the mechanism (d), it just changes the local metal ion concentration around the immobilized working enzymes in the bioreaction solutions. In fact, the turbulent flow in the microfluidic channel (schematically shown as Figure 11) will guarantee the well-mixed and uniform concentration of overall bioreactions except the spot, on which the working enzymes are immobilized, focused by the locally intensified electric field. Besides, by site-directed mutagenesis, this bioregulator scheme will also provide the bioresearch group a novel skill to study the allosteric mechanisms and the real conformational change in bioreactions.

Table 2 The comparison between the operation conditions of different regulating modes by the proposed regulators.

Mechanisms / Operattion Condition	(a) conformational change of polar enzymes induced electric field	(b) allosteric effect due to stressed conformation enhanced by electric field	(c) allosteric effect due to ion concentration variations controlled by electric field
Need apparently polar property? (for immobilized enzymes)	Must !	Need	Need Not
Need extra-added redox agents? (for reaction solution)	Need Not	Must !	Need Not
Need extra-added metal ions? (for reaction solution)	Need Not	Need Not	Must !

Integrating the highly sensitive SiNW-FET biosensor and the highly efficient bioregulator, both developed at the first two phases respectively, to a multi-functioned bionic system is the goal of the third phase of this project. Subprogram 2 at this research phase will be responsible for designing the cascade of bioreactions and studying the dynamic bioregulation.

The transfer of the charged sulfonate moiety to an acceptor steroid catalyzed by human dehydroepiandrosterone sulfotransferase (DHEAST; SULT2A1; EC 2.8.2.2) decreases the biological activity of the steroid. In fact, steroid sulfates resulting from this reaction are not

capable of binding to or activating steroid receptors. Steroid sulfonation has been recognized as an important means for maintaining steroid hormone levels in their metabolism. In humans, dehydroepiandrosterone sulfate (DHEAS) is the most prodigious steroid precursor and one of the major secretory products of both adult and fetal adrenals.

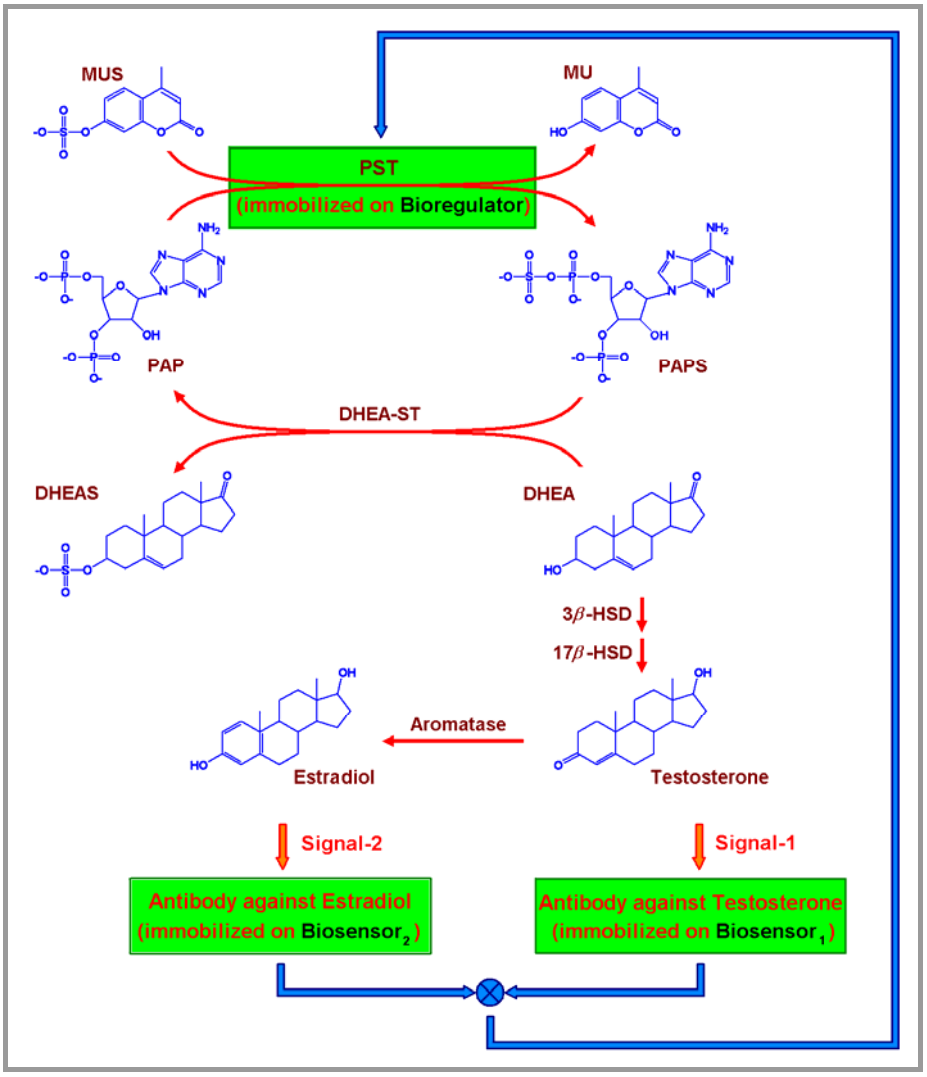

Figure 10 A bionic system, which includes two biosensors and one bioregulator (shown as three green boxes), is set up to detect the concentration variations of testosterone and estradiol and to modulate the catalysis of PST. There are at least five enzymes included in this cascade of bioreactions; they are PST, DHEA-ST, 3b-HDS, 17b-HDS, and aromatase, respectively. The direction of blue line shows the commanding from the sensors, through signal processor,

and then to the regulator. (The signal processor deals with the weighting between signals or other commanding inputs.)

An example of overall experimental design for bionic cascade reactions is shown as Figure 10. First, using methylumbellifery sulfate (MUS) as sulfuryl group donor to biosynthesize the universal sulfuryl group donor, 3'- phosphoadenosine 5'-phosphosulfate (PAPS), the reaction is catalyzed by phenol sulfotransferase (PST). This step has been well-controlled and used to couple to another sulfotransferase for measuring its activity in our laboratory.[34] Many different enzymes involved in this system are to maintain the bionic cascade reactions. For example, dehydroepiandrosterone sulfotransferase (DHEA-ST) is used to transfer the sulfuryl group of PAPS to dehydroepiandrosterone (DHEA). The product, DHEA sulfate (DHEAS) had been demonstrated to act as sex hormone precursor and neurosteroid.[35] Therefore, by supplying the enzymes involved in both catalyzing sex steroid hormone and steroid biosynthesis, such as 3β-hydroxysteroid dehydrogenase (3β-HSD), 17β-hydroxysteroid dehydrogenase (17β-HSD), and aromatase, it will be easy to obtain testosterone (T) and estradiol (E2) in this system.

There are two biosensors and one regulator involved in this case of bionic system; the related antibodies against T and E2 will be immobilized on SiNWs of FET biosensors, respectively, and PST immobilized on a SiNW of the electrically-controlled bioregulator. Clearly, these two biosensors are set up to detect the dynamic variations of T and E2, respectively, and then the system will command the catalysis of PST on the regulator after weighting these two signals from Sensor 1 and Sensor 2. These sensors will be developed at the phase 1 of this project. To our anticipation, this bionic system can provide the further research of dynamic bioreactions and the simulation study of biomedical engineering. In fact, this bionic system will be exactly a highly efficient, but mild, artificial reactor, so it has very

great potentiality in medical diagnosis, pharmaceutical or ferment industry, environmental defense and national security.

1.4 Interface Study and System Integration between Nanoelectronic Devices and Biomolecules

1.4.1 Perspective and background

The biggest hurdle to bio-electronics development is the biosensor technique. This is because any complex system requires a very sensitive sensor to characterize the status. For any bio-detective system, it is almost impossible to fully understand the status of the system by simply only obtaining 1 or 2 parameters. Instead, a few tens of determinative parameters are required to describe the performance of a complicated bio-system. In the past, scientists have developed the smell and taste sensors, while the function of these sensors is still limited.

Mirkin's group has developed the DNA array sensors which are based on the conductivity changes through the binding of oligonucleotides and gold nanoparticles. The gold nanoparticles are assembled within the electrodes and the silver deposition is facilitated by these nanoparticles bridging the gap and lead to readily measurable conductivity changes. Using this method, they can detect the target DNA concentration down to 500 fM. Star et al. have fabricated the nanoscale field effect transistor (FET) devices with carbon nanotubes (CNTs) as the conducting channel to detect protein binding. In order to avoid the alternation of physical properties of the FET due to the covalent binding of biomolecule with the CNTs, they propose a new technique of overcoating polyethylene imine and poly (ethylene glycol) onto the nanotubes. Prior to recognizing the streptavidin molecule, a biotin (molecular receptor) is immobilized onto the polymer's surface. This sensor is very sensitive and the detection level is estimated to be of the order of 10 streptavidin molecules.

Lieber's group fabricated the 20nm p-type silicon nanowire electronic devices in the channel of 500μm by 3mm, which functions as ultrasensitive (10fM) and selective detectors of DNA. The surfaces of the silicon nanowire devices were modified with peptide nucleic acid receptors designed to recognize wild type versus in the mutation site in the cystic fibrosis

transmembrane receptor gene. This nanowire-based approach represents a step forward for direct, label-free DNA detection with extreme sensitivity and good selectivity, and could provide a pathway to integrated, high-throughput, multiplexed DNA detection for genetic screening and biothreat detection.

The electronic device has much better sensitivity than optical method, and the application of electrical sensing to biomolecule will become the major role in the future. Hence, this interdisciplinary technology attracts much attention from academic and industry. There still exist a couple of problems that need to be overcome. For examples, how to set up a fluid channel in an electrical device? How to transport biosamples? How to immobilize the biomolecules onto the sensing channel? The integration of nanodevice and biomolecule involves the research on heterogeneous interface. The interdisciplinary cooperation shall soon become the main issue of bioelectronics field.

1.4.2 Specific aims and research approaches

The 20nm poly-Si NWs fabricated from the spacer of gate line from subprogram 1 is intended to immobilize the biomolecules offered from subprogram 2 through the linker molecule. This subprogram is aimed to study the interface and system integration. It is essential for surface chemistry to occur to clean the FET surface from the contaminants. The use of acid wash solution, a mixture of H_2O_2 and H_2SO_4, simultaneously removes organic and metal contamination from the poly-Si NWs. There are two ways to immobilize the surface linker molecule, i.e. monolayer and multilayer, and the spatial structure exhibits various effects on the conductance of FET. We predict the monolayer method has better signal reliability on biomolecule sensing due to the lower thickness variation of surface electrical double layer, but exhibits poor sensitivity. On the contrary, the multilayer structure has better

sensitivity, but demonstrates the poor reliability. Hence, we need to compromise the deposition method. Considering the sensitivity issue, the multilayered immobilization is a possible means to reach the single molecule detection capability with the FET.

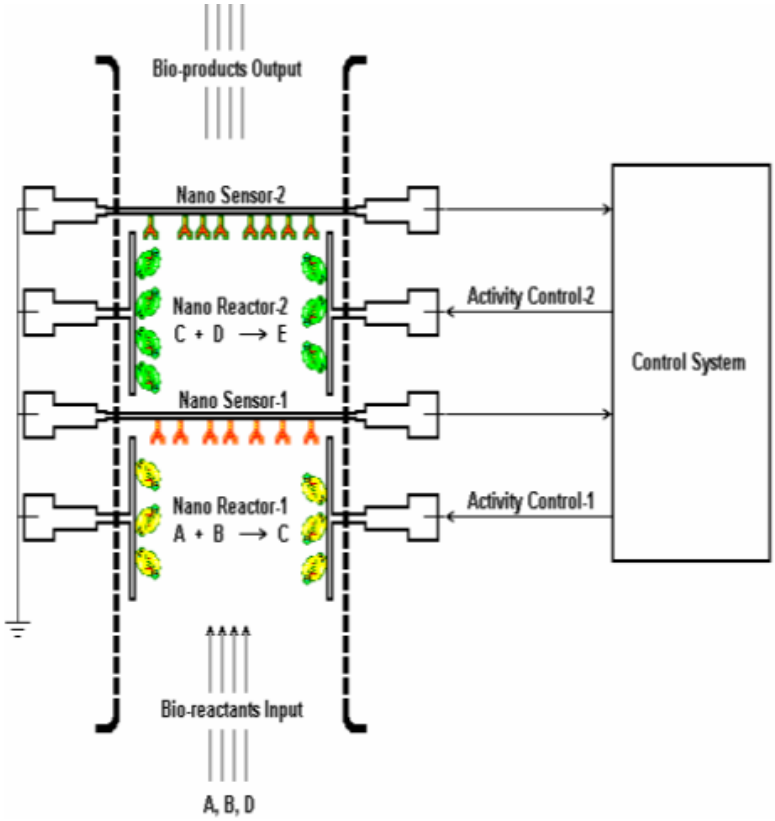

Figure 11 This schematically shows the set-up of a bionic system developed in this project. The bionic system integrates three major subsystems, they are: (1) the bio-system, which includes bioreactions, bio-recognized pairs for biosensors and bioregulators; (2) the nano-electronics system, which comprises SiNW biosensor devices, SiNW bioregulator devices, and the control system; (3) the nano-tech system, which includes the microfluidic channel and the related fluid system, immobilized zones, the related packing parts, etc.

We will utilize the liquid immersion method to assemble multilayered structure, while gas phase silanization under vacuum environment to achieve monolayer molecule. In order to specific assembly the linker, the polymeric soft mask is spin-coated, exposed and development to open the area of interest. Prior to lift-off the polymer by organic solvent, the

linker molecule is assembled onto the NWs. In the multilayer structure, the sample is immersed in the linker solution. Then, the sample is washed and drying. In the monolayer assembly, the sample is putted in a vacuum chamber. After waiting a moment, the linker is deposited onto the NWs through the inert gas carrier. We will study the thickness and surface morphology by ellipsometer and atomic force microscope.

As we known our system should meet the purpose of sensing and regulation, Figure 11 illustrates the schematic diagram of our model system. The covering plastic material is made with poly (dimethylsiloxane) (PDMS). The silicone elastomer base and curing agent are mixed at a ratio of 10:1, and connect the tubes for latter solution delivery. After drying the plastic mold at 65^{o}C for 1 hour, the cover material and the FET device are activated with oxygen plasma and then bonding together. We don't known whether the plasma damages the linker molecule in the proposal stage. If it happens, we will use the flow system to re-immobilize the linker onto the NWs for sensing. Using the on-line flow system, we will study the biomolecular reaction, immobilization, electrical detection, washing, re-immobilization, detection and so on under 37^{o}C. The system will apply to control and regulate the biomolecular reaction once the reliability of the system has no problem. The barriers, such as (1) signal interference from micro/nano scale bubbles, defect particles and memory effect, and (2) poor sensitivity from low immobilization efficiency, assembling molecular instability and contaminated element diffusion into the sensing gate, will be studied carefully.

1.5 Bottle-neck Technologies on Bio-interface for Bio-sensor and Bio-regulator on Silicon-based Material

1.5.1 Spatially Controlled Immobilization of Biomolecules on Silicon Surface

Immobilization of biomolecules on silicon-based material is the common crucial technology for the research and development of bio-sensor and bio-regulator. However, how to control the positioning, orientation, and conformation of immobilized biomolecules is the key. Chapter 2 will show our strategy and preliminary result of enzyme immobilization.

1.5.2 An Approach to Analyzing and Modeling Immobilized Enzyme Kinetics

Many biomolecules, such as membrane proteins, perform their specific biorecognition or biocatalytic activities while they are immobilized on the surface of cells or organelles.[36, 37] Artificial technologies also take advantage of immobilized enzymes for a variety of applications such as bioconversion, bioremediation, and biosensors.[38-42] Methods developed for the analysis of the function of biomolecules that move and rotate freely in the homogeneous solution may not be adequate to describe the behavior of immobilized biomolecules. The immobilized enzyme is not distributed evenly and freely in the solution and may have a unique microenvironment for each enzyme molecule. For example, the specific orientation is important for the function of proteins.[43, 44] However, free protein in solution can have many orientations, while the rotation for an immobilized protein is restricted. Unique kinetic behaviors of membrane-bound enzymes have also been reported.[45, 46]

The leading-edge semiconductor devices[47, 48] have attracted researches into the emerging fields of biomolecular sensors,[3, 4, 49, 50] hybrid (biotic-abiotic) nanomaterials,[51] lab-on-a-chip platform for further biomedical applications,[52] enzyme-coupled biosensor,[53] and novel enzyme-based devices.[54-56] The immobilization of a variety of biomolecules including proteins and nucleic acids onto silicon-based material is essential for specific biorecognition and electronic signal manipulation required for the bio-silicon hybrid devices. How to characterize the reaction kinetics for immobilized enzyme on silicon-based supporting material has become the object of study.[57-61] Kinetic properties of immobilized alkaline phosphatase have been determined in a microfluidic reaction with packed bed.[62] The kinetics of immobilized horseradish peroxidase has been studied using a microfluidic packing reaction[63] and modeling system.[64] Using batch-assay method, the kinetic parameters of immobilized glutathione S-transferase has been determined in porous silicon.[65] The kinetics and transport of this immobilized enzyme has also been simulated by an embedding method in sessile hydrogel drops.[66] Fractal and jamming effects were also used to model the kinetics of heterogeneous enzymatic catalysis.[67] The batch method used for the analysis of immobilized enzyme described above is similar to conventional method used for the analysis of free enzyme in solution. However, the apparent kinetic values determined may differ significantly from the intrinsic values for the factors that affect diffusion of product and substrate cannot be ignored in a non-homogeneous solution. Enzyme kinetics determined in a microfluidic system must consider mass transfer factors that may be significantly affected by the model system used.

To embed biomolecules onto the technology of standard IC (integrated circuit)[68] and MEMS (Micro Electro Mechanical Systems), the planar surface of Si or SiO_2 is frequently used as the substrate of immobilization. It is very important to be able to determine the kinetics of enzyme immobilized on these planar surfaces within the microfluidic system in order to evaluate the function of the whole system. So far, there is no such method reported.

In this paper, we were developing a novel kinetic model, based on systematized and standardized approach, for measuring K^*_m and V^*_{max} of rat phenol sulfotransferase (PST) immobilized on planar silicon oxide surface within a microfluidic bioreactor. Sulfonation catalyzed by PST in biological system is a popular and important biotransformation that involves in detoxication of a broad range of endobiotics and xenobotics and activation and deactivation of hormones and carcinogens.[69-72] We first tried to derive a mathematic model that can be used to extract the K^*_m and V^*_{max} of an immobilized enzyme in a microfluidic system. To deal with the diffusion effect of enzyme substrate, the ratio of the reaction volume to the catalytic planar surface must be reduced. We built a microfluidic bioreactor with a much smaller channel height than the diffusion layer in semi-infinite diffusion process according the derived mathematic model. Finally, experiments were performed in order to extract the intrinsic kinetic characteristics of the immobilized enzymes.

1.5.3 A Scheme to Measuring and Calculating Immobilized Enzyme Kinetics

Biomolecules immobilized on membranes of cells or organelles is widespread in nature, and in many cases, their activities are highly regulated in response to changes of biochemical environment. [36, 37] While today man-made systems, such as bioconversion, bioremediation and biosensors, [38-42] also take advantage of immobilized enzymes based on their properties of specific biorecognition or biocatalytic activities. Many studies of new and emerging fields, which integrate biotechnology and mature semiconductor technology, like biomolecular sensors,[3, 4, 49, 50, 73] hybrid (biotic-abiotic) nanomaterials,[51] lab-on-a-chip platform for further biomedical applications,[52] enzyme-coupled biosensor,[53] and novel enzyme-based devices,[54-56] have generated considerable attention.

To embed a variety of biomolecules including proteins and nucleic acids onto the technology of standard IC (integrated circuit)[68] and MEMS (Micro Electro Mechanical Systems) for specific biorecognition and electronic signal manipulation required for the bio-silicon hybrid devices, the planar surface of Si or SiO_2 is frequently used as the substrate of immobilization. For evaluating the performance in this kind of bio-embedded application, the kinetics of enzymes (or substrates) immobilized on these planar surfaces within a microfluidic system should be known and has become the object of study.[57, 58, 61, 74, 75]

The immobilized enzyme is not distributed evenly and freely in the solution, so there are many extra constraints to the enzyme molecule: conformation, specific orientation, substrate diffusion, ion charge profile near the surface of supporting material, to which enzymes are bound.[43-46]

The experimental methodology of measuring enzyme activity with homogeneous assay based on Michaelis–Menten equation has been developed completely during the past century and become standard material in whole modern textbooks of enzyme assays.[76, 77] Similarly, we tried to establish a standard scheme for measurement and data analysis of immobilized enzyme assays based on the surface reaction limited model, constructed and reported in our previous studies.[5] However, the apparent kinetic values determined may differ significantly due to not only different models adopted but different methods of data treatment, so the standardization of corresponding measurement and calculation is especially necessary to focus on besides establishment of model system for immobilized enzyme assay.

So far, there is no such platform combined a complete solution, through a systematized and standardized consideration, to set up a standard scheme, which can be used to compare the performance of immobilized enzyme operated by different research groups. Using the covalent linkages with sulfhydryl enzymes[78] and the high affinity of Gold nanoparticles (AuNPs) for biomolecules,[79] in this paper, rat phenol sulfotransferase (PST) and *Candida rugosa* lipase (CRL) were immobilized on planar silicon oxide surface within a microfluidic

bioreactor, respectively, and, we were providing a novel method for kinetic measurement and corresponding data analysis, based on our previous kinetic model,[5] for measuring K^*_ms and V^*_{max}s. Sulfonation catalyzed by PST in biological system is a popular and important biotransformation that involves in detoxication of a broad range of endobiotics and xenobotics and activation and deactivation of hormones and carcinogens.[69-72] Lipase are used industrially as detergent enzymes, in paper and food technology, in the preparation of specialty fats, and as biocatalysts for the synthesis of organic intermediates, and in various clinical studies and drug delivery.[80] Facing these two enzymes with different immobilization schemes and limitations of enzyme assays, we developed a standard measuring and calculating procedure to extract the near intrinsic kinetic characteristics of the immobilized enzymes.

Chapter 2 Enzyme Immobilization

2.1 Introduction

The interdisciplinary study of biology, chemistry, and electronics becomes more and more important than ever before. Combining the biotechnology and semiconductor technology, various types of biochips and biosensors have now been developed to detect and monitor the specific binding of biomolecules on the solid-state substrates.[81] The choice of suitable chip surface for the purpose of biomolecular immobilization has gradually received attraction in recent years. For example, (3-mercaptopropyl)trimethoxysilane linker first assembles onto the silicon oxide film. Through the assistant of gold nanoparticles, the deoxyribonucleic acid (DNA) molecule can be tethered.[82] DNA molecule can also be assembled onto the platinum-silicide surface through the linkers of (3-aminopropyl)trimethoxysilane, N-cyclohexyl-N'-[2-(N-methylmorpholino)-ethyl]-carbodiimide-4-toluene sulfonate and imidazole.[83] Genomics and proteomics research has elucidated many new biomarkers that exhibit the potential to greatly improve the correctness of disease diagnosis.[84, 85]

There were three important enzymes as the studying targets in this research for the evaluation of immobilized enzyme kinetics; they were rat-phenol-sulfotransferase (rat-PST, E.C. 2.8.2.1), D-hydantoinase (or imidase, E.C. 3.5.2.2), and *Candida rugosa* lipase (CRL, E.C. 3.1.1.3). Sulfotransferase is an important enzyme in a variety of organisms and can specifically catalyze the transfer of the sulfuryl group (SO_3). The reaction involves the transfer of the donor of universal sulfuryl group (3'-phosphoadenosine 5'-phosphsulfate, PAPS) to the variety of nucleophiles ranging from endobiotics (i.e., monoamines, phenyl compounds, hormones, proteins and carbohydrate) to xenobiotics.[69, 70] Hence, sulfonation catalyzed by sulfotransferase is an important pathway in detoxification of a broad range of endobiotics and xenobotics. They have been implicated in the activation and deactivation of

hormones and carcinogens through the formation of sulfate conjugates.[71] In the recent review,[72] membrane-associated proteins have been used in several influential biological processes, including viral entry of cells, leukocyte adhesion, and anticoagulation. More generally, enzymatic transformations of cell-surface proteoglycans by sulfotransferases appear to trigger vital molecular-recognition and signal-transduction events. Redox modification of Cys residues provides a mechanism for protein regulation.[86, 87] Proteins can be S-glutathionylated or S-nitrosylated, especially for the environment of oxidative stress. Oxidative stress is involved in the pathogenesis of various degenerative diseases including cancer.[88]

Due to its broad substrate specificity, hydantoinase, a zinc enzyme, is also known as dihydropyrimidinase, hydantoinase, dihydropyrimidine hydrase, dihydropyrimidine amidohydrolase, or imidase,[89-96] which catalyzes a reversible ring-opening hydrolysis of hydantoin/pyrimidine and their 5'-monosubstituted analogues.[97] It is an industrial enzyme[98] used as a biocatalyst for the efficient production of optically pure D- or L-amino acids via the enantioselective hydrolysis of corresponding hydantoins.[99-101] These intermediates are widely used for the synthesis of semisynthetic antibiotics, peptide hormones, pyrethroids, and pesticides.[101]

Among the many enzymes used in biocatalytic processes, lipases have gained particular interest as catalysts in organic synthesis. The hydrolytic enzymes are relatively insensitive towards non-aqueous solvents, can tolerate fairly broad Ph and temperature ranges, and most importantly, exhibit high chemoselectivites.[102, 103] Lipases have found applications ranging from kinetic asymmetric resolutions[104-106] to polymerizations.[107]

The use of "state-of-the-art semiconductor technology" for sensor technology guarantees the high fabrication reliability and yield. However, the assembly of biomolecules onto the popular films used in semiconductor is still challenged, especially for the enzyme molecule. Most recent literatures are focused on the glucose oxidase immobilization because the

diabetes disease is a major world health problem.[39, 41, 84] To the best of our knowledge, the immobilization of PST or imidase onto the silicon-based films of semiconductor manufacturing and its activity has not been reported. The active enzymes on the silicon-based surfaces serve as the basis for the enzyme sensor. Nanoparticles are attracting substantial interest in the rapidly developing area of nanobiotechnology.[108, 109] Gold nanoparticles (AuNPs), which have high affinity for biomolecules, have been used as biosensors,[24] immunoassays,[110] therapeutic agents,[111] and vectors for drug delivery;[112] thus, the conjugation of AuNPs and biomolecules has become a major area of research for advancing the use of nanotechnology in biomedical applications.[113-115]

Besides covalent linkages with sulfhydryl PST and imidase enzymes, we have also tried to use the high affinity of AuNPs for CRL's immobilization. Nanoparticles are attracting substantial interest in the rapidly developing area of nanobiotechnology.[108, 109] AuNPs, which have high affinity for biomolecules, have been used as biosensors,[24] immunoassays,[110] therapeutic agents,[111] and vectors for drug delivery;[112] thus, the conjugation of AuNPs and biomolecules has become a major area of research for advancing the use of nanotechnology in biomedical applications.[113-115]

In this study, we first evaluate the pattern surface often encountered in the semiconductor technology to assemble the fluorescent rhodamine molecule. The suitable pattern material is adopted for modification and functionalization to immobilize PST, imidase, CRL.

2.2 Experiment Procedures

2.2.1 Pattern formation processes

P-type Si(100) wafers (14-21 Ω-cm, MEMC, MO, USA) with 15 cm diameter were deposited and etched to form the structure with silicon oxide pattern on poly-Si film, and silicon nitride pattern on poly-Si film, respectively. They were cut into 2x2 cm^2 pieces to serve as test samples. To prepare the silicon oxide pattern on poly-Si film, the poly-Si film was first deposited with silane gas (SiH_4) at 60 cm^3/min and 620^oC. Prior to photolithography, the silicon oxide film was grown by wet oxidation with a gas mixture of hydrogen (8000 cm^3/min) and oxygen (5000 cm^3/min) at 978^oC. The mask with the pattern of interest was used to define the photoresist (TMER-iP3650, Tokyo Ohka Kogyo, Tokyo, Japan) pattern. A 365nm light emitted from high pressure mercury lamp (SUV-2001CIL, USHIO, Tokyo, Japan) induced the photo-active reaction for the photoresist film. After the dissolution of exposure area with 2.38% tetramethylammonium hydroxide, the plasma was used to etch the silicon oxide film without passivation by photoresist pattern. The reactive-ion etch system (TE5000, Tokyo Electron Limited, Tokyo, Japan) was operated at 500W RF power under 0.2 Torr high vacuum, and the gas mixture of 20 cm^3/min of CF_4, 20 cm^3/min of CHF_3, and 400 cm^3/min Ar. Finally, the residual photoresist was removed and cleaned by the mixing chemical of H_2SO_4 and H_2O_2 (volume ratio = 3:1) at 120^oC for 10min. The chemicals used were of higher grade from Merck (Darmstadt, Germany).

Similar with the processes for the above sample of silicon oxide pattern on poly-Si film, the silicon nitride film was deposited with a mixture of ammonium (130 cm^3/min) and dichlorosilane (30 cm^3/min) at 780^oC. The silicon nitride film with photoresist pattern passivation was etched by the same reactive-ion etch system. The instrument was operated at 250W RF power under 0.8 Torr high vacuum, and the gas mixture of 50 cm^3/min of CF_4, 20

cm^3/min of O_2, and 1000 cm^3/min Ar. After the surface cleaning, the silicon nitride pattern on poly-Si film was achieved.

2.2.2 Chemicals, Apparatus and Procedures for Immobilization

Prior to immobilization, the patterned sample should be carefully cleaned in the piranha solution, H_2SO_4 and H_2O_2 (volume ratio is 3:1), twice, each time for 30 min. The temperature of the solution of must be maintained above 85°C to possess the oxidative power. The clean effect is based on the dehydrating effect of the H_2SO_4, and the oxidizing effect of the H_2O_2.[116] If the temperature dropped, hydrogen peroxide was required to replenish. It should be noted that the cleaning solution was very corrosive and dangerous; we must handle it carefully. After pure water rinsing and drying, the patterned sample of interest was immersed in the (3-aminopropyl)triethoxysilane (APTES) solution for 30 min in room temperature. The APTES (Sigma-Aldrich, MO, USA) solution was prepared by the following procedures: (1) mixing pure water with acetone (volume ratio is 5:1), (2) adjusting the above solvent pH to 3.5 by 1M HCl, and (3) preparing the 5% APTES solution by diluting with above solvent. Then, the patterned sample was rinsed with pure water thoroughly. The succeeding step was to bake the pattern sample at 120°C for 30 min. Then, the sample was immersed in the linker solution (2.5 % glutaraldehyde, i.e. pentane-1,5-dial) for 30 minutes in room temperature. The 2.5% glutaraldehyde solution was diluted with phosphate buffered saline solution (pH 7.4 PBS buffer, containing 120mM NaCl, 2.7mM KCl, and 10mM phosphate buffer, Sigma-Aldrich) from 25% glutaraldehyde (in water, Sigma-Aldrich). Then, the pattern sample was rinsed with PBS. Finally, the patterned sample was immersed in the rhodamine B amine ($C_{28}H_{31}N_3O_3$, Sigma-Aldrich) solution for 16 h at room temperature. The powder of rhodamine B amine was first weighted and then dissolved in the dimethylformamide (DMF, Sigma-Aldrich).

Then, it was diluted by 0.1 M carbonate buffer (pH 9.6) to reach the concentration of 0.1 mM rhodamine B amine solution. The rhodamine B amine is a light-sensitive molecule. Hence, the solution should be prepared freshly and the vessel should be covered with aluminum foil. Prior to observing these pattern samples by fluorescent microscope (BX51, OLYMPUS, PA, USA), all the samples were cleaned sequentially by 0.1 M carbonate buffer, pure water, and drying.

The home-made apparatus in Figure 12(a) was designed and used to evaluate the enzyme activity on the sample surface of interest. Figure 12(b) and (c) show the pilot platform of bio-regulator, a batch-type reactor regulated by electric field. The Teflon ring tightly contacted with the substrate and sealed with the silicon resin glue. Prior to conducting the enzyme immobilization, we needed to test the reliability of the home-made apparatus to avoid leakage problem. The clean and APTES immobilization methods for enzyme immobilization were conducted in the home-made apparatus with the same procedures as rhodamine mentioned above. We prepared the linker solution by dissolving sulfosuccinimidyl 4-(N-maleimidomethyl)-cyclohezane-1-carboxylate (sulfo-SMCC, Sigma-Aldrich) into the 50mM sodium borate buffer (Sigma-Aldrich). To immobilize the sulfo-SMCC, the 0.5 mM sulfo-SMCC solution was dipped into the apparatus in Figure 12 for 1 h at room temperature. Then, the enzyme solution (200 μg/mL rat-phenol-sulfotransferase, rat-PST, EC.2.8.2.1) was also put into the vessel for 1 h at 4^{o}C. Finally, the enzyme-immobilized sample was immersed by the 50 mM 2-mercaptoethanol solution (the solution was prepared in the 50mM sodium phosphate buffer) for 30 min at 4^{o}C both to block the maleimide group of unreactive sulfo-SMCC and to keep immobilized sulfotransferase in reduced state. (The reduced sulfotransferase is in its active form.) The sample was repeatedly immersed by fresh 50mM sodium phosphate buffer for three times to wash away the residual 2-mercaptoethanol solution. Observation of the activity of the enzyme was a direct method to know whether the enzyme was successfully immobilized or not. The reaction solution was prepared by adding

the 1mM 4-nitrophenyl sulfate, 50μM 2-naphthol, and 2μM 3'-phosphoadenosine 5'-phosphate (PAP) into the solvent of 100 mM 1,3-bis[tris(hydroxymethyl)methylamino]propane buffer at pH 7. Then, we added the above solution into the home-made apparatus. At the reaction time of interest, the liquid was siphoned out from the home-made apparatus to an UV-Vis spectrophotometer (Hitachi UV-Vis-3300, Tokyo, Japan) for characterization. We analyzed the absorbance of 4-nitrophenol (the catalytic product of 4-nitrophenyl sulfate) at 400 nm wavelength to determine the activity of sulfotransferase.

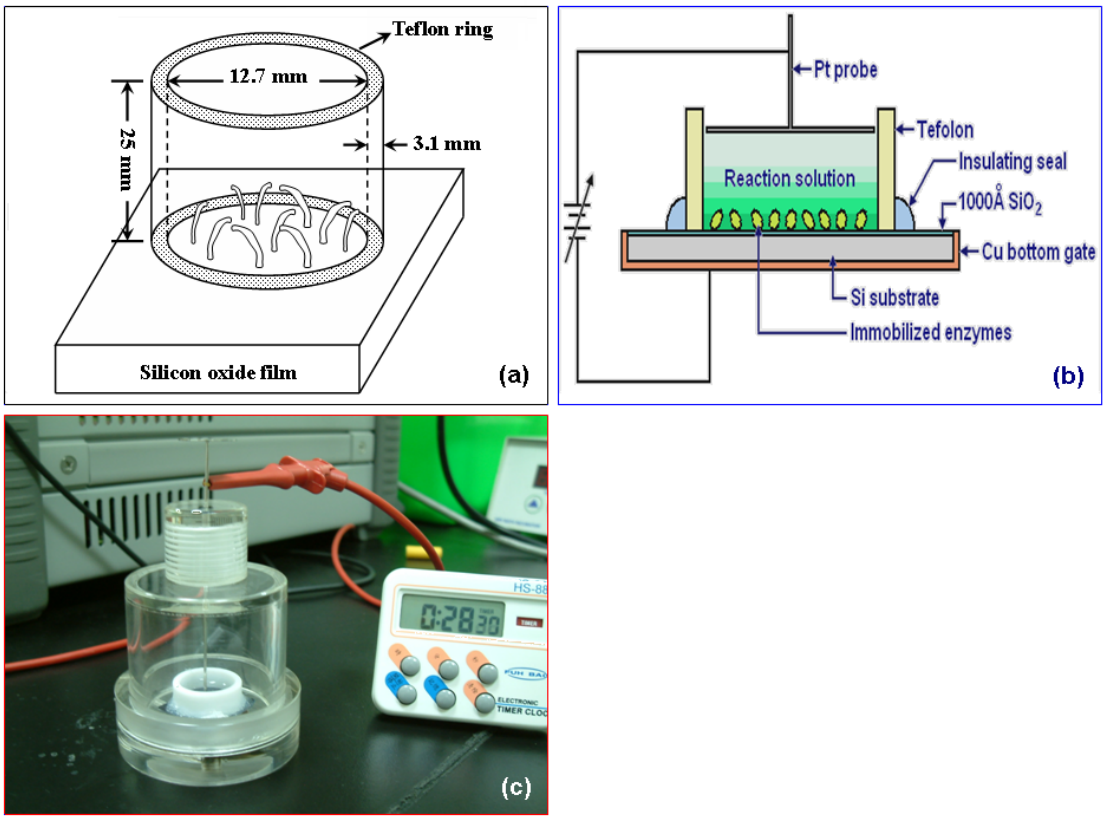

Figure 12 (a) Schematic diagram of the home-made apparatus for immobilization of sulfotransferase onto the silicon dioxide surface; (b) schematic diagram for the pilot apparatus of bio-reactor regulated by electric field; (c) real setup of test platform for bio-reactor regulated by electric field.

2.3 Results and Discussion

2.3.1 Immobilization of Fluorescent Material onto Various Pattern Substrates

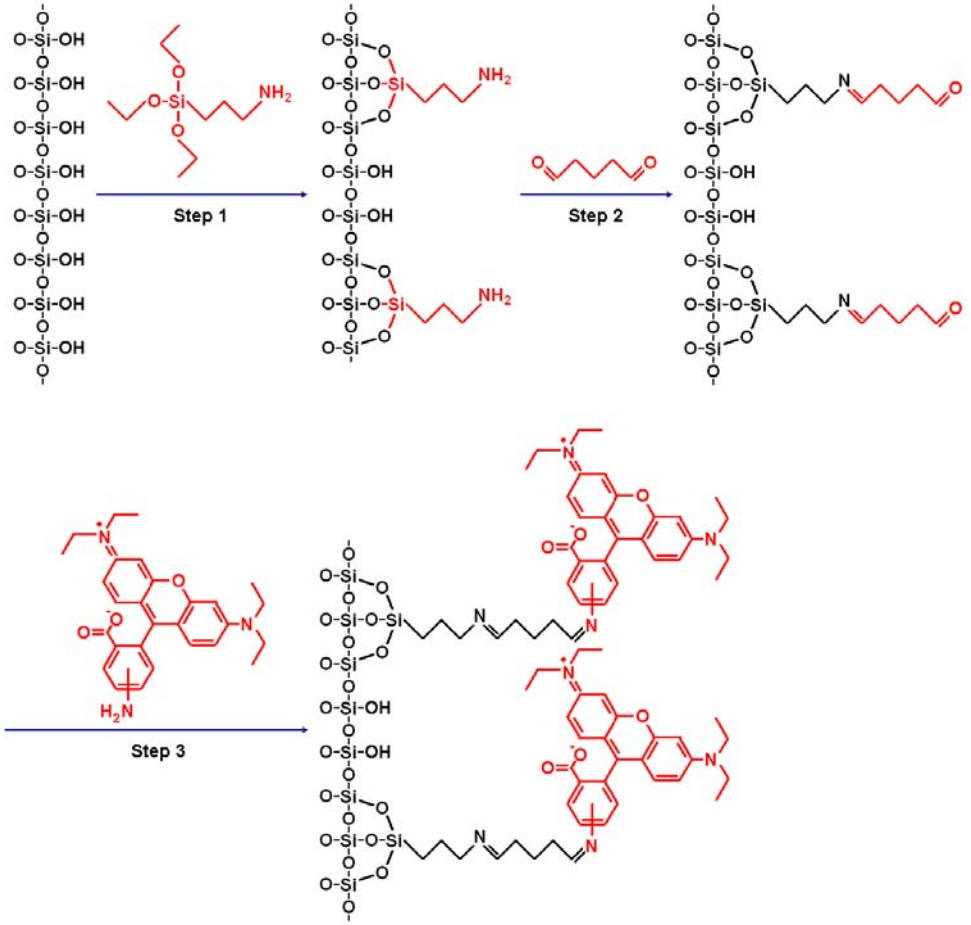

Figure 13 The immobilization steps for rhodamine B amine onto silicon oxide surface.

Rhodamine and its derivatives are popular fluorescent materials for labeling all types of biomolecules. The integration of the rhodamine derivatives onto the semiconductor-based pattern structures is very important for developing the biosensors. In Figure 13, the successful immobilization of rhodamine B amine onto silicon oxide surface requires three mail steps. In first step, the ethoxysilane group (CH_3CH_2O-Si) in APTES reacts with the surface silanol group (Si-OH) on silicon dioxide film. The elimination of ethanol to form the Si-O-Si link, leaving a primary amine group on the surface. Glutaraldehyde in second step is subsequently

used to react with the surface amine group, yielding an imine linkage (C=N) with one end aldehyde group in glutaraldehyde. At last, the other end aldehyde group reacts with the amine group in rhodamine. The elimination of water helps to immobilize the fluorescent molecule.

Two types of pattern structures (silicon oxide on poly-Si, and silicon nitride on poly-Si) are used to evaluate the immobilization capability for the rhodamine B amine. The successful immobilization can be evaluated from the red fluorescent rhodamine molecule. The pattern sample in Figure 14(a) has finished the whole procedures mentioned in Figure 13. We find only the red color emitted from the silicon oxide pattern, while no color in poly-Si region. This observation clearly suggests the rhodamine molecule can only be immobilized in silicon oxide pattern, but not in poly-Si. This result is beneficial for future biosensor construction by means of semiconductor process. As to the same pattern but skip the APTES and glutaraldehyde procedures in Figure 13, no image contrast can be seen from Figure 14(b). This observation suggests the rhodamine molecule has not yet assembled onto the sample surface. The amine group of rhodamine molecule can not react either with the silicon oxide or the poly-Si film.

The other structure of silicon nitride pattern on the poly-Si film is also studied. Figure 14(c) demonstrates the sample with the entire processes in Figure 13. Except for the contamination area, no colour can be seen from this Figure. This result means the silicon nitride and poly-Si can not immobilize the rhodamine molecule. This finding is attributed to no surface active group appeared for silicon nitride and poly-Si. Therefore, there has no reaction for the surface with the linker molecules (such as APTES or glutaraldehyde). Together with the observation in Figure 14(a) and 14(b), only the silicon oxide film, pre-assembled linker, can immobilize rhodamine molecule.

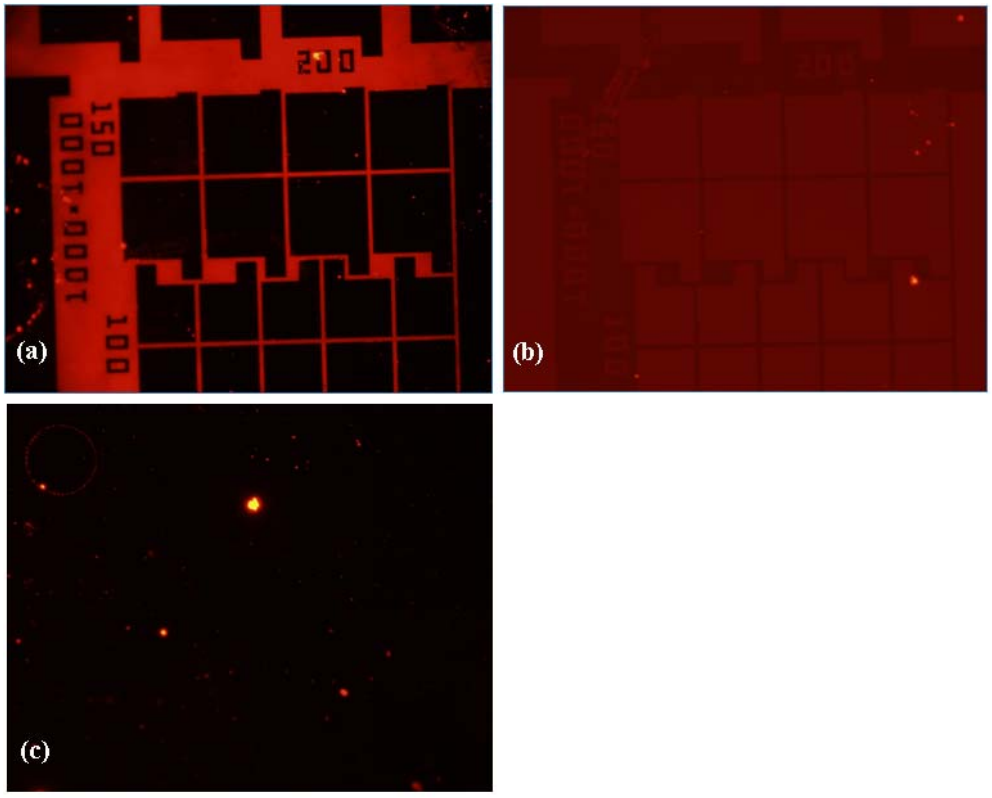

Figure 14 (a) The sample has previously assembled linkers of APTES and glutaraldehyde. The red region of fluorescent image represents the rhodamine molecule has immobilized onto the silicon oxide surface, and the black region represents no rhodamine molecule has immobilized onto the poly-Si surface. (b) The sample omits the linker processes of APTES and glutaraldehyde. The rhodamine molecule can be immobilized onto the silicon oxide and poly-Si surface without the aid of linkers. (c) The sample has previously tried to assemble linkers of APTES and glutaraldehyde. The black color means the rhodamin molecule can not immobilize onto silicon nitride and poly-Si surface, irrespective of linkers.

2.3.2 Enzyme Immobilization and Its Activity

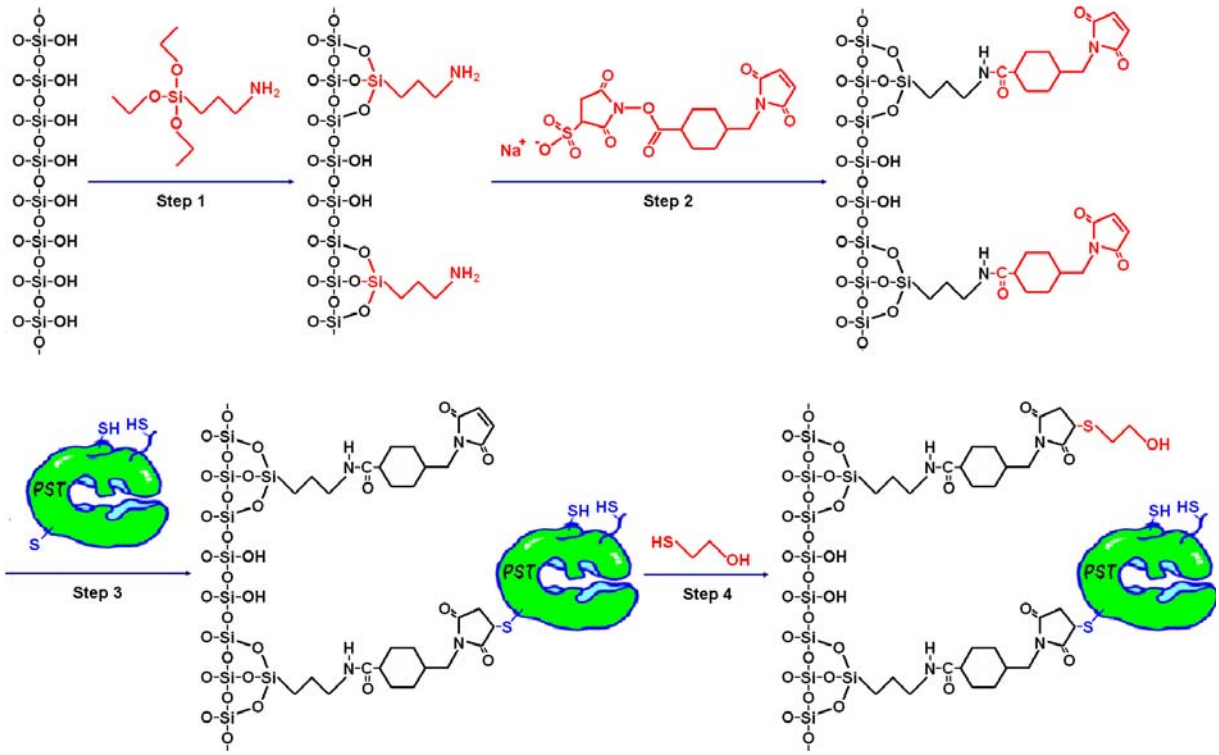

Figure 15 Schematic diagramof the immobilization of PST (or imidase) onto silicon oxide surface.

It is obvious that the surface of silicon nitride and poly-Si have no active group for immobilization. The bio-important enzyme, i.e. PST, can be only assembled onto the silicon dioxide film. The reaction having three main steps is illustrated in Figure 15. The first step for APTES immobilization is the same with Figure 13. In second step, we substitute the linker from glutaraldehyde to sulfo-SMCC. The sulfo-SMCC reacts with the terminal amine group in Figure 15 to form the stable amide bond, and with the release of sulfo-N-hydroxysuccinimide (sulfo-NHS) group. At third step, the sulfuryl group of enzyme (PST) reacts with the terminal maleimide group on the surface. One of the carbons adjacent to the double bond undergoes nucleophilic attack by the thiolate anion to generate the addition product. Hence, the PST is successfully immobilized onto the surface of silicon oxide film. Prior to testing the activity of surface enzyme, the region without enzyme immobilization, but

still has terminal maleimide group, is deactivated by the 2-mercaptoethanol (step 4 in Figure 15).

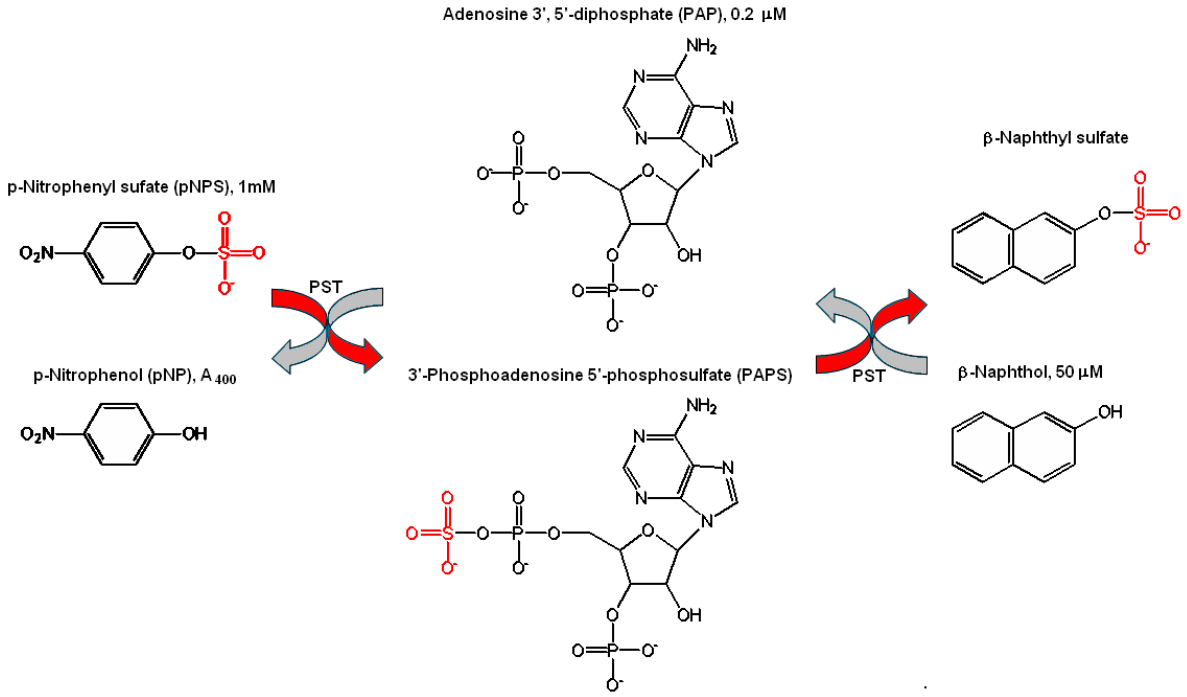

Figure 16 The couple reactions in the home-made apparatus are catalyzed by phenol sulfotransferase.

The analysis of surface enzyme (PST) activity is very complex. Figure 16 illustrates the three simultaneous chemical reactions appeared in the home-made apparatus. The sulfate group in the 4-nitrophenyl sulfate is transferred into the PAP molecule under the catalysis by the PST enzyme, yielding the products of 4-nitrophenol and 3'-phosphoadenosine 5'-phosphatesulfate (PAPS). The molar ratio of PAP to 4-nitrophenyl sulfate is 500. As a result, the reaction by enzyme will terminate soon. However, the coexisted 2-naphthol can be catalyzed to form the 2-naphthyl sulfate. This reaction can recover the PAP from PAPS, and continue the sulfuryl group transformation between 4-nitrophenyl sulphate and 4-nitrophenol. Once the enzyme is still active, the concentration of 4-nitrophenol is gradually accumulation. Therefore, the absorbance at 400nm wavelength also gradually increases. This reaction design,

together with the home-made apparatus, provides an easy characterization way by using UV-Vis spectrophotometer to evaluate the enzyme activity after surface immobilization.

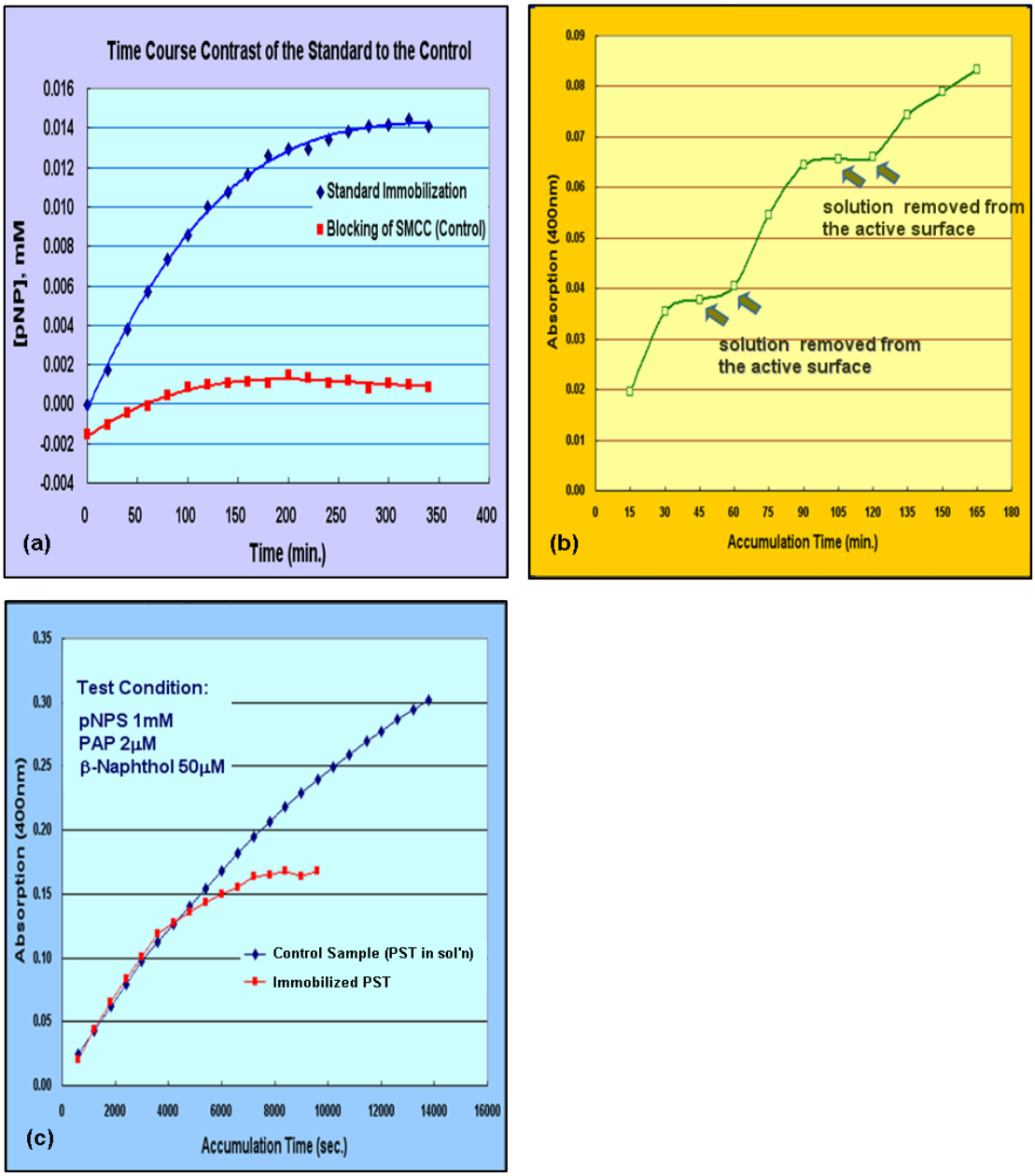

Figure 17 The absorbance of 4-nitrophenol; (a) time course contrast of the standard process of PST immobilization to the blocking control; (b) time course with two termination periods caused by removing reaction mixture from catalytic surface, (c) at various enzyme reaction times for the control sample (sulfotransferase in solution) and the enzyme target sample (sulfotransferase immobilized onto the silicon oxide surface).

Based on the standard assay for PST immobilized on patterned SiO_2/Si substrate, the concentration of *p*NP increased with time course of reaction, shown as Figure 17. Figure 17(a) shows the little increment of *p*NP concentration for enzyme-blocked control (keep all immobilization procedures as Figure 15, but exchange step-3 and step-4; so the maleimide on SMCC was blocked by the thiol on 2-mercaptoethanol through Michael addition reaction) was saturated under 0.002 mM. The insufficient reaction time of blocking step should be the cause of a small leakage control. In order to confirm the PST was immobilized tightly onto the patterned SiO_2/Si substrate, we withdrew the reaction mixture from catalytic surface to a cuvette, when reaction had proceeded 30 min; then incubated in a cuvette for more 30 min, in this period, two times of detection followed at accumulation time 45 min and 60 min respectively. No increment of *p*NP concentration was found, that was no *p*NP was produced if the reaction mixture was removed from catalytic surface. Reload the previous reaction mixture to catalytic surface at accumulation time 60 min; the reaction immediately started again. At accumulation time 90 min, we withdrew the reaction mixture, and the reaction terminated again, shown as Figure 17(b).

The immobilization of enzyme onto the substrate surface can promote the controllability for the future enzyme sensor. However, the immobilization confines the enzyme geometry and the enzyme may be denatured reversibly or irreversibly after a couple of times. To elucidate the activity of the surface immobilized enzyme, we need to compare the activity of enzyme either from the surface phase or in the solution phase. There exist various degrees of freedom for the enzyme on the surface or in the solution. Figure 17(c) shows the PST activity under two different experiments. The control experiment is conducted in the home-made apparatus, but the sample surface without immobilization. We add the mixture solution of 1 mM 4-nitrophenyl sulfate, 50 μM 2-naphthol, and 2 μM PAP into the apparatus. Then, 50 mg/L PST is spiked into the apparatus to induce the catalytic reaction. The absorbance of 4-nitrophenol

in the control sample gradually increases with the reaction time. No saturation effect is observed during the time period of $1.4x10^4$ sec. The time course trend of enzyme reaction meets the enzyme kinetics in the solution. On the contrary, the surface immobilized enzyme exhibits a quite different tendency. The time course trend of surface-immobilized enzyme exhibits the same behavior with the control sample for the duration within $4.8x10^3$ sec, but gradually loss the activity thereafter.

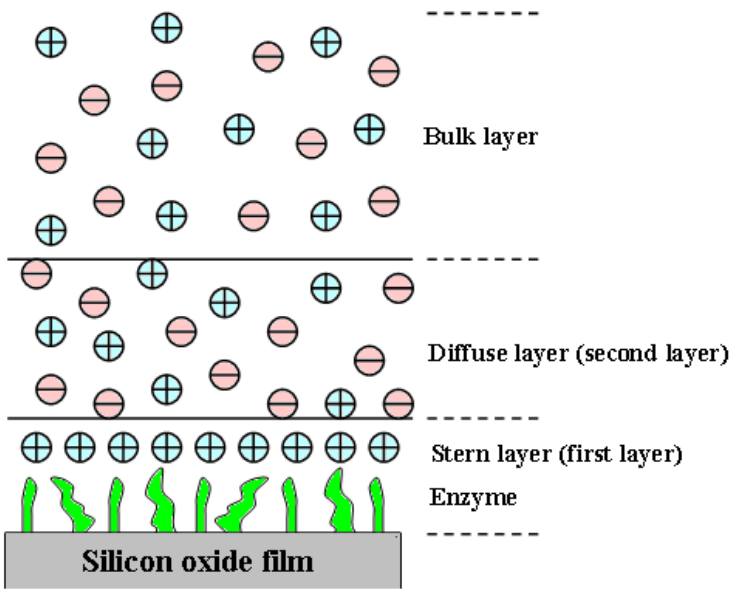

Figure 18 The surface diffusion model for the catalytic reaction of sulfotransferase.

There arises a question- why the surface immobilized enzymes loss their activity than suspended enzyme in solution after $4.8x10^3$ sec? The surface diffusion model (in Figure 18) based on the Stern-Gouy-Chapman prediction[117, 118] can be used to explain this finding for the enzyme immobilized surface. The PST enzyme and its counter ions are located in the first layer. The second layer contains both the positive and negative charged ions, and forms the formal charge gradient for these ions form the interface (i.e. shear plane). The other ions are randomly dispersed in the bulk layer. For example, the initial formal charge in the first layer is mainly from the molecules of 4-nitrophenol sulphate, PAP and 2-naphthol. The total charge in the first layer should be kept constant, irrespective of reaction time. Once the 2-naphthyl

sulphate in the second layer or bulk layer diffuses into the first layer, the enzyme will catalyze the reaction and produce the 4-nitrophenol. As previous mention in Figure 16, the PAP also diffuses near the surface enzyme, and reacts to produce PAPS. Similarly, 2-naphthol also needs to diffuse into the first layer to recover the PAPS into PAP. After a couple of reaction times, the 2-naphthyl sulphate and 4-nitrophenol increases to a relatively high concentration. The diffusion rate of reactant from the second or bulk layer into the first layer will be restricted. Hence, the reaction rate will decrease, and saturate finally. On the contrary, the behavior of enzyme in the control sample is different with the case of surface immobilized enzyme. The boundary for the solution enzyme and the reagents is not significant due to the homogeneous mixing in the solution type. Hence, the saturation effect during the time period of $1.4x10^4$ sec can not be seen for the solution enzyme (control sample) in Figure 17(c).

To prove the above viewpoint, we siphon the solution from the home-made apparatus at time of interest to observe the absorbance of 4-nitrophenol. With the help of surface-immobilized enzyme, the 4-nitrophenol concentration increases from $9.0x10^2$ sec duration to $1.8x10^3$ sec duration. The solution is then drawn from the vessel after $1.8x10^3$ sec. Interestingly, the absorbance remains constant at $2.7x10^3$ sec and $3.6x10^3$ sec due to the separation of solution with the surface immobilized enzyme. The solution refills back into the home-made apparatus. The surface-immobilized enzyme again catalyzes the reaction, and the absorbance of 4-nitrophenol is increases at $4.5x10^3$ sec and $5.4x10^3$ sec. The solution is again drawn from the vessel after $5.4x10^3$ sec. Similarly, the absorbance is unchangeable at $6.3x10^3$ sec and $7.2x10^3$ sec. We put the solution again into the enzyme-immobilized vessel, and the absorbance is increase. This observation confirms that the PST enzyme can be immobilized onto smooth surface, and the enzyme activity can be efficiently controlled. This idea is beneficial for the future design of advanced enzyme regulators. The bio-reaction can be conducted only at the enzyme-immobilized silicon oxide region, while terminated at the enzyme-free silicon nitride or poly-Si region.

2.3.3 Stability of Immobilized Enzymes

Enzymes are biocatalysts that accelerate many biochemical reactions. Immobilizing enzymes to supporting materials can make enzymes reusable and greatly affect their stability.[43] Any strain onto the enzyme during immobilization process, like higher temperature or extreme pH, is likely to enhance the inactivation of the enzymes. Though examining the stability of immobilized enzymes has been deeply concerned in traditional biochemical engineering,[119] that study of enzymes immobilized onto silicon-based supporting material is still a new and potential field in near future applications.[54] For developing stable research platform or analytic devices in analytic and medical application, the reliability of bio-purposed devices and the stability of immobilized enzymes are both crucial. In fact, there are common methods and similar concepts in analyzing the failure or inactivation of them. A generally accepted definition of reliability is the probability that an item will perform a required function under stated conditions for a stated period of time.[120] Similar to this definition, table 3 illustrates the analog but specific items to themselves; this allows us to reasonably use the mathematical model of reliability, widely used in engineering field, to analyze and characterize the inactivation data of immobilized enzymes. A more advanced consideration, mathematical model of reliability will still be the key how to evaluate the reliability of future artificial-bio hybrid devices or systems, though the stability of immobilized enzyme in majority of literature was represented by raw-data plotting of normalized activity versus time. The Weibull model is based on the extreme value distribution that applies when many small defect sites compete with each other to be the causes the earliest time of failure. Proteins are the most abundant macromolecules present in membranes, cytosol, organelles, and chromosomes of living cells. There are also many micro-scale mechanisms, which may affect the shape or conformation of loop, motif, domain, active side of protein, and compete with each other, to cause denaturation of a protein. Based on this

concern, using the Weibull distribution function to analyze enzyme stability is described as follows:

Assume that an enzyme is operating at t = 0, right after immobilization process, the activity of all immobilized enzymes are equal, and the activity rate is proportional to the number of active enzymes. Let there be N immobilized enzymes in a population; assume that at time t it is observed $N_i(t)$ of the enzymes have been inactivated and that $N_a(t) = N - N_i(t)$ enzymes are still active. The ratio N_a/N is defined as the stability of enzyme, which equals to normalized activity of enzyme (the ratio of survived activity to original activity of enzyme). N_i/N is the instability of enzyme, and can be termed by the cumulative function I(t) with the following properties

$$\begin{cases} I(t) = 0 & t < 0 \\ 0 \le I(t) \le I(t') & 0 \le t \le t' \\ I(t) \to 1 & t \to \infty \end{cases} \qquad (1)$$

Table 3 Analog between the reliability of bio-purposed device and the stability of immobilized enzyme.

	Reliability of a device or system	Stability of immobilized enzyme
Assumption	the system is a series system, and failure is due to component or part failures. all compoents are constant failure rate and independent.	the activity of all immobilized enzymes are equal, and the catalytic rate is proportional to the number of active enzymes.
Required function	a definition of satisfactory operation and unsatisfactory operation or failure. "good" or "bad"	"active" or "inactive"
Stated conditions	the total physical environmnt, icluding the mechanical, thermal, and electrical conditions of expected use.	temperature, redox agents, pH, buffer concentration, etc.
Stated period of time	the time during which satisfactory operation is required.	the time during which an imaginary enzyme is active.

The stability function S(t) is the probability that the enzyme will survive to time t without deactivation. The function is related to I(t) and is given by

$$S(t) = 1 - I(t) \tag{2}$$

The probability density function i(t) is defined by the derivative of I(t) with respect to time. The i(t) is related to the I(t) by

$$i(t) = \frac{d}{dt} I(t) \qquad or \qquad I(t) = \int_0^t i(t)dt \tag{3}$$

In our scheme to measure the kinetics of immobilized enzyme, which will be examined in chapter 3, the quantity that is of most concern is the instantaneous inactivation rate λ(t), or the denature rate, given by

$$\lambda(t) = \frac{i(t)}{1 - I(t)} = \frac{dI(t)/dt}{1 - I(t)} \approx \frac{\Delta I(t)/\Delta t}{1 - I(t)} \tag{4}$$

The distinctive shape of the λ(t) curve makes it the more useful measure of the stability of a enzyme. This "bathtub-shaped" curve can be divided into three regions, which means three different mechanisms of inactivation is dominant,[121] as shown in Figure 20. That is there are, at least, three micro-scaled states in this population of immobilized enzyme; so there must be three different sets of apparent kinetics constants corresponding to each phase in bathtub curve.

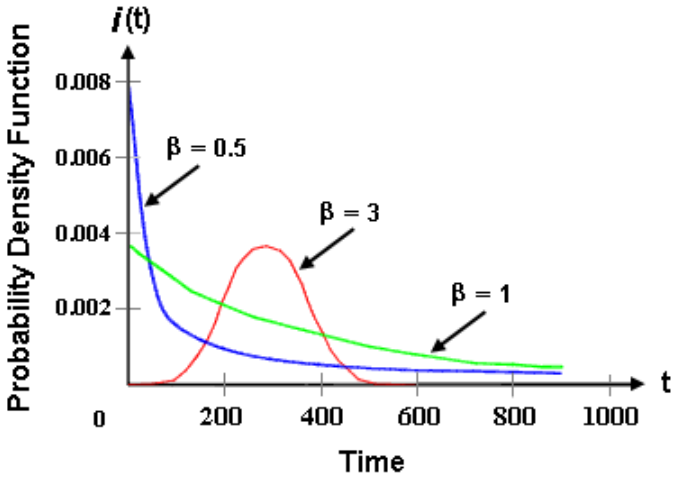

Figure 19 The typical plots for the Weibull distribution.

In the Weibull distribution function the inactivation rate varies as a power of the age of the enzyme. The inactivation rate is represented as

$$\lambda(t) = \frac{\beta}{\alpha} t^{\beta-1} \tag{5}$$

where α is a scale parameter, and β is a shape parameter. For $0 < \beta < 1$ the inactivation rate decreases with time, and the Weibull distribution may used to present the early inactivation period of an enzyme. For $1 < \beta < \infty$ the inactivation rate increases with time, and the Weibull distribution may be used to represent the wear-out period of a enzyme. If $\beta = 1$ the inactivation rate is constant, and the exponential distribution is a special case of the Weibull distribution with $\beta = 1$. This distribution is highly adaptable, and can be used to provide a variety of shapes, as shown in Figure 19.

From eq (5) we can calculated that

$$I(t) = 1 - \exp(-\frac{1}{\alpha} t^{\beta}) \tag{6}$$

When experimental data is fitted to an assumed cumulative inactivation function to determine the function parameters as well as the goodness of fit, appropriate plotting paper must be used. That is, the scales of the paper must be such that the experimental data will lie on a straight line if the data is well represented by assumed distribution. Such plotting paper is available for use with the Weibull distribution function. For the Weibull distribution function

$$\ln\{\ln(\frac{1}{1-I(t)})\} = \beta \ln t - \ln \alpha \tag{7}$$

which is linear in the form y = mx + c. Figure 22 shows an example of Weibull plotting paper.

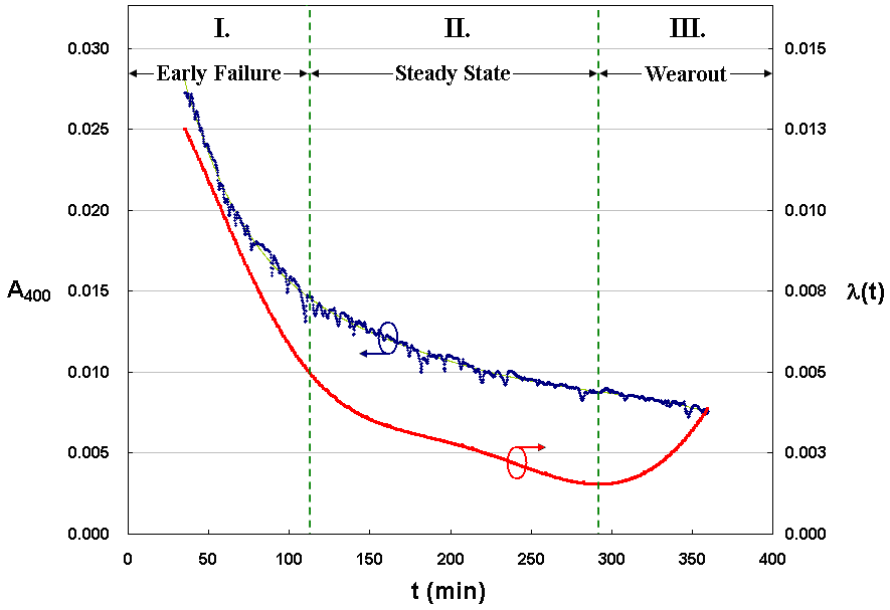

Figure 20 The absorbance A_{400} and inactivation rate λ(t) v.s. time for sulfuryl-group transfer reaction of rat-phenol-sulfotransferase. The volume of this channel reactor, scheme shown in Figure 25, is 1.29 mL; space time is 20min; reaction assay condition at the inlet of channel is 1 mM pNPS, 2 μM PAP, and 50 μM b-naphthol in pH 7.0 100 mM bis-trispropane buffer solution.

To study the stability of rat-phenol-sulfotransferase immobilized onto a plane of Si-based support, we used couple of sulfuryl-group transfer reactions as Figure 16 and a microfluidic system with one-side catalytic surface as Figure 25, which will be discussed in chapter 3; keep the flow rate at 64.5 μL/min. Figure 20 shows the continuous data of absorbance A_{400} and instantaneous inactivation rate λ(t). During the entire test period, three distinct regions were observed in the curve of inactivation rate; therefore, three micro-scaled inactivated mechanisms was involved and dominative in these three different phases. The phenomena may be closely related to that different covalent bonding sites exist in the population of immobilized rat-PST. In immobilization process, we used the five cystines (Cys66, Cys82, Cys232, Cys283, Cys289 shown in Figure 21) on the surface of rat-PST to proceed maleimide reaction with sulfo-SMCC, so there must be different orientations and conformations,

corresponding to these linkage sides. These must strongly affect the enzyme kinetics, therefore there are also different impacts on Michelis constant K_m and turnover number k_{cat} in the population of immobilized rat-PST.

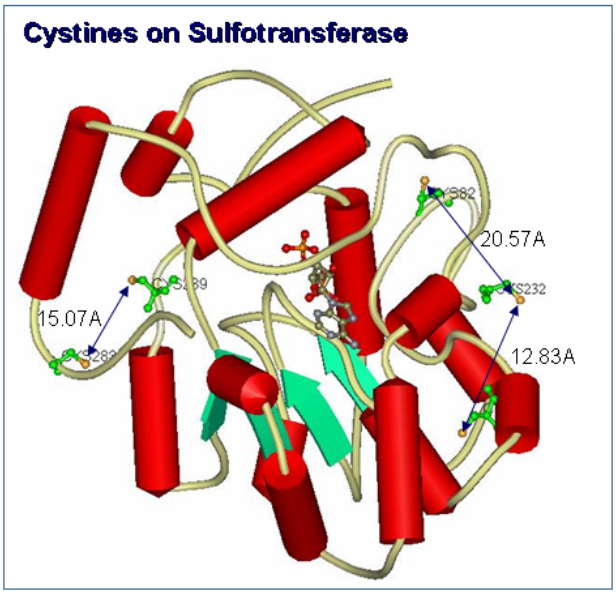

Figure 21 The structure of rat-phenol-sulfotransferase; five cystine locations and PAP binding site are clearly marked. The distances between cystines are also indicated.

In order to study the effect of pH value on the stability of immobilized D-hydantoinase on the silicon-based surface, we analyzed the data of cumulative function of inactivation I(t) v.s. log(t) by the Weibull plotting paper, shown as Figure 22. In this hydrolysis catalytic reaction (shown as eq (8)), the phthalimide is both a substrate and a reporter, absorbance at 298 nm. Our preliminary results (shown in Figure 22) indicated that the trend of the inactivation rate was located in early failure mode or steady state mode during whole measurement procedure, and the stability of immobilized D-hydantoinase at pH 8 is much higher than that at pH 7. Table 4 shows the evident difference the values of the cumulative function (instability) at t = 10^3 min are about 60% and 30% for the reaction conditions at pH 7 and pH 8, respectively.

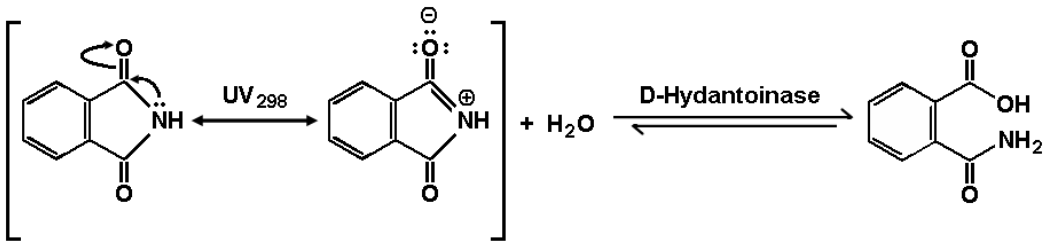

(8)

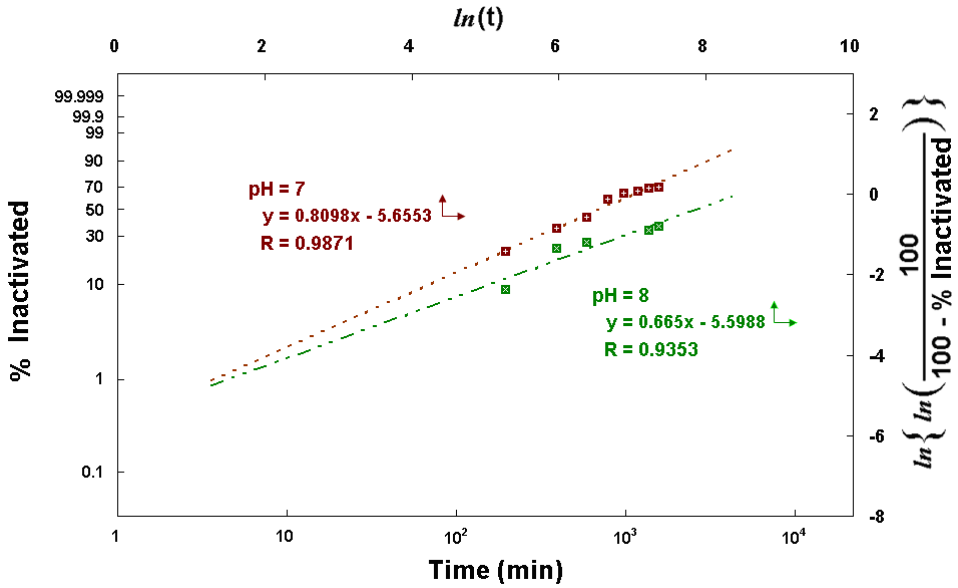

Figure 22 The Weibull plotting of inactivation distribution for hydrolysis reaction of D-hydantoinase at 25°C. The size of this channel reactor, scheme shown in Figure 25, is L = 72.6cm, W = 0.194cm, H = 0.0167cm; reaction assay condition at the inlet of channel is 1mM phthalimide, in 100mM bis-trispropane buffer solution. The dark-red curve and the green curve represent the experimental data at pH 7 and pH 8, respectively.

Table 4 Based on the fitting data of Weibull plotting in Figure 22, the inactivation rate and the cumulative function of inactivation for hydrolysis reaction of D-hydantoinase at pH 7 and pH 8 are calculated, respectively.

	$y = mx + c$		Inactivation Rate $\lambda(t) = (\beta/\alpha)\, t^{\beta-1}$			Cumulative function of Inactivation $I(t) = 1 - \exp(-\frac{1}{\alpha} t^{\beta})$			
pH	m	c	α	β		10 s	10^2 s	10^3 s	10^4 s
7.0	8.098×10^{-1}	-5.655	285.8	0.8098	$\lambda(t) = 2.833\times10^{-3}\, t^{-0.1902}$	2.23%	13.56%	60.95%	99.77%
8.0	6.550×10^{-1}	-5.599	270.1	0.6650	$\lambda(t) = 2.462\times10^{-3}\, t^{-0.3350}$	1.70%	7.61%	30.65%	81.59%

According to the slopes in Figure 22, we can calculate the scale parameter α and the shape parameter β of the inactivation rates in eq (5) for pH 7 and pH 8 conditions, the result shows as following table.

2.3.4 Morphology of Immobilized Enzymes on Silicon Dioxide Surface

Biomolecules such as proteins, on silicon-based surfaces are extreme importance in various applications including biosensor, bioregulator, and therapeutics. Though to measure the exact value of surface density for immobilized enzyme on silicon dioxide is very difficult, we still tried to use the atomic force microscopy (AFM) to predict the order of density in this experiment. In AFM, the tip is positioned on one end of a cantilever, which must be extremely sensitive to small force changes between the tip and the sample. The use of a piezocrystal to generate minute movements of either tip or surface allows for accurate measurement of the surface topography.

To understand the morphological changes in the silicon dioxide surface with respect to immobilization process, a step by step morphological analysis was conducted. Figure 23 is the morphological changes in silicon dioxide during immobilization process; Figure 23 (b) shows only little change in morphological images of surface functionalized with chemical links APTES and sulfo-SMCC. After enzymes (rat-phenol-sulfotransferase and D-hydantoinase) linking to the surface of silicon dioxide, the roughness was evidently increased with the drop about height 5nm, of which value is near to the diameter of unit enzyme. It means the immobilized enzyme is monolayer.

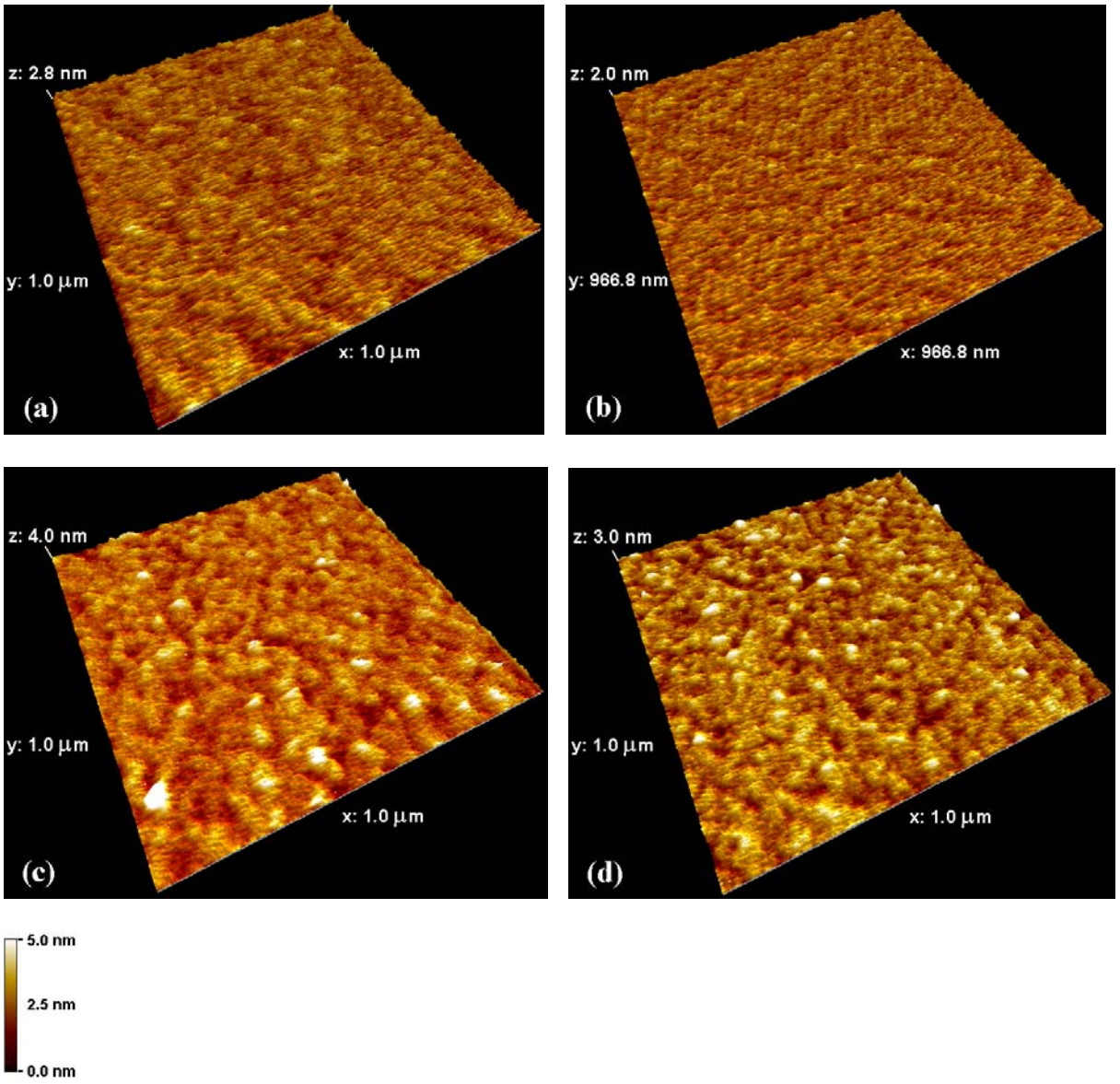

Figure 23 AFM contact-mode topographical images at different stages of immobilization process; (a) silicon dioxide surfaces, (b) after APTES and Sulfo-SMCC modification, (c) immobilized rat-phenol-sulfotransferase, and (d) immobilized D-hydantoinase.

Chapter 3 A Surface Limited Model for the Evaluation of Immobilized Enzyme on Planar Surface

3.1 Introduction

Many biomolecules, such as membrane proteins, perform their specific biorecognition or biocatalytic activities while they are immobilized on the surface of cells or organelles.[36, 37] Artificial technologies also take advantage of immobilized enzymes for a variety of applications such as bioconversion, bioremediation, and biosensors.[38-42] Methods developed for the analysis of the function of biomolecules that move and rotate freely in the homogeneous solution may not be adequate to describe the behavior of immobilized biomolecules. The immobilized enzyme is not distributed evenly and freely in the solution and may have a unique microenvironment for each enzyme molecule. For example, the specific orientation is important for the function of proteins.[43, 44] However, free protein in solution can have many orientations, while the rotation for an immobilized protein is restricted. Unique kinetic behaviors of membrane-bound enzymes have also been reported.[45, 46]

The leading-edge semiconductor devices[47, 48] have attracted researches into the emerging fields of biomolecular sensors,[3, 4, 49, 50] hybrid (biotic-abiotic) nanomaterials,[51] lab-on-a-chip platform for further biomedical applications,[52] enzyme-coupled biosensor,[53] and novel enzyme-based devices.[54-56] The immobilization of a variety of biomolecules including proteins and nucleic acids onto silicon-based material is essential for specific biorecognition and electronic signal manipulation required for the bio-silicon hybrid devices. How to characterize the reaction kinetics for immobilized enzyme on silicon-based supporting material has become the object of study.[57-61] Kinetic properties of immobilized alkaline

phosphatase have been determined in a microfluidic reaction with packed bed.[62] The kinetics of immobilized horseradish peroxidase has been studied using a microfluidic packing reaction[63] and modeling system.[64] Using batch-assay method, the kinetic parameters of immobilized glutathione S-transferase has been determined in porous silicon.[65] The kinetics and transport of this immobilized enzyme has also been simulated by an embedding method in sessile hydrogel drops.[66] Fractal and jamming effects were also used to model the kinetics of heterogeneous enzymatic catalysis.[67] The batch method used for the analysis of immobilized enzyme described above is similar to conventional method used for the analysis of free enzyme in solution. However, the apparent kinetic values determined may differ significantly from the intrinsic values for the factors that affect diffusion of product and substrate cannot be ignored in a non-homogeneous solution. Enzyme kinetics determined in a microfluidic system must consider mass transfer factors that may be significantly affected by the model system used.

To embed biomolecules onto the technology of standard IC (integrated circuit)[68] and MEMS (Micro Electro Mechanical Systems), the planar surface of Si or SiO_2 is frequently used as the substrate of immobilization. It is very important to be able to determine the kinetics of enzyme immobilized on these planar surfaces within the microfluidic system in order to evaluate the function of the whole system. So far, there is no such method reported. In this paper, we were developing a novel kinetic model, based on systematized and standardized approach, for measuring K^*_m and V^*_{max} of rat phenol sulfotransferase (PST) immobilized on planar silicon oxide surface within a microfluidic bioreactor. Sulfonation catalyzed by PST in biological system is a popular and important biotransformation that involves in detoxication of a broad range of endobiotics and xenobotics and activation and deactivation of hormones and carcinogens.[69-72] We first tried to derive a mathematic model that can be used to extract the K^*_m and V^*_{max} of an immobilized enzyme in a microfluidic system. To deal with the diffusion effect of enzyme substrate, the ratio of the reaction volume

to the catalytic planar surface must be reduced. We built a microfluidic bioreactor with a much smaller channel height than the diffusion layer in semi-infinite diffusion process according the derived mathematic model. Finally, experiments were performed in order to extract the intrinsic kinetic characteristics of the immobilized enzymes.

3.2 Theoretical Considerations

3.2.1 Channel Reactor with a One-sided Planar Catalytic Surface

A model that combined a plug-flow reactor[122] in surface reaction limited conditions[123] was developed to analyze the kinetics of PST catalyzed reaction (Figure 1). A rectangular channel reactor with proper dimension was designed as shown in Figure 2. This reactor possesses a one-sided catalytic surface with scale size $L >> W >> H$ (Figure 25(a)). We assume that the reaction mixtures flow through the channel at equal velocities, and the diffusion effect, as compared to convection in x-direction, can be neglected (Figure 25(b)). At steady state, the substrate concentration, determined by diffusion in z-direction, convection in x-direction, and consumption at catalytic surface ($z = H$) is given by eq (9) and the related boundary conditions (BCs) are given by eq (10).

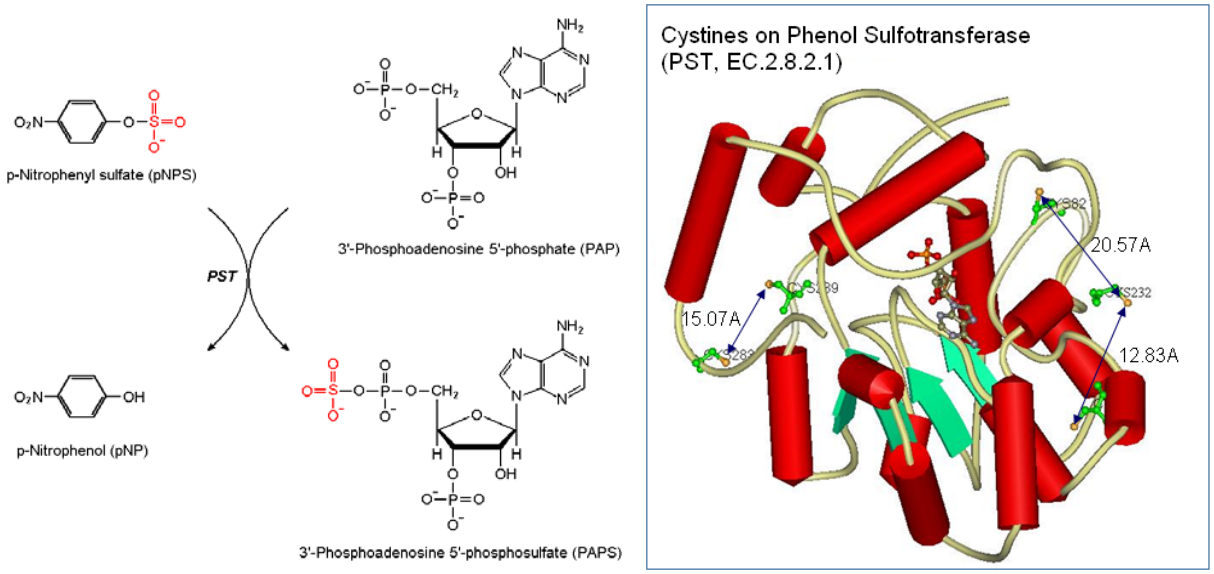

(a) **(b)**

Figure 24. PST catalyzed sulfuryl group transfer reaction. (a) PAP and pNPS were used as substrates for rat PST. The product, pNP, that gives strong 400 nm absorption in neutral or alkaline solution served as the reporter molecule for the progress of the enzyme catalyzed reaction. (b) The structure of rat PST (PDB:1LS6). Five cystines and PAP are shown with their molecular structrues. The distances between near-by cystines are also indicated.

$$v_x \frac{\partial [S]}{\partial x} = D \frac{\partial^2 [S]}{\partial z^2} \tag{9}$$

$$BCs \begin{cases} [S](0,z) = [S]_o \\ \dfrac{\partial [S]}{\partial z}(x,0) = 0 \\ -D \dfrac{\partial [S]}{\partial z}(x,H) = k_s [S](x,H) \end{cases} \tag{10}$$

v_x is the velocity of flow between two parallel plates. D is diffusion coefficient of substrate and k_s (dm min^{-1}) is rate constant of surface reaction. Substrate concentration profile of the rectangular reactor, $[S](x,z)$, can be obtained by solving eq (9) coupled with eq (10) and is given as eq (11),

$$[S](x,z) = 4[S]_o \sum_{n=1}^{\infty} [\frac{\sin \beta_n}{\sin(2\beta_n) + 2\beta_n} \cos(\frac{\beta_n}{H} z)] \exp(-\frac{D\beta_n^2}{v_x H^2} x) \tag{11}$$

where eigenvalues, β_n, that fit in eq (11) are given as follows:

$$\tan(\beta_n) = \frac{k_s}{(D/H)\beta_n} \quad \text{or} \quad Da = \beta_n \tan(\beta_n) \tag{12}$$

Dimensionless Damkohler number (Da) in eq (12), is defined as ratio of the rate constants of chemical reaction to mass transfer factor, $Da \equiv k_s / (D/H)$, for this system. $Da >> 1$ indicates that the system is mass transfer limited, while the system becomes surface reaction limited when $Da << 1$. In Figure 26(a), computer-generated graphs of eq (11) are shown to illustrate substrate concentration profiles at different Da. Average substrate concentration over the cross section on the outlet, $\overline{[S]}_\tau \ (at\ x = L)$, is equal to the outlet substrate concentration $[S]_{UV}$ detected by UV-Vis spectrophotometer; therefore

$$\overline{[S]}_\tau = \frac{4[S]_o}{H} \sum_{n=1}^{\infty} [\frac{\sin \beta_n}{\sin(2\beta_n) + 2\beta_n}] \exp(-\frac{D\beta_n^2 \tau}{H^2}) \int_0^H \cos(\frac{\beta_n z}{H}) dz = [S]_{UV} \tag{13}$$

where space time τ is the time required to process the volume of reaction mixture in reactor. Let α_τ be the average reaction conversion fraction at the outlet, $\alpha_\tau \equiv \frac{[S]_o - \overline{[S]_\tau}}{[S]_o} = \frac{[S]_o - [S]_{UV}}{[S]_o}$, and eq (13) becomes eq (14).

$$\alpha_\tau = 1 - \frac{[S]_{UV}}{[S]_o} = 1 - 4\sum_{n=1}^{\infty} \frac{\sin^2 \beta_n}{\beta_n [\sin(2\beta_n) + 2\beta_n]} \exp(-\frac{D\beta_n^2 \tau}{H^2}) \qquad (14)$$

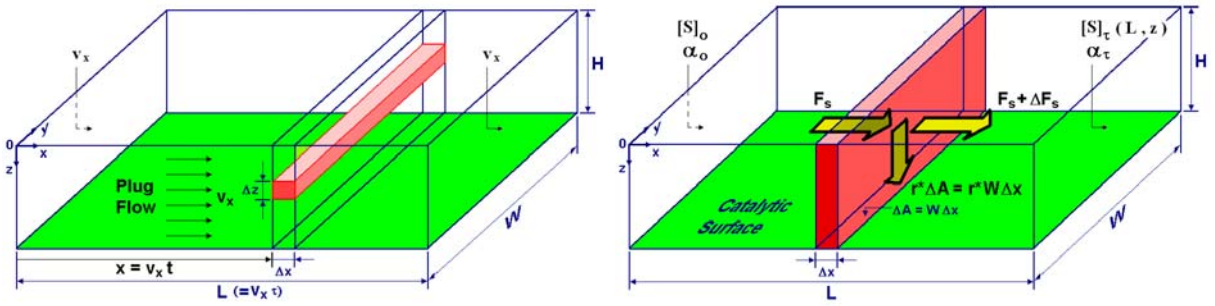

(a) **(b)**

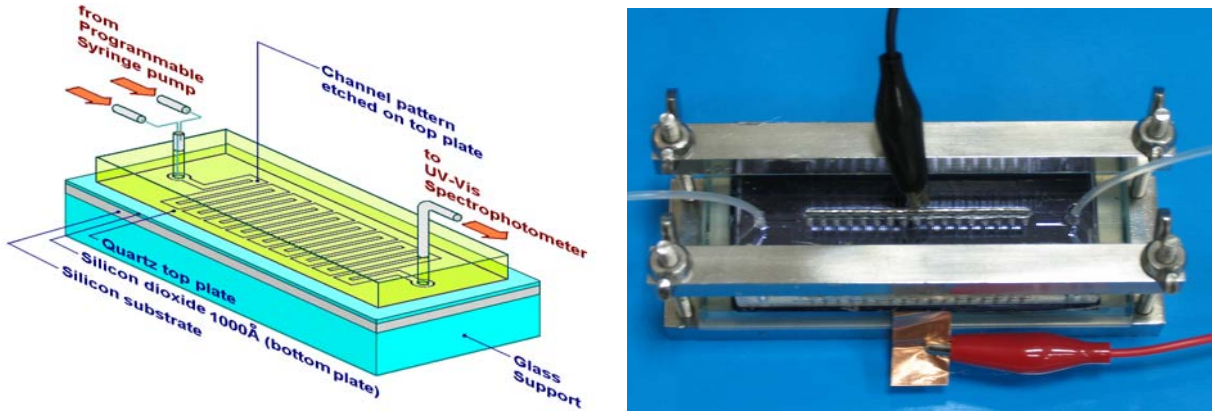

(c) **(d)**

Figure 25. Bioreactor design for the determination of kinetic constants of immobilized enzyme. (a) Rectangular reactor with a catalytic surface on the bottom plate. The channel size is $L \times W \times H$ (where $L >> W >> H$). v_x is the velocity of flow between two parallel plates. τ means space time ($\tau = L/v_x$ in this case). (b) The reaction flow in a rectangular bioreactor. The yellow arrows illustrate the material balance of substrate S in the control volume $\Delta x \times W \times H$ at x position, where F_s is molar flow rate of substrate S, (μmol min^{-1}) and r^* is surface

reaction rate on the catalytic surface, (μmol dm^{-2} min^{-1}). $[S]_o$ and $[S]_\tau(L,z)$ are the inlet and the outlet substrate concentrations, respectively, and their corresponding reaction fractions are α_o (= 0, for common case) and α_τ (for average $\overline{[S]}_\tau$ at $x = L$), respectively. (c) Schematic diagram of the microfluidic reactor. The reactor composes a sandwich structure, the quartz top plate, the Si bottom plate, and the glass supporting plate. The enzyme was immobilized on the SiO_2 surface of the Si bottom plate and the fluidic channel pattern was etched on the top quartz plate. (d) Photography of the bioreactor. The reaction solution was pumped into the channel by a programmable syringe pump and eluted to a spectrophotometer for the determination of the concentration of reporter molecules.

By coupling eqs (12) and (14), the magnitude of *Da* can be evaluated by numerical analysis method (detailed analysis and prediction of *Da* is given in Appendix IV) when the substrate conversion α_τ is known. The height, *H*, of the channel, the space time, τ, and the substrate concentration at inlet of the channel, $[S]_o$, can be set as experimental parameters in eqs (12) and (14). The substrate concentration at outlet of the channel, $[S]_{UV}$, is a measurable value. In addition, liquid mass diffusivity of substrate, *D*, can be predicted by experimental methods and theoretical formula.[123, 124] The diffusion coefficient, *D*, of most small molecules in a dilute solution has 10^{-6} cm^2/s order.[125]

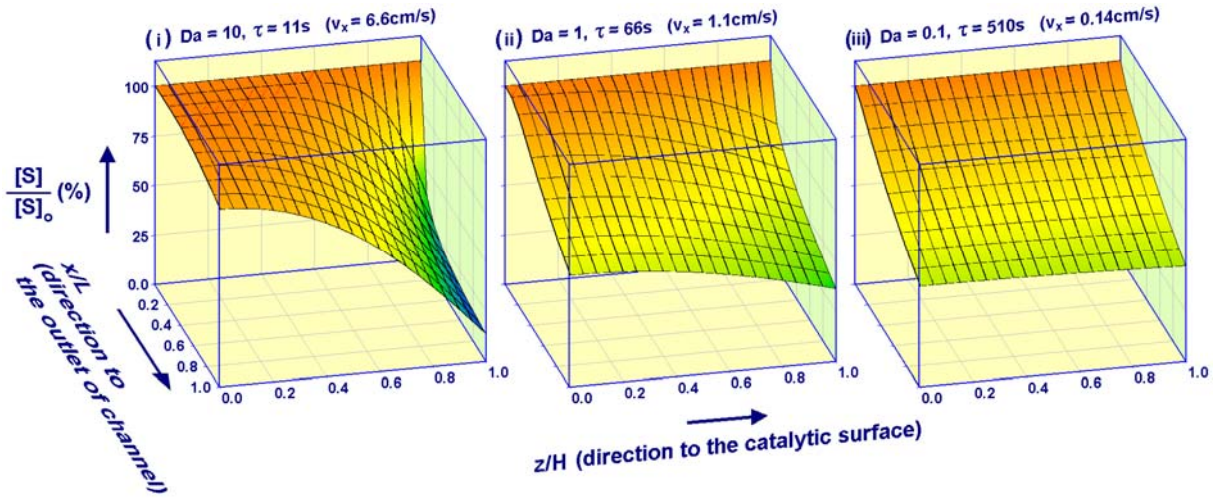

(a)

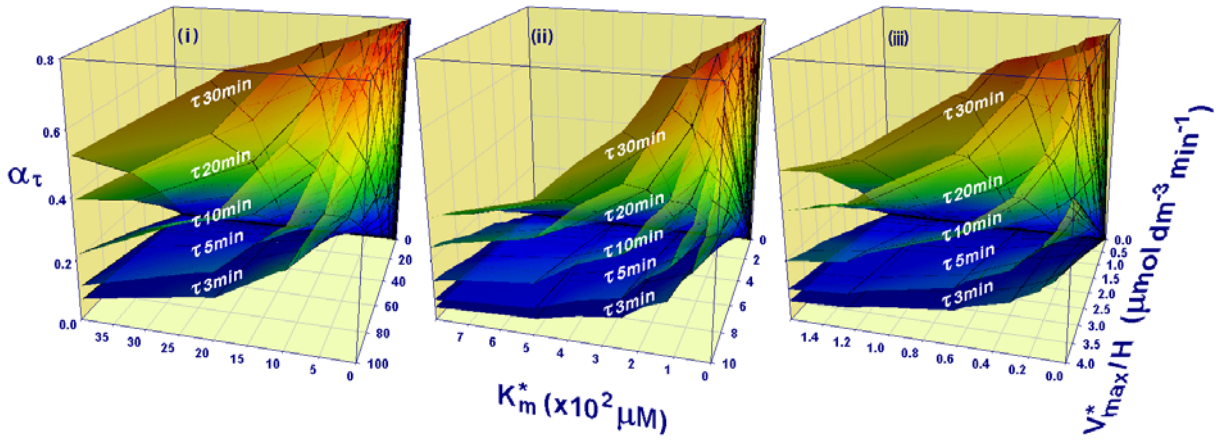

(b)

Figure 26. Simulation of reaction conditions and the derivation of kinetic constants. (a) Effect of Damkohler number on substrate concentration. Substrate concentrations at varied *Da*s in a rectangular reactor with a catalytic surface on the bottom plate are simulated. The substrate concentration profiles are obtained in a steady state condition using diffusion coefficient $D = 3.92 \times 10^{-6}\ cm^2 / s$ in a rectangular reactor with a catalytic surface at $z = H$ (167 μm). The axes depict the substrate concentration $[S](x,z)$ relative to the inlet substrate concentration $[S]_o$, the distance z from the non-catalytic plate (at $z = 0$) to the catalytic plate (at $z = H$), and the distance x from the inlet ($x = 0$) to the outlet ($x = L$) of the channel as shown in Figure 2. These profiles are created at the conditions of conversion fraction, $\alpha_\tau = 0.5$, that is, $\overline{[S]}_\tau / [S]_o = [S]_{UV} / [S]_o = 0.5$. (i), (ii), and (iii) are produced using $Da = 10$, $Da = 1$, and $Da = 0.1$, respectively. (b) Three-dimensional graph of K^*_m and V^*_{max}/H surface. Eq (8) at $[S]_o$ = 40 μM is used for the plot. Each surface represents a certain space time, τ. Different scales of K^*_m and V^*_{max}/H are shown in (i), (ii), and (iii).

3.2.2 Surface Reaction Limited Model

As shown in Figure 26(a)(iii), the substrate concentration is nearly uniform in z-direction under $Da = 0.1$ condition based on the channel reactor with a one-sided planar catalytic

surface as described above. In this condition, [*S*] becomes the function of *x* only and can be used to derive equation to extract the kinetic constant of immobilized enzyme.

In a steady state condition (at a constant flow rate), the enzyme reaction rate on the catalytic surface is

$$r^*(x) = \frac{V^*_{\max}[S](x,H)}{K^*_m + [S](x,H)} \approx \frac{V^*_{\max}[S](x)}{K^*_m + [S](x)} \tag{15}$$

where V^*_{max} is maximum reaction rate per unit surface area of catalyst (μmol dm^{-2} min^{-1}), K^*_m is the Michaelis-Menten constant (μmol dm^{-3}) for immobilized enzymes on the planar surface. Substituting eq (15) into the mass balance of substrate S gives eq (16),

$$\tau = \frac{-K^*_m}{V^*_{\max}/H} Ln(1-\alpha_\tau) + \frac{[S]_o}{V^*_{\max}/H}\alpha_\tau \tag{16}$$

A computer-generated plotting based on eq (16) at a certain $[S]_o$ is shown in Figure 26(b). The optimum value of $-K_m^*/(V_{max}^*/H)$ and $[S]_o/(V_{max}^*/H)$ can be found based on certain parameters, including $[S]_o$, H, and the set of experimental data between space time, τ, and conversion fraction, α_τ. Therefore, K^*_m and V^*_{max} can be evaluated by regression analysis using eq (16).

If reaction conversion fraction, α_τ, is smaller than 1%, and $[S]_o$ is much greater than K^*_m, then eq (16) can be degenerated as follows:

$$\alpha_\tau \approx \left(\frac{V^*_{\max}}{H}\right)\left(\frac{\tau}{[S]_o}\right) \qquad (for\ [S]_o >> K^*_m) \tag{17}$$

This means that the whole immobilized enzymes (from the entrance to the outlet of reactor shown in Figs. 24(a) and 24(b) as green surface) are under saturating substrate conditions. Under this degenerated condition, eq (17) provides us the opportunity to determine the simultaneous value of V_{max}^*/H. Simultaneous determination of enzyme activity is important because the inactivation of immobilized enzyme is generally expected (Figure 27).

3.3 Experimental Section

3.3.1 Surface Modification on Silicon Wafer

P-type Si(100) wafers (14-21 Ω-cm, MEMC, MO, USA) with 15 cm diameter, on which 100 nm oxide layers were grown using wet oxidation with a gas mixture of hydrogen (8000 cm^3/min) and oxygen (5000 cm^3/min) at 978°C, were cut into 4×8 cm^2 pieces of samples to serve as a supporting material for enzyme immobilization. Prior to immobilization, the piece of oxidized silicon wafer was carefully cleaned in the piranha solution, H_2SO_4 and H_2O_2 (volume ratio is 3 : 1), twice, each time at above 85 °C for 30 min. It should be noted that the cleaning solution is very corrosive and dangerous. After rinsing with pure water and drying, the sample was immersed in the (3-aminopropyl)triethoxysilane (APTES, Sigma-Aldrich, MO, USA) solution to proceed the silanization reaction for 30 min at room temperature to create an amine-functional surface (Figure 15). The APTES solution was prepared by the following procedures: (1) mixing pure water with acetone (volume ratio is 5:1), (2) adjusting the pH value of the above solvent to 3.5 by 1 M HCl, and (3) preparing the 5% APTES solution by diluting with above solvent. Following the APTES treatment, the silicon wafer was rinsed with pure water thoroughly. Then, the treated silicon wafer was baked at 120 °C for 30 min to complete the Si-O bond formation.[126] To create a maleimide group for the immobilization of enzyme through its sulfhydryl group, sulfosuccinimidyl 4-(N-maleimidomethyl)-cyclohexane-1-carboxylate (sulfo-SMCC, Sigma-Aldrich) was used to link to the amino group of APTES on the surface of silicon wafer (Figure15). The 0.5 mM sulfo-SMCC linker solution was prepared by dissolving sulfo-SMCC into 50 mM sodium borate buffer (Sigma-Aldrich), and then the linker solution was dipped onto the silanized surface of the sample for 1 hour at room temperature. Finally, the surface was extensively rinsed with water and dried with nitrogen gas.

3.3.2 Reactor System and Enzyme Immobilization

The microfluidic channel of reactor shown in Figs. 24(c) and (d) composed two plates. The bottom plate was the silicon wafer on glass support. The silicon surface was modified with APTES and maleimide as described above. The top plate, made of quartz, contained a tortuous fluidic guide on its surface formed by etching. The fluidic channel was 72.6 cm long, 0.194 cm width, and 167 μm depth. To avoid leakage during pumping operation, the edges between the two plates were sealed with glue and the two plates was tightly clamped together using a screwed clamp holder. The enzyme solution (200 μg/mL rat PST, EC.2.8.2.1, in 0.1 M sodium phosphate buffer at pH 7.0) prepared according to published procedure[127, 128] was pumped into the microfluidic system by a programmable syringe pump (KD Scientific, KDS260P) at space time τ = 0.5 min (equivalent to 28.2mL/hr or v_x=2.4 cm/sec) and stopped to incubate for 15 min at room temperature. Next, 50 mM 2-mercaptoethanol solution (in 50 mM sodium phosphate buffer at pH 7.0) was pumped into the microfluidic system and stopped to incubate for 8 min at room temperature. Finally, 50 mM sodium phosphate buffer was pumped into the microfluidic system to wash away the residual 2-mercaptoethanol solution. Reactions involved in the surface modification and the immobilization of rat PST are shown in Figure 15.

3.3.3 Enzyme Assay

Two different concentrations of 3'-phosphoadenosine 5'-phosphate (PAP), 400 μM and 2 μM, were used to create saturating and non-saturating substrate condition, respectively, for the immobilized PST-catalyzed reaction. The PAP concentrations used were determined according to the K_m of free rat PST[127, 128] and eq (16) in a surface reaction limited model. The

reaction mixtures for immobilized rat PST contained PAP (400 μM or 2 μM) and 20 mM p-nitrophenyl sulfate (pNPS) in 100 mM 1,3-bis[tris(hydroxymethyl)methylamino]propane buffer at pH 7. Injection of the reaction mixtures into the reactor was controlled by automatic pumping system and operated at desired flow rate to have space time, τ, at 1 min, 2 min, 4 min or 8 min. The output solution was directed into a quartz flow cell mounted in the UV-Vis spectrophotometer (Hitachi UV-Vis-3300, Tokyo, Japan) for pNP detection at 400 nm (Figure 24).

3.4 Results and Discussion

3.4.1 Development of Surface Reaction Limited Model for the Derivation of K^*_m and V^*_{max}

Computer-generated figures (Figure 26) and equations derived (eqs (16) and (17)) based on a rectangular bioreactor (Figure 25) demonstrated that a surface reaction limited model can be used to obtain kinetic constants of immobilized enzyme in an appropriate reaction condition. Figure 26(a) illustrates three types of reaction kinetics based on the same average conversion fraction α_τ = 50% across the outlet area (Figure 25). Dimensionless *Da*, defined as ratio of the rate constants of chemical reaction to mass transfer factor, is used to distinguish the three types of reaction kinetics. The mass transfer limited condition ($Da >> 1$) indicates that the perpendicular diffusion rate is much slower than the rate of reaction on the catalytic surface (as shown in Figure 26(a)(i), $Da = 10$). The transition condition ($Da \approx 1$) indicates that the diffusion rate is comparable to the surface reaction rate (as shown in Figure 26(a)(ii), $Da = 1$). The surface reaction limited condition ($Da << 1$) shown in Figure 26(a)(iii) indicates that the perpendicular diffusion rate is much higher than the surface reaction rate. At $Da = 0.1$ (Figure 26(a)(iii)), the concentrations of substrate and products can be evenly distributed on the *z* (or *H*) direction (Figure 25).

Figure 26(b) illustrates computer-generated curved surfaces under the $Da << 1$ condition at certain space times according to eq (16). One set of K^*_m and V^*_{max}/H can be obtained on the curved surface at specific substrate concentration and space time. This indicates that, following the regression analysis, the K^*_m and V^*_{max} of immobilized enzyme can be obtained using different flow rates (or space time) to determine the rate of substrate conversion to product in the bioreactor. The curve surfaces shown in Figure 26(b) were simulated at $[S]_o$ = 40 μM with space time τ = 3, 5, 10, 20 and 30 min. Figs. 25(b)(i), 25(b)(ii) and 25(b)(iii) are shown with different scales of K^*_m and V^*_{max}/H to reveal the variation of the curve surfaces. In order to obtain a better K^*_m and V^*_{max}/H following regression analysis, it is desirable that

α_τ (converted from space time, τ) is chosen where curve surfaces vary more drastically with respect to K^*_m and V^*_{max}/H axes shown in Figure 26(b). For example, as shown in Figure 26(b)(iii), it would be suitable to determine the kinetic constants of an immobilized enzyme with K^*_m < 40 μM and V^*_{max}/H < 3 μM min^{-1} using the reaction condition of $[S]_o$ = 40 μM, τ = 3, 5, 10, 20 and 30 min. However, this reaction condition is inappropriate for an immobilized enzyme with K^*_m > 600 μM and V^*_{max}/H = 2~10 μM min^{-1} (Figure 26(b)(ii)). Because at this region, the variation on the curve surface is small and thus even small errors produced by the α_τ data determination may significantly affect the values of K^*_m and V^*_{max}/H following regression analysis. In other words, after K^*_m and V^*_{max}/H were obtained experimentally, Figure 26(b) can provide us to check for the accuracy of these values and, if necessary, further guide us to select appropriate experiment parameters, set of space times, for more accurate measurement of K^*_m value.

3.4.2 Stability and V^*_{max}/H of Immobilized Enzyme on Planar Si Surface

The stability of enzyme is a concern for all bio-related applications when it is used as a catalyst. It is important that the stability and activity of the immobilized enzyme can be monitored or predicted during the whole reaction process. It is reasonable to assume that the loss of total enzyme activity is due to the inactivation of part of the protein molecules. That is, each enzyme molecule is either fully active or completely dead and its K_m and k_{cat} remain the same for each active enzyme molecule. The determination of V^*_{max}/H can be achieved easily using eq (17) degenerated from eq (16) under saturating substrate condition. As shown in Figure 27(a), V^*_{max}/Hs were obtained experimentally at several progress times after immobilization in a surface reaction limited condition at high substrate concentration. The

decrease in total activity indicated inactivation of enzyme following immobilization. Three sets of immobilized PST whose activities were determined at different stage following immobilization all followed the same deactivation pattern shown in Figure 27(a). The deactivation curve indicates that the activity of PST can be predicted, and the resulting V^*_{max}/H obtained can be normalized at any given time following its immobilization on the reactor surface. The decay curves (Figure 27) were used to normalized V^*_{max}/H at various progress times and to derive K^*_m at low substrate concentration (Figure 28).

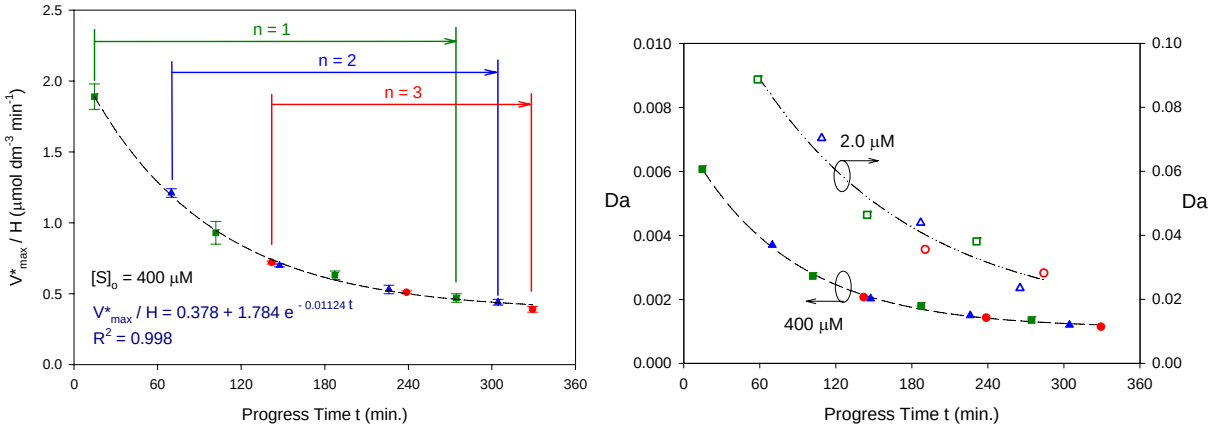

(a) **(b)**

Figure 27. Stability of PST and its effect on Damkohler number. (a) Deactivation curve of rat PST under saturating substrate condition. High substrate concentration (400 µM PAP) was used to give the characteristic curve of rat PST determined according to eq (9). Three data sets, dark-green rectangles, blue triangles, and red circles, were collected at different times (simultaneously, one hour, and two hours) after immobilization of PST. (b) Effect of substrate concentration and enzymatic activity on *Da*. Typical *Da* was obtained at space time $\tau = 4$ min. The curves decayed gradually due to the deactivation of enzyme. Dark green squares, blue triangles, and red circles were recorded independently at different times after immobilization of PST. The upper (open symbols) and lower lines (solid symbols) represent low (2.0 µM) and high (400 µM) substrate concentration conditions, respectively.

To assure that the required condition, $Da << 1$, can be satisfied in this study for the surface reaction limited model, the Da in low and high substrate concentration, respectively, were shown in Figure 27(b). Both the substrate concentration and the decay of enzyme activity following immobilization at various progress times significantly affected the Da. This observation is expected for the catalytic reaction on the planar surface is to be affected by the amount of active enzyme and substrate concentration. This indicates that the relative substrate consumption on the reaction surface was more significant than those perpendicularly from the reaction surface. At $[S]_o$ = 2 μM, the Da was about an order higher than that of $[S]_o$ = 40 μM. However, all the Da shown in Figure 27(b) are lower than 0.1. Under such condition, the concentration profile in z (or H) direction can be considered constant and satisfies the requirement for surface reaction limited model shown in Figure 26(a)(iii).

3.4.3 Determination of K^*_m(PAP) through Regression Analysis

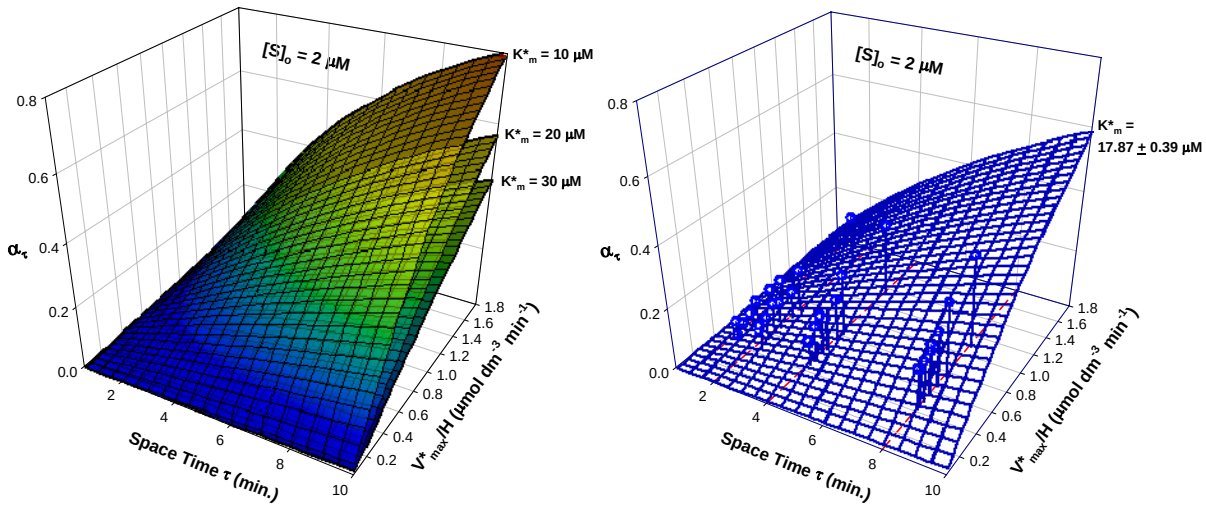

(a) **(b)**

Figure 28. The curved surfaces of K^*_m in the space of $\tau - V^*_{max}/H - \alpha_\tau$. (a) Computer-generated plots of eq (8) at moderate low concentration of substrate. Each K^*_m curved surface clearly separates one another at comparable low substrate concentration. (b) K^*_m curved

surface produced by experimental data. The curved surface of K^*_m = 17.87±0.39 μM was generated through regression analysis of experimental data at $[S]_o$ = 2 μM.

As shown in Figure 28(a), a specific curved surface of a certain K^*_m can be obtained according to eq (16) by giving any set of values τ, V^*_{max}/H, and α_τ. The computer-generated Figure 28(a) also shows that K^*_m can be determined through a series of τ and V^*_{max}/H values when $[S]_o$ and K^*_m values are in the same order of magnitude. Experimental data, using $[S]_o$ = 2 μM, were obtained and fit into Eq (16) as shown in Figure 28(b). Regression analysis of the experimental data matched very well with curved surface of K^*_m(PAP) = 17.87 ± 0.39 μM. The original V^*_{max}/H (PST activity just after immobilization) was determined as 2.16 μM/min (or $V^*_{max} = 3.62\times10^3$ s^{-1} μm^2) according to Figure 27(a). The K_m(PAP) and V_{max} of free PST in a homogenous system were 4.10 ± 0.26 μM and 295 ± 3 nmol/min/mg, respectively. The K^*_m(PAP) of immobilized PST was significantly higher than that of the free enzyme. It is reasonable for immobilized enzyme to exhibit a higher K^*_m because, as compared to free enzyme in solution, it decreases its degree of freedom and may be difficult to maintain its flexible and proper conformation in a more stressful environment. Thus, the affinity of the substrate with enzyme may be weakening and higher substrate concentration may be needed to give the maximum enzyme activity as compared to that of free enzyme in solution. The V^*_{max} of immobilized PST was about ten folds less than that of free PST. Since PST is a cytosolic enzyme, it would not be surprising that its activity was found to be considerably lower following immobilization. Other factors may also affect PST activity such as the orientation of PST immobilization, the formation of monomer following immobilization and the change of PST environment due to PST immobilization on silicon oxide surface. All these possible factors may be studied one by one in the near future. Multipoint immobilization is possible since there are five cysteins in a rat PST (Figure 24(b)). This may lead to the

distortion of tertiary structure of immobilized PST and therefore to a decrease in its activity. Different orientations, conformations, and degree of freedom can be expected following PST immobilization. Therefore the kinetic parameters of immobilized PST determined in this research should be considered the average behavior of the enzyme in various conditions. This research focused on the establishment of measurement platform and model. In the near future, we plan to use site-directed mutagenesis to produce PST with single free cystein to clarify immobilizing issue and to study redox-regulating mechanism of immobilized rat PST.

3.5 Conclusions

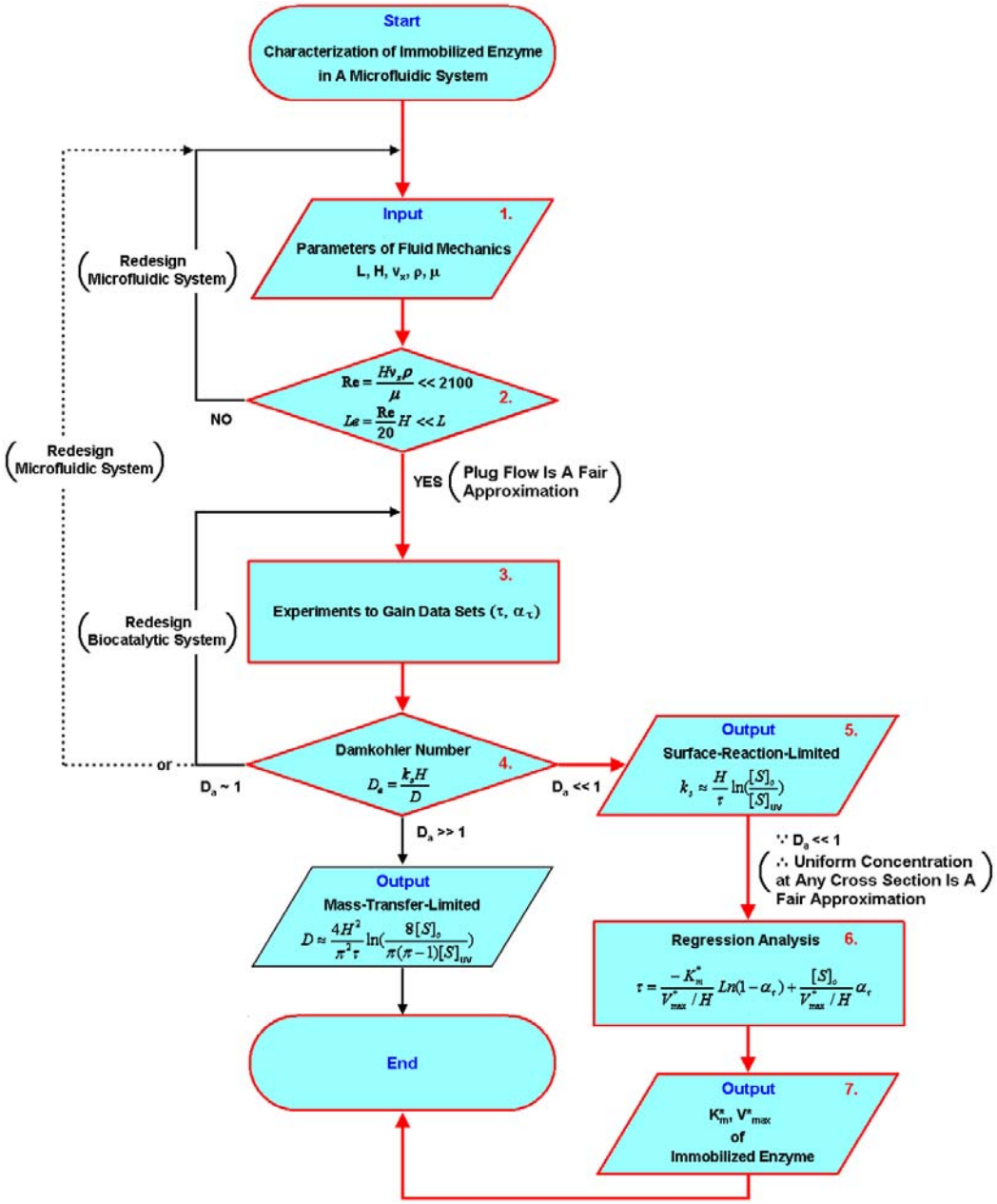

Scheme 1. A step-by-step consideration for the determination of K^*_m and V^*_{max} of an immobilized enzyme on planar surface using surface reaction limited model.

We have developed a novel scheme for the determination of kinetic parameters of an immobilized enzyme on planar surface through a systematized and standardized consideration shown in Scheme 1. This scheme can be followed step-by-step to evaluate kinetic properties of immobilized enzyme *in situ* based on surface reaction limited experimental condition. It is

important because a standard scheme is necessary to compare the performance of immobilized enzyme operated by different research groups. In the real life application, the catalytic activity can be significantly increased by immobilizing enzyme on all walls surrounding the microfluidic channel.

Chapter 4 A New Approach to Measuring Immobilized Enzyme Kinetics Using Continuous-flow Assays

4.1 Introduction

Biomolecules immobilized on membranes of cells or organelles is widespread in nature, and in many cases, their activities are highly regulated in response to changes of biochemical environment. [36, 37] While today man-made systems, such as bioconversion, bioremediation and biosensors, [38-42, 129] also take advantage of immobilized enzymes based on their properties of specific biorecognition or biocatalytic activities. Many studies of new and emerging fields, which integrate biotechnology and mature electronic or novel electronic technology, like biomolecular sensors, [3, 4, 49, 50, 73, 130] hybrid (biotic-abiotic) nanomaterials, [51] lab-on-a-chip platform for further biomedical applications, [52] enzyme-coupled biosensor, [53, 131-133] and novel DNA-based or enzyme-based devices, [54-56, 134, 135] have generated considerable attention.

To embed a variety of biomolecules including proteins and nucleic acids onto the technology of standard IC (integrated circuit)[68] and MEMS (Micro Electro Mechanical Systems) for specific biorecognition and electronic signal manipulation required for the bio-silicon hybrid devices, the planar surface of Si or SiO_2 is frequently used as the substrate of immobilization. For evaluating the performance in this kind of bio-embedded application, the kinetics of enzymes (or substrates) immobilized on these planar surfaces within a microfluidic system should be known and has become the object of study. [57, 58, 61, 74, 75]

The immobilized enzyme is not distributed evenly and freely in the solution, so there are many extra constraints to the enzyme molecule: conformation, specific orientation, substrate diffusion, ion charge profile near the surface of supporting material, to which enzymes are bound. [43-46]

The experimental methodology of measuring enzyme activity with homogeneous assay based on Michaelis–Menten equation has been developed completely during the past century and become standard material in whole modern textbooks of enzyme assays.[76, 77] Similarly, we tried to establish a standard scheme for measurement and data analysis of immobilized enzyme assays based on the surface reaction limited model, constructed in Chapter 3.[5] However, the apparent kinetic values determined may differ significantly due to not only different models adopted but different methods of data treatment, so the standardization of corresponding measurement and calculation is especially necessary to focus on besides establishment of model system for immobilized enzyme assay.

So far, there is no such platform combined a complete solution, through a systematized and standardized consideration, to set up a standard scheme, which can be used to compare the performance of immobilized enzyme operated by different research groups. Using the covalent linkages with sulfhydryl enzymes[78] and the high affinity of Gold nanoparticles (AuNPs) for biomolecules,[79] in this paper, rat phenol sulfotransferase (PST) and *Candida rugosa* lipase (CRL) were immobilized on planar silicon oxide surface within a microfluidic bioreactor, respectively, and, we were providing a novel method for kinetic measurement and corresponding data analysis, based on our previous kinetic model,[5] for measuring K^*_ms and V^*_{max}s. Sulfonation catalyzed by PST in biological system is a popular and important biotransformation that involves in detoxication of a broad range of endobiotics and xenobotics and activation and deactivation of hormones and carcinogens.[69-72] Lipase are used industrially as detergent enzymes, in paper and food technology, in the preparation of specialty fats, and as biocatalysts for the synthesis of organic intermediates, and in various clinical studies and drug delivery.[80] Facing these two enzymes with different immobilization schemes and limitations of enzyme assays, we developed a standard measuring and calculating procedure to extract the near intrinsic kinetic characteristics of the immobilized enzymes.

4.2 Methods

According to the model in Chapter 3,[5] we have constructed a microfluidic system, which combined plug flow[122, 136] approximation, Michaelis-Menten equation, and surface reaction limited condition,[123] to model the kinetics of immobilized enzyme on one-side planar surface as eq (18.1).

$$\tau = \frac{-K_m^*}{V_{\max}^*/H} Ln(1-\alpha_\tau) + \frac{[S]_o}{V_{\max}^*/H}\alpha_\tau \qquad (18.1)$$

where space time τ is the time required to process the volume of reaction mixture in reactor, K^*_m is the Michaelis constant (μmol dm^{-3}) for immobilized enzymes on the planar surface, V^*_{max} is maximum reaction rate per unit surface area of catalyst (μmol dm^{-2} min^{-1}), H is the height of rectangular channel reactor, α_τ is reaction conversion fraction, and $[S]_o$ is the substrate concentration at inlet of the channel. Surface reaction limited condition means that diffusion is fast compared to surface reaction. To meet this requirement, the ratio of the reaction volume to the catalytic planar surface must be reduced. We built a microfluidic bioreactor with a much smaller channel height than the diffusion layer in semi-infinite diffusion process, and the corresponding dynamic model was discussed in detail in Chapter 3.[5] By using a series of variant flow rates (or space time τs), this equation could allow us to precisely predict the kinetics of immobilized enzyme at different inlet concentration of substrate; details are as followings:

If reaction conversion fraction, α_τ, is smaller than 1%, and $[S]_o$ is much higher than K^*_m, then eq (18.1) can be degenerated as follows:

$$\alpha_\tau \approx < \frac{V_{\max}^*}{H} >_0 \left(\frac{\tau}{[S]_{o,H}}\right) \qquad (for\ [S]_{o,H} >> K_m^*) \qquad (19)$$

where the subscript H of $[S]_{o,H}$ refers to this saturating assay condition, the subscript 0 of $< \frac{V_{\max}^*}{H} >_0$ refers to initial approximation without regard to K^*_m factor. This condition means

that the highest available concentration of substrate is much larger than K_m. If we could choose $[S]_{o,H} \geq 19K_m$, then the error involved in the approximation of $< \frac{V^*_{\max}}{H} >_0$ based on eq (19) would be less than 5%. Eq (19) provides us to determine $< \frac{V^*_{\max}}{H} >_0$ using linear regression, and the discrete determined values of $< \frac{V^*_{\max}}{H} >_0$ could be used to fit a decay curve concerning the issue of deactivation of immobilized enzyme; therefore the any simultaneous value of $< \frac{V^*_{\max}}{H} >_0$ can be determined in experiment progress. Eq (18.1) obviously indicates that we should choose as low as possible the $[S]_o$ concentration, as long as the output concentration of reporter is not beyond the limit of detection, to increase the accuracy of K^*_m evaluation after $\frac{V^*_{\max}}{H}$ determined as above. Eq (18.1) can be arranged into the following eq:

$$< \frac{V^*_{\max}}{H} >_0 \tau - [S]_{o,L} \alpha_\tau = - < K^*_m >_0 Ln(1-\alpha_\tau) \qquad (18.2)$$

where the subscript L of $[S]_{o,L}$ refers to at low concentration of substrate, the subscript 0 of $< K^*_m >_0$ refers to an initial approximation. With linear regression of eq (18.2), and using a set of space time τs and the corresponding measured data of conversion fraction α_τs, we can derive estimated value for $< K^*_m >_0$, the slope of eq (18.2). If the $[S]_{o,H}$ can be prepared to guarantee the saturating assay condition, then $< \frac{V^*_{\max}}{H} >_0$ and $< K^*_m >_0$ determined by eq (19) and eq (18.2) respectively, will be good approximations.

Nevertheless, the saturating substrate condition can't always be achieved in some assays because of high-substrate inhibition or limit of substrate solubility. If the highest available concentration of substrate is larger than the level of $3K_m$, then accurate estimates of kinetics for immobilized enzymes can still be achieved. For this case, considering an iterative scheme,

we can re-arrange eq (18.1) as eq (18.3), and combine eq (18.3) with eq (18.2) to set up the following set of equations.

$$\begin{cases} < \frac{V^*_{\max}}{H} >_{\mathrm{r}} = \frac{1}{\tau}\{- < K^*_m >_{\mathrm{r-1}} Ln(1-\alpha_\tau) + [S]_{o,H}\alpha_\tau\} & (18.3) \\ < \frac{V^*_{\max}}{H} >_{\mathrm{r}} \tau - [S]_{o,L}\alpha_\tau = - < K^*_m >_{\mathrm{r}} Ln(1-\alpha_\tau) & (18.4) \end{cases}$$

Where r = 1, 2, 3, …, and $< K^*_m >_0$ obtained by eq (18.2) as the initial approximation for eq (18.3). For optimum estimations of $\frac{V^*_{\max}}{H}$ and K^*_m, the detected values of α_τ in eq (18.3) and eq (18.4) are based on two measurement conditions – high inlet concentration of substrate, $[S]_{o,H}$, and low inlet concentration of substrate, $[S]_{o,L}$, respectively. After successively finite computing, we will get repetitions of decimal places being used for $< \frac{V^*_{\max}}{H} >_{\mathrm{r}}$ and $< K^*_m >_{\mathrm{r}}$, and these values are then the final approximate solutions to eq (18.3) and eq (18.4), respectively.

As mentioned above, this method will fail or gain a large deviation from true value of kinetics when the highest available concentration of substrate is far lower than saturation (i.e., $\leq 3K_m$). This is similar to the limitations of Michaelis-Menten plot to estimate the kinetic value of homogeneous catalytic reaction.[76] The strategy of measurement and calculation is briefly outlined as Scheme 2, and has been used to analyze the kinetics of immobilized PST- and CRL-catalyzed reactions, respectively.

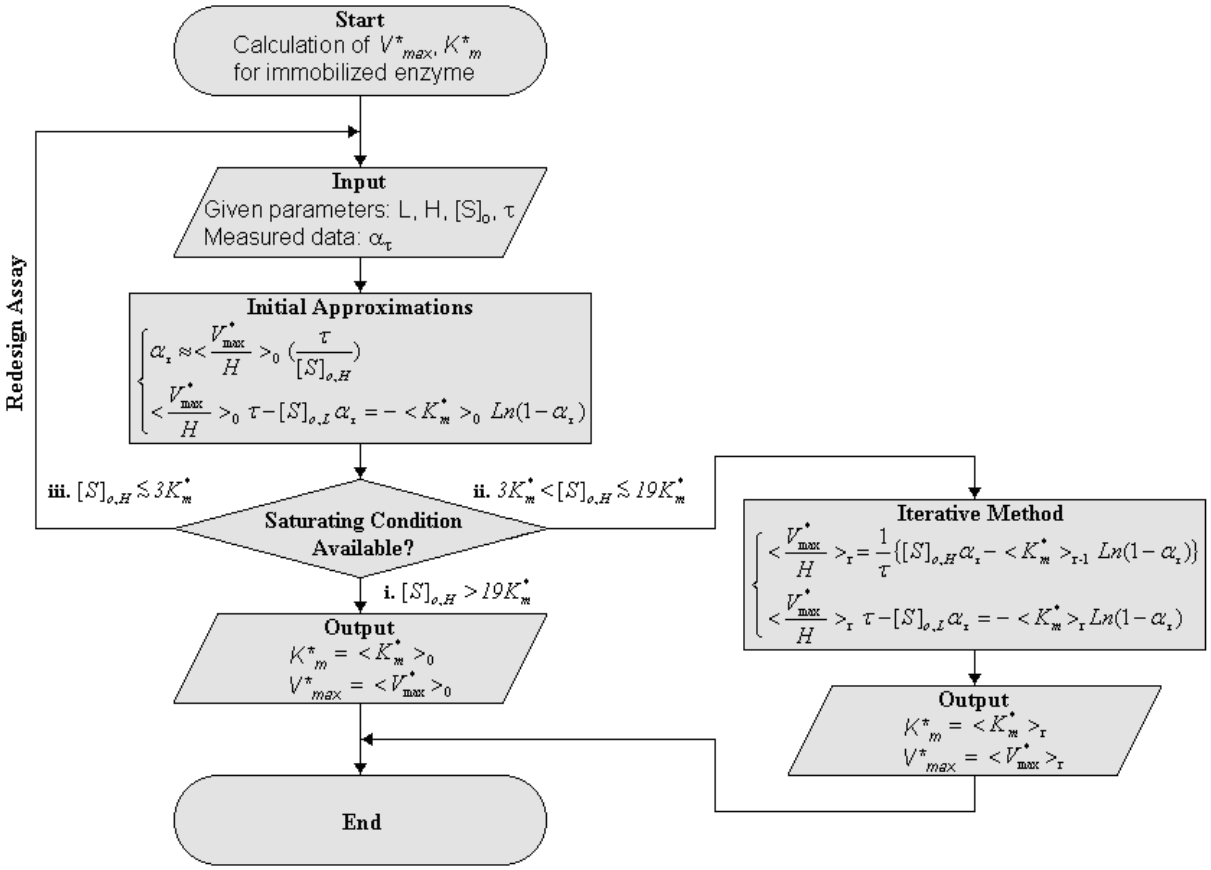

Scheme 2. A systematic and standardized data analysis. Flow chart showing the scheme of solving eq (1.1) to determine the apparent kinetics of immobilized enzyme when i) saturating condition is available; ii) enough high, but not saturating, concentration of substrate is available; iii) the highest available concentration of substrate is still lower than $3K_m$. These conditions of choice can be also regarded as the final check for the reasonableness of calculating results.

4.3 Experimental Section

4.3.1 Cleaning and Silanization of Silicon Wafer

P-type Si(100) wafers (14-21 Ω-cm, MEMC, MO, USA) with 15 cm diameter, on which 100 nm oxide layers were grown using wet oxidation with a gas mixture of hydrogen (8000 cm^3/min) and oxygen (5000 cm^3/min) at 978°C, were cut into 4×8 cm^2 pieces of samples to serve as a supporting material for enzyme immobilization. Prior to immobilization, the piece of oxidized silicon wafer was carefully cleaned in the SPM (sulfuric-peroxide mixture), H_2SO_4 and H_2O_2 (volume ratio is 3:1), twice, each time at above 85 °C for 30 min. It should be noted that the cleaning solution is very corrosive and dangerous. After rinsing with pure water and drying, the sample was immersed in the (3-aminopropyl)triethoxysilane (APTES, Sigma-Aldrich, MO, USA) solution to proceed the silanization reaction for 30 min at room temperature to create an amine-functional surface (Figure S2). The APTES solution was prepared by the following procedures: (1) mixing pure water with acetone (volume ratio is 5:1), (2) adjusting the pH value of the above solvent to 3.5 by 1 M HCl, and (3) preparing the 5% APTES solution by diluting with above solvent. Following the APTES treatment, the silicon wafer was rinsed with pure water thoroughly. Ultrapure water (>18 MΩ cm at 25 °C) was used throughout the experiments. Then, the treated silicon wafer was baked at 120 °C for 30 min to complete the Si-O bond formation.[126]

4.3.2 Reactor System and Enzyme Immobilization

The fabrication of microfluidic reactor and the associated enzyme immobilization were described in our previous reports,[5, 137] and the step by step process flow is briefly illustrated in Figure 29(a). For sealing step of reactor assembly implemented under near-dry condition,

which will significantly cause PST deactivated, the immobilization process of PST must be practiced after reactor assembly and directly before assay not like CRL. The reactor composed two plates; the bottom plate was a silicon wafer on glass support, and the top plate, made of quartz, contained a tortuous fluidic guide on its surface. The fluidic channel was 72.6 cm long (L), 0.194 cm width (W), and 167 μm depth (H).

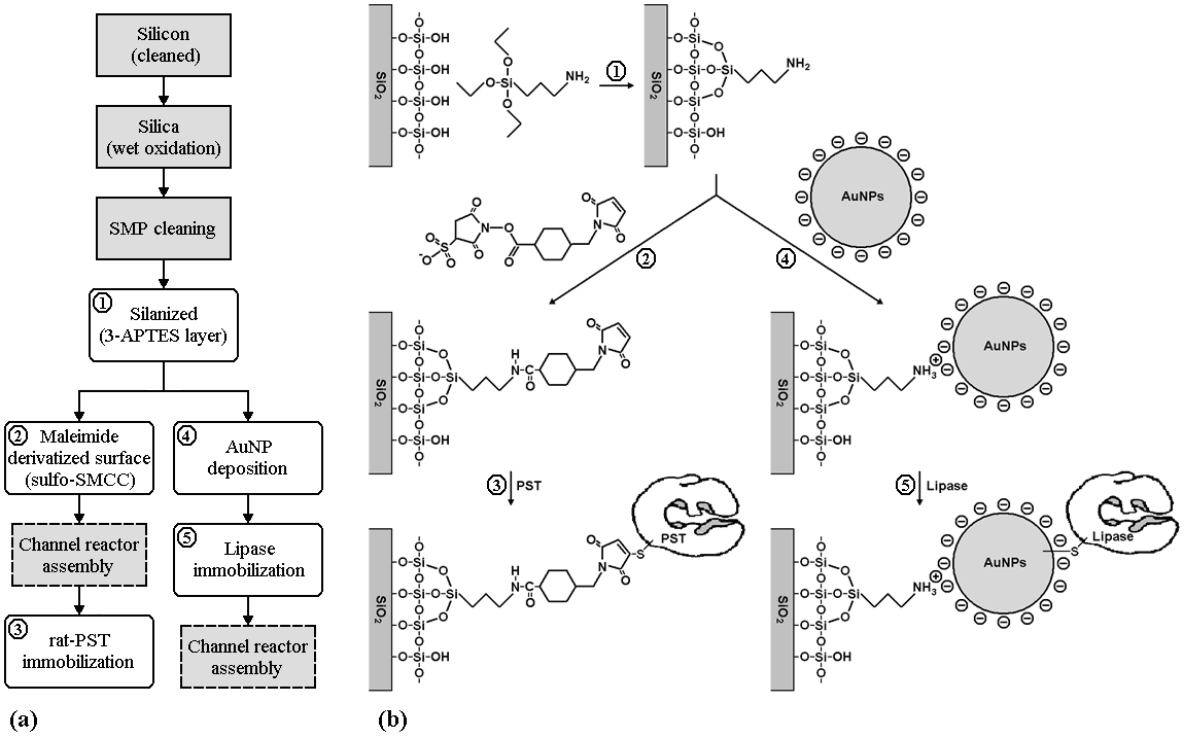

Figure 29. Step-by-step and chemical procedures of enzyme immobilization. (a) Process flow showing the samples used and their preparation technique and (b) schematic diagram of the chemical linking method of enzymes, rat-PST and CRL, binding to the silica substrate.

The two approaches to biding enzymes, PST and CRL, that we have investigated were coupling of thiols (cysteine residues) to maleimide groups and to gold nanoparticles (AuNPs), respectively, as follows:

(a) PST immobilization: To create a maleimide group for the immobilization of enzyme through its sulfhydryl group, sulfosuccinimidyl 4-(N-maleimidomethyl)-cyclohexane-1-

carboxylate (sulfo-SMCC, Sigma-Aldrich) was used to link to the amino group of APTES on the surface of silicon wafer (Figure 29(b)). The 0.5 mM sulfo-SMCC linker solution was prepared by dissolving sulfo-SMCC into 50 mM sodium borate buffer (Sigma-Aldrich), and then the linker solution was dipped onto the silanized surface of the sample for 1 hour at room temperature. Finally, the surface was extensively rinsed with water and dried with nitrogen gas. The enzyme solution (200 μg/mL rat PST, EC.2.8.2.1, in 0.1 M sodium phosphate buffer at pH 7.0) prepared according to published procedure[127, 128] was pumped into the microfluidic system by a programmable syringe pump (KD Scientific, KDS260P) at space time τ = 0.5 min (equivalent to 28.2 mL/hr or v_x = 2.4 cm/sec) and stopped to incubate for 15 min at room temperature. Next, 50 mM 2-mercaptoethanol solution (in 50 mM sodium phosphate buffer at pH 7.0) was pumped into the microfluidic system and stopped to incubate for 8 min at room temperature. Finally, 50 mM sodium phosphate buffer was pumped into the microfluidic system to wash away the residual 2-mercaptoethanol solution.

(b) CRL immobilization: As a connecting bridge linking enzyme via its sulfhydryl groups with Si substrate via the silanized surface, the AuNPs were prepared in aqueous solution using a previously reported chemical reduction method.[83] Aqueous solution of 10mL 1mM $HAuCl_4$ ($HAuCl_4 \cdot 3H_2O$, Sigma-Aldrich) and 1mL 38.8 mM trisodium citrate dehydrate (Showa Chemical Co., Japan) were mixed, and then heated under reflux for 15 min with vigorous stirring. The color of the solution gradually changed from yellow to purplish-red. After cooling to room temperature, colloidal AuNPs were formed in the solution, and then this AuNPs solution was used to rinse the silanized surface of the sample for 15 min at room temperature. The surface was extensively rinsed with water immediately after removing from AuNPs colloid suspension, and dried with nitrogen gas. 1.5 μM CRL (crystallized and lyophilized, EC 3.1.1.3, Sigma-Aldrich) solution prepared was dipped onto the AuNPs modified surface of the sample, and incubated for 10 min; CRL concentration was determined using UV-Vis spectroscopy (molar extinction coefficient 3.7×10^4 $M^{-1}cm^{-1}$ at 280 nm). Finally,

the surface was immersed in water for 5 min and dried with nitrogen gas, and then the CRL-immobilized samples were stored at 4°C until enzyme activity assay. Reactions involved in the surface modification and the immobilization of rat PST and CRL are shown in Figure 29(b).

4.3.3 PST Activity Assay

Two different concentrations of 3'-phosphoadenosine 5'-phosphate (PAP), 400 μM and 2 μM, were used to create saturating and non-saturating substrate condition, respectively, for the immobilized PST-catalyzed reaction (Figure 30(a)). The PAP concentrations used were determined according to the K_m of free rat PST[127, 128] and eq (18.1) in a surface reaction limited model. The reaction mixtures for immobilized rat PST contained PAP (400 μM or 2 μM) and 20 mM p-nitrophenyl sulfate (*p*NPS) in 100 mM 1,3-bis[tris(hydroxymethyl) methylamino]propane buffer at pH 7.

4.3.4 CRL Activity Assay

Two different concentrations of 4-nitrophenyl palmitate (*p*NPP, Sigma-Aldrich), 80 μM and 4 μM, were used to create relative high and low substrate condition, respectively, for the immobilized CRL-catalyzed reaction (Figure 30(b)). According to the K_m of free CRL[137] and eq (18.1) in a surface reaction limited model, the 80 μM *p*NPP prepared was only up to a relative high concentration not a saturating substrate condition in this assay due to the limit of solubility of *p*NPP. The assays were performed for immobilized CRL in mixtures as

following volume ratio: 1.3mL phosphate-buffered saline (PBS) buffer solution (tablets, 140 mM NaCl, 2.7 mM KCl, 10 mM Na_2HPO_4, 1.8 mM KH_2PO_4, pH 7.4, Sigma-Aldrich); 0.5mL propan-2-ol containing *p*NPP at 1.2 mM and 0.06mM concentrations, respectively; and 0.1 mL water (as a control compared to homogeneous reaction, which AuNPs-CRL complex was prepared and suspended in 0.1 mL water before assay[137]).

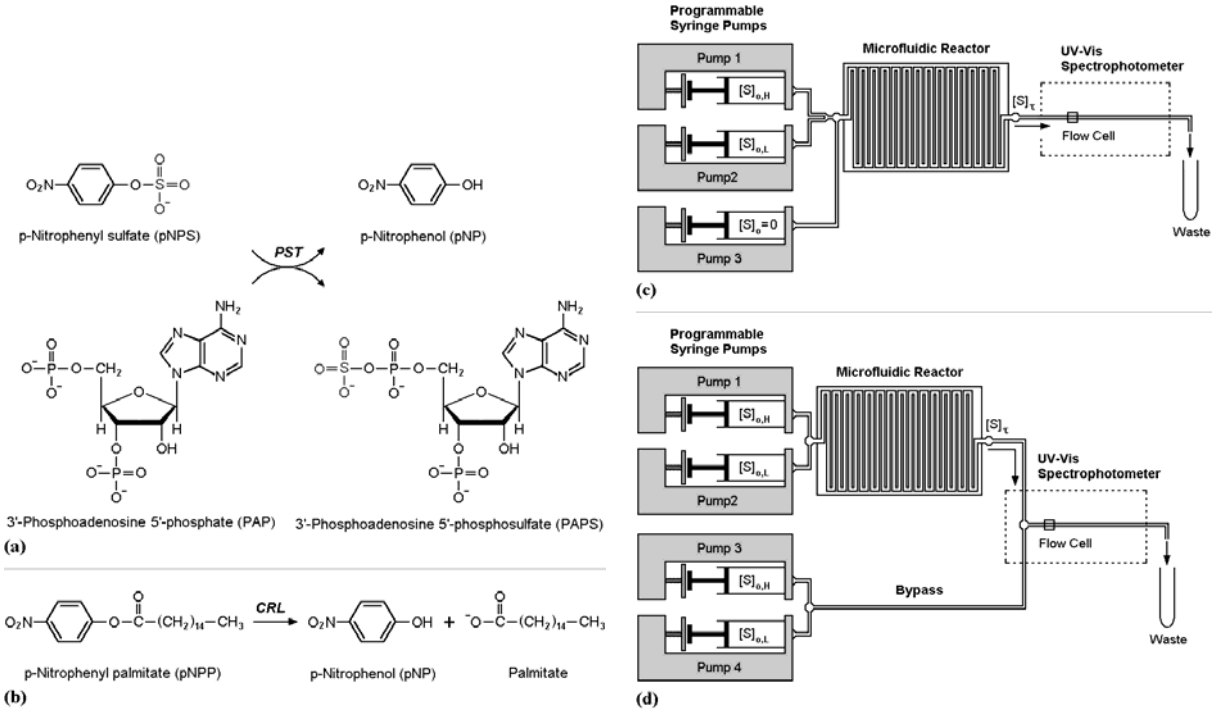

Figure 30. PST-catalyzed sulfuryl group transfer reaction, CRL-catalyzed hydrolysis reaction, and the corresponding setups of assay systems. (a) PAP and *p*NPS were used as substrates for rat PST; (b) *p*NPP was used as substrate for CRL. The common product, *p*NP, which gives strong absorption at 400 nm in neutral or alkaline, served as the reporter molecule for the progress of these two enzyme-catalyzed reactions. Schematic diagram of a typical microfluidic-reactor instrument for continuous kinetic measurements; (a) for the PST assay system with substrate-free as base line; the substrate S is PAP, $[S]_{o,H} = [PAP]_{o,H} = 400$ μM, $[S]_{o,L} = [PAP]_{o,L} = 2$ μM. (b) for the CRL assay system with enzyme-free (via bypass) as base line. In the lipase assay; the substrate S is *p*NPP, $[S]_{o,H} = [pNPP]_{o,H} = 80$ μM, $[S]_{o,L} = [pNPP]_{o,L} = 4$ μM.

Injection of the reaction mixtures into the reactor was controlled by automatic pumping

system throughout the experiments and operated at desired flow rate to have space time τs, at 0.5, 2, 4 or 8 min for PST assay, and at 0.5, 1, 2, 4 min for CRL assay, respectively. The output solution was directed into a quartz flow cell mounted in the UV-Vis spectrophotometer (Hitachi UV-Vis-3300, Tokyo, Japan) for *p*NP detection at 400 nm and 410 nm in PST and CRL assays, respectively. The essential components of microfluidic-reactor instrument for kinetics analysis are shown as Figure 30(c) and 29(d). The molar extinction coefficients of *p*NP absorbance were 10,500 M^{-1} cm^{-1} for PST assay; 14,100 M^{-1} cm^{-1} and 15,000 M^{-1} cm^{-1} for CRL assays at 80 μM and 4 μM *p*NPP, respectively.

4.4 Results and Discussion

4.4.1 Enzymatic Activities of Surface-Immobilized PST, CRL Based on Corresponding Running Controls

The typical time course plots of product yield are presented in Figure 31 were the *p*NP absorbance responses to high/low feed concentration of substrate with a series of space times τs, after subtracting blank controls, at 400 and 410 nm in PST and CRL assays, respectively. It should be emphasized that two assays were set up by different schemes (Figure 30(c) and 29(d)) to obtain respective running blank controls: (1) substrate PAP free for PST assay, (2) enzyme free, by use of bypass scheme to skip reaction solution directly to UV-Vis spectrophotometer, for CRL assay. Because the values of *p*NP absorbance at high concentration of substrate *p*NPP were significantly different from those at low concentration of substrate *p*NPP, bypass was an essential strategy to continuous-flow assay of surface-immobilized CRL in order to subtract accurate blank controls (Figure 30(d)). In this study, the average background absorbance of 80 μM *p*NPP at 410 nm was 0.1033 larger than that of 4 μM *p*NPP. The breaks in x-axis, progress time t, of Figure 31(b) were due to bypass steps.

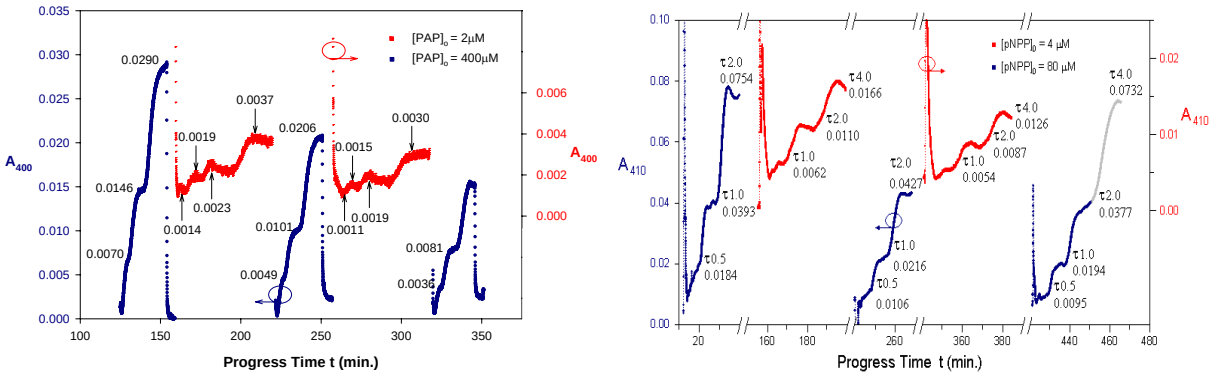

(a) **(b)**

Figure 31. The typical progress curves of enzymatic assays. The absorbance measurements of time courses were obtained after (a) setting zero on a control solution containing no PAP substrate in the PST assay; and (b) setting zero with no enzyme via bypass in the CRL assay, respectively.

4.4.2 Immobilized PST Kinetics: Saturating Substrate Condition to Determine V^*_{max}/H and Corresponding Deactivation Curve; Graphical Scheme to Determine K^*_m(PAP)

The determination of V^*_{max}/H for Immobilized PST can be achieved easily using eq 19 degenerated from eq 18.1 under saturating substrate condition, which was 400 μM substrate PAP. Figure 32(a) shows a typical fits of eq 19. The slopes of the fits were evaluated to yield V^*_{max}/H values corresponding to different progressing average times, t = 12.4, 101.8, 187.3, 269.1 min. Using exponential decay regression with three parameters to fit these V^*_{max}/H data, the deactivation curve of immobilized PST could be determined by $\frac{V^*_{max}}{H} = 0.4035 + 1.714e^{-0.01142t}$ with R^2 = 0.9994, and the V^*_{max}/H value at any time was estimated within all progressing period, shown as the inset of Figure 32(a). The original V^*_{max}/H (PST activity just after immobilization) and the time average $(V^*_{max}/H)_{ave}$ over the whole activity assays are 2.12 μM/min and 0.884 μM/min, respectively; i.e. original V^*_{max} = 3.55×10^3 $s^{-1}\mu m^{-2}$, $(V^*_{max})_{ave}$ = 1.48×10^3 $s^{-1}\mu m^{-2}$. Using $[PAP]_o$ = 2 μM, space time τs = 1, 2, 4, 8 min, and the determined V^*_{max}/H values as experimental parameters, Figure 32(b) shows the linear regression analysis based on eq (18.2), in which the K^*_m(PAP) values were the slopes of the least-squares regression lines, and the average K^*_m(PAP) of four independent experiment data was 16.95 ± 1.32 μM. As a check, the relation $[PAP]_{o,H}$ = 400 μM ≥ $5K^*_m$(PAP) = 84.75 μM was satisfied, and then the assumption of the saturating condition has established (i. condition in Scheme 2).

As shown in Figure 32(c), the K_m(PAP), specific V_{max}, and k_{cat} of free PST in a homogenous system were 4.10 ± 0.26 μM, 295 ± 3 nmol/min/mg, and 0.167 ± 0.002 s^{-1}, respectively. The K^*_m(PAP) of immobilized PST was four times higher than that of the free enzyme. It is reasonable for immobilized enzyme to exhibit a higher K^*_m because, as compared to free enzyme in solution, it decreases its degree of freedom and may be difficult to maintain its

flexible and proper conformation in a more stressful environment. Thus, the affinity of the substrate with enzyme may be weakening and higher substrate concentration may be needed to give the maximum enzyme activity as compared to that of free enzyme in solution. Using the k_{cat} value of free PST in a homogenous system combined with the original V^*_{max} of immobilized PST, we can estimate the immobilized PST density on silicon dioxide in this experiment, and obtain the value 0.0213 μm^{-2}. The true density should be larger than this, because there is, theoretically, smaller k_{cat} value of immobilized PST due to a steric barrier, an orientation issue, etc.; however, this estimated density means the average nearest-neighbor distance between immobilized PST macromolecules (diameter $d \approx 7.38$ nm), which still maintain active, will reach to about 7.36 μm. Moreover, with the same distance the free enzymes suspended apart in a homogenous system, the enzyme concentration will be lowered to 5.89 pM, which is far lower than the μM level used in ordinary enzymatic assay. Two important points, here, must be noted for the so low estimated surface density of immobilized PST based on the original V^*_{max} value: (1) it much guaranteed that the perpendicular diffusion rate of substrate to catalytic surface was much higher than the surface catalytic reaction rate, i.e. surface reaction limited condition was fairly well satisfied in this experiment; (2) A further improvement or an alternative scheme in the immobilization procedure to increase the surface density of immobilized PST required for expending research in new fields based on this assay platform.

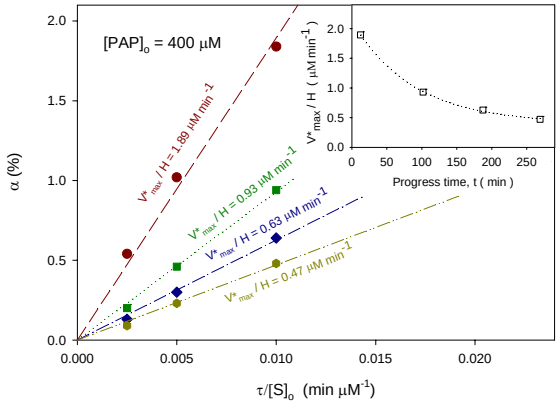

(a)

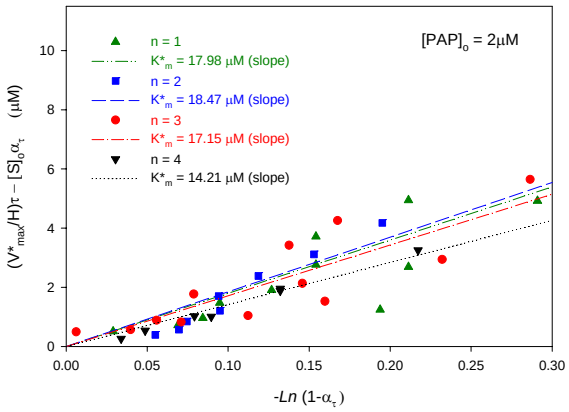

(b)

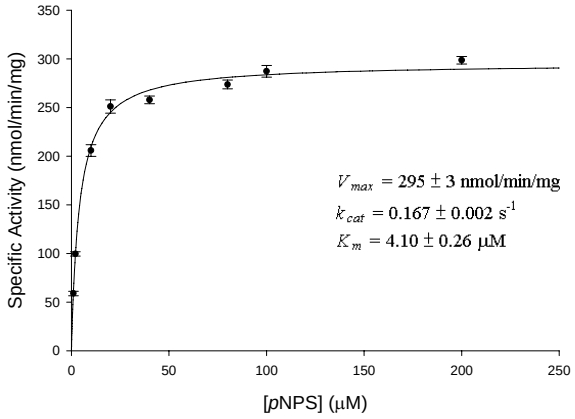

(c)

Figure 32. PST kinetics. (a) According to eq (19), the α_τ versus $\tau/[S]_o$ plot was used to determine V^*_{max}/H at high substrate concentration. Under saturating substrate condition, $[PAP]_o$ = 400 μM >> K_m, in the PST assay, the slope of linear regression, V^*_{max}/Hs, were fitted to an exponential decay curve shown as the inset, of which interpolated value was used to predict V^*_{max}/Hs at any time in the experimental intervals. (b) Fitting line of eq (18.2) to the data sets, $(V^*_{max}/H)\tau$-$[S]_o\alpha_\tau$ versus $-Ln(1-\alpha_\tau)$, of which slope was used to predict the optimum apparent Michaelis-Menton constant K^*_m. The predicted values of K^*_m of immobilized PST are the result of four set of independent experiment data (n = 1~4). (c) Michaelis-Menten plots for sulfuryl group transfer reaction by free PST.

4.4.3 Immobilized CRL Kinetics: Iterating Scheme to Determine V^*_{max}/H, Corresponding Deactivation Curve, and K^*_m

Due to solubility limit of substrate *p*NPP in immobilized CRL assay, the initial approximations of V^*_{max}/H and corresponding deactivation curve (r = 0 in Figure 33(a)) were obtained from eq (19) using 80 μM *p*NPP as inlet condition of high substrate concentration. This decay curve (r = 0) and 4 μM *p*NPP as inlet condition of low substrate concentration were then used to obtain the initial approximation of K^*_m (r = 0 in Figure 33(b)) from eq (18.2). Substituting $< V^*_{max}/H >_o$ and $< K^*_m >_o$ as the initial estimations into the set of two iterating eqs (18.3) and (18.4), the converged results of immobilized CRL were got, through five successive approximations as Figures 32(a) and 32(b), as follows: the deactivation curve $\frac{V^*_{max}}{H} = 1.603 + 2.226e^{-0.007047t}$ with R^2 = 0.9854, original V^*_{max}/H = 3.83 μM/min (or V^*_{max} = 6.41×10^3 $s^{-1}\mu m^{-2}$), and average K^*_m = 23.74 μM (Figure 33(c)), etc. Because the relation $0.33K^*_m$ = 7.83 μM ≤ $[p\text{NPP}]_{o,H}$ = 80 μM ≤ $5K^*_m$ = 84.75 μM was satisfied well, the kinetic parameters could be correctly obtained through this iterating calculation (ii. condition in Scheme 2). Comparing immobilized CRL K^*_m (23.74 μM) with homogeneous CRL K^*_m (23.91 μM)[43] implied that there was almost no influence on the affinity of substrate *p*NPP with immobilized CRL. Being a membrane enzyme, CRL would not be at the natural optimal conformation both in free-state in solution and immobilized-state on supporting material.

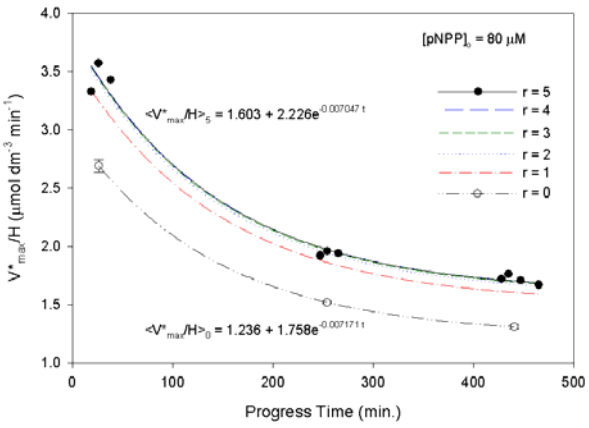

(a)

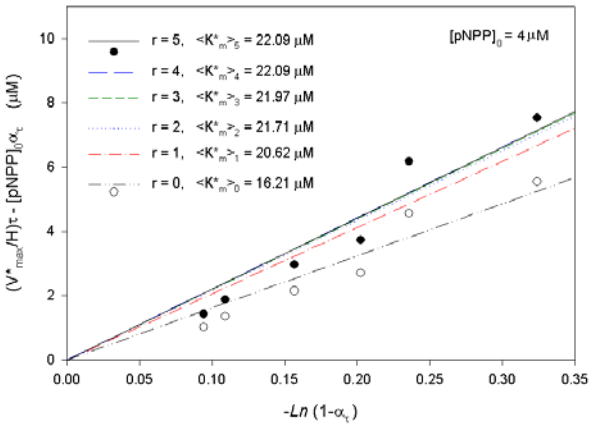

(b)

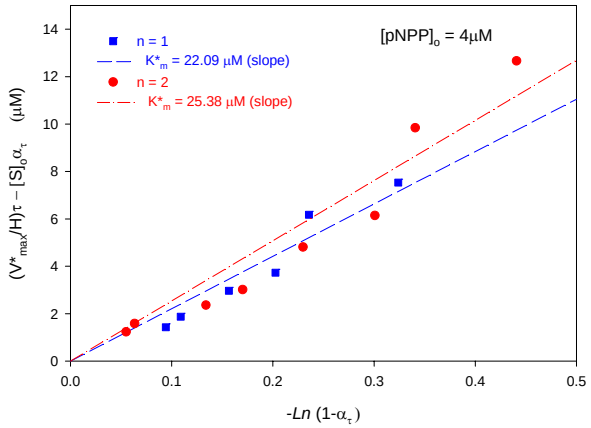

(c)

Figure 33. CRL kinetics. The typical iterative plots (a) and (b) were the output values of eqs (18.3) and (18.4), respectively; (a) for the solubility limit of substrate [*p*NPP]$_o$ in the CRL assay, [*p*NPP]$_o$ = 80 μM concentration used in this experiment, the initial approximation $<V^*_{max}/H>_0$ (open symbol) were still obtained from eq (19), and fitted to the exponential decay curve (dash-dot-dot). The r = 1~5 curves mean the fitting curves of five successive approximations of eq (18.3); the solid symbol means the optimum value of V^*_{max}/H, which has converged to three significant figures. (b) The open symbol and solid symbol mean the initial and the fifth approximations of eq (18.4), respectively. The value of K^*_m of immobilized CRL has converged to 22.09μM with three four significant figures after five successive approximation (r = 1~5). (c) The predicted values of K^*_m of immobilized CRL are the result of two set of independent experiment data (n = 1~2).

Physical Meanings of the Axes in Graphical Determinations of K^*_m. As mentioned above, $(\frac{V^*_{max}}{H})\tau - [S]_{o,L}\alpha_\tau = -K^*_m Ln(1-\alpha_\tau)$, in eqs (18.2) and (18.4), would predict K^*_m using linear regression plots as Figures 31(b) and 32(c). However, what were the physical meanings of these plots? First, the x-axis $-Ln(1-\alpha_\tau)$ can be expressed as a Maclaurin series: $-Ln(1-\alpha_\tau) = \alpha_\tau + \frac{\alpha_\tau^2}{2} + \frac{\alpha_\tau^3}{3} + \cdots + \frac{\alpha_\tau^n}{n} + \cdots$ Apparently, we can regard x-axis as only the conversion factor α_τ when α_τ value is still at low to moderate level (ex: $\alpha_\tau = 0.1$, $-Ln(1-\alpha_\tau) = 0.1054$; $\alpha_\tau = 0.3$, $-Ln(1-\alpha_\tau) = 0.3567$). Secondly, the y-axis $(V^*_{max}/H)\tau - [S]_{o,L}\alpha_\tau$ was the difference in reaction yield between two extreme substrate levels; the former, $(V^*_{max}/H)\tau$, means the change in product concentration in the time period τ at substrate saturating condition (or at the maximum velocity), and the latter, $[S]_{o,L}\alpha_\tau$, is the change in product concentration of a plug reactor at a low inlet substrate concentration and at a certain space time τ. The corresponding plots clearly reflect the relation: "the larger the yield difference between $(V^*_{max}/H)\tau$ and $[S]_{o,L}\alpha_\tau$ is, the higher K^*_m value is." For further explanation, the smaller difference between $(V^*_{max}/H)\tau$ and $[S]_{o,L}\alpha_\tau$ means that the reactor velocity (the latter) still keeps at higher velocity even at a low inlet concentration; i.e. the relative binding affinity of substrate is higher (or K^*_m is lower), and vice versa.

4.5 Conclusions

Enzyme immobilization is indispensable for biosensing, bio-regulation and many other bioengineering applications. Following our previously proposed approach for the determination of the kinetics of the immobilized enzyme, we were able to further establish procedures for the evaluation of two important enzymes immobilized on silicon substrate. Well-known procedures are available for the kinetic analysis of homogenous enzymes in solution. On the contrary, generally accepted method for the evaluation of immobilized enzymes in a systematic way is still needed to compare the kinetic parameters obtained from different laboratories. Based on our previously proposed model, we constructed practical design and analysis of kinetics of immobilized enzymes. Using this prototype platform, it allowed us to observe the kinetic in-situ change of immobilized enzyme, and the advanced fundamental research about kinetic mechanism under different stress conditions could be possible.

Appendix

I. Solution of A Partial Differential Equation[138, 139]

Consider eq (9)

$$D\frac{\partial^2[S]}{\partial z^2}=\frac{\partial[S]}{\partial t} \tag{9}$$

with the initial and boundary conditions as follows:

$$IC \qquad [S](z,0)=[S]_o \tag{10.1}$$

$$BCs \quad \begin{cases} \dfrac{\partial}{\partial z}[S](0,t)=0 & (10.2) \\ -D\dfrac{\partial}{\partial z}[S](H,t)=k_s[S](H,t) & (10.3) \end{cases}$$

where diffusion coefficient $D > 0$, and rate constant of surface reaction $k_s > 0$

To apply the separation of variables method, we carry out the following steps:

STEP 1 – Separating the partial differential equation into two ordinary differential equations

Substituting $[S](z,t)=Z(z)T(t)$ into eq (9) gives

$$ZT'=DZ''T$$

or

$$\frac{T'}{DT}=\frac{Z''}{Z}$$

setting them both equal to $-\lambda$ gives two ordinary differential equations

$$T'+D\lambda T=0 \tag{A1}$$

$$Z''+\lambda Z=0 \tag{A2}$$

with initial and boundary conditions

$$\begin{cases} Z(z)T(0) = [S]_o & \text{(A3.1)} \\ Z'(0) = 0 & \text{(A3.2)} \\ -DZ'(H) = k_s Z(H) & \text{(A3.3)} \end{cases}$$

STEP 2 – Finding the separation constant

First of all, λ must not be negative or else $T(t)$ will grow exponentially to infinity.

Secondly, suppose $\lambda = 0$, this being the case, we have

$$Z'' = 0$$

and thus

$$Z = C_1 z + C_2$$

Substituting it into eq (A3.2), eq (A3.3), we could conclude that

$$\begin{cases} C_1 = 0 \\ -DC_1 = k_s(C_1 H + C_2) \end{cases} \rightarrow \begin{cases} C_1 = 0 \\ C_2 = 0 \end{cases}$$

which would mean $[S](z,t) = 0$. We throw out this uninteresting case.

Finally, if $\lambda > 0$, we set $\lambda = \mu^2$ (also set $\mu > 0$) and rewrite eq (A1) and eq (A2)

$$T' + D\mu^2 T = 0$$
$$Z'' + \mu^2 Z = 0$$

which gives us solutions

$$T(t) = Ae^{-D\mu^2 t} \quad \text{(A4.1)}$$
$$Z(z) = B_1 \cos(\mu z) + B_2 \sin(\mu z) \quad \text{(A4.2)}$$

Substituting eq (A4.2) into eq (A3.2), we could conclude

$$B_2 \mu = 0 \;\rightarrow\; B_2 = 0 \;\rightarrow\; Z(z) = B_1 \cos(\mu z),$$

substituting this into eq (A3.3) gives

$$DB_1 \mu \sin(\mu H) = k_s B_1 \cos(\mu H)$$

or

$$\cot(\mu H) = \frac{D}{k_s}\mu \quad \text{(A5)}$$

$$\text{Let} \begin{cases} \beta = \mu H \ \text{ or } \mu = \dfrac{\beta}{\mathrm{H}} & \text{(A6.1)} \\ Da \equiv \dfrac{k_s H}{D} & \text{(A6.2)} \end{cases}$$

, then

$$\cot(\beta) = \frac{\beta}{Da} \quad \text{transferred from eq (12)} \qquad \text{(A6)}$$

Equation (A6) allows us to solve the eigenvalues β_n with graphical construction as Figure A3(a) (or with numerical analysis methods)

STEP 3 – Finding the fundamental solution

Hence we have an infinite series of the form for the fundamental solution

$$[S](z,t) = \sum_{n=1}^{\infty} Z_n(z) T_n(t) = \sum_{n=1}^{\infty} a_n \cos(\frac{\beta_n}{H} z) \exp(-\frac{D\beta_n^2}{H^2} t) \qquad \text{(A7)}$$

Setting $t = 0$ and making use of the initial condition eq (10.1), we have

$$[S](z,0) = [S]_o = \sum_{n=1}^{\infty} a_n \cos(\frac{\beta_n}{H} z) \qquad \text{(A8)}$$

This brings us to our final step

STEP 4 – Expansion of the initial condition as a sum of eigenfunctions

To find the constant a_n in eq (A8), we must multiply each side of the equation by $\cos(\frac{\beta_m}{H} z)$ and integrate z from 0 to H; that is;

$$\int_0^H [S]_o \cos(\frac{\beta_m}{H} z) dz = \sum_{n=1}^{\infty} a_n \int_0^H \cos(\frac{\beta_m}{H} z) \cos(\frac{\beta_n}{H} z) dz$$

$$[S]_o \frac{H}{\beta_m} \sin(\beta_m) = a_m \int_0^H \cos^2(\frac{\beta_m}{H} z) dz$$

$$= a_m H \{\frac{(\sin(2\beta_m) + 2\beta_m)}{4\beta_m}\}$$

Solving for a_m, we get our desired result

$$a_m = \frac{4[S]_o \sin(\beta_m)}{\sin(2\beta_m) + 2\beta_m} \tag{A9}$$

In other words, our solution to eq (9) is

$$[S](z,t) = 4[s]_o \sum_{n=1}^{\infty} \frac{\sin(\beta_n)}{\sin(2\beta_n) + 2\beta_n} \cos(\frac{\beta_n}{H} z) \exp(-\frac{D\beta_n^2}{H^2} t) \tag{A10}$$

Substituting the time of stream $t = \frac{x}{v_x}$ into eq (A10), substrate concentration [S] can be transferred as a function of position (z, x) in the reactor, and we obtain steady state expression of substrate concentration [S] profile for the whole space of rectangular reactor

$$[S](z,x) = 4[S]_o \sum_{n=1}^{\infty} [\frac{\sin\beta_n}{\sin(2\beta_n) + 2\beta_n} \cos(\frac{\beta_n}{H} z)] \exp(-\frac{D\beta_n^2}{v_x H^2} x) \tag{11}$$

II. Viscosity Measurement of Liquid[140, 141]

The coefficient of viscosity e μ (cP) of a fluid is conveniently measured by determination of the time t (s) of flow of a given volume V (cm^3) of the liquid through a vertical capillary tube of radius r and length L, both in cm, under the influence of gravity. For a liquid, this flow is governed by Poiseuille's law in the form

$$\mu = \frac{\pi \Delta P r^4}{8VL} t \qquad \text{(A11)}$$

where ΔP ($dyne/cm^2$) is the difference in pressure between the two ends of the capillary tube. The Ostwald viscosimeter arrangement is shown in Figure A1.

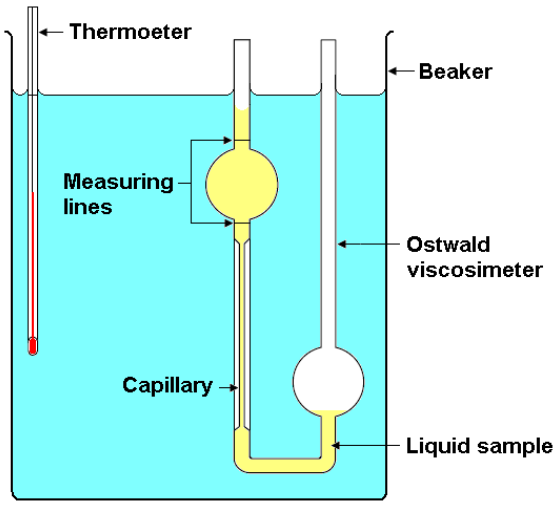

Figure A1. Ostwald viscosimeter arrangement to be used if a glass-walled thermostat bath is not available.

In eq (A11), the difference in pressure between the two ends of the capillary tube $\Delta P = gL\rho$; substitute this into eq (A11), then,

$$\mu = \frac{\pi g r^4 \rho}{8V} t \qquad \text{(A12)}$$

Since r and V are constants for some one fixed viscosimeter, eq (A11) can be rewritten

$$\mu = C\rho t \qquad \text{(A13)}$$

where C (cSt/s) is a constant for a fixed viscosimeter. If a standard liquid (like water) with known viscosity is available, then eq (A14) allows us to measure an unknown viscosity of solution,

$$\mu = \frac{\rho t}{\rho_o t_o}\mu_0 \qquad \text{(A14)}$$

Using Ostwald viscosimeter, we have determined the viscosity of reaction solutions A and B in Table A1. Table A2 shows the measuring raw data and the determined result of viscosity at 25 ^{o}C.

Table A1. The contents of reaction solutions A and B for enzyme kinetics assay are designed for rat-phenol-sulfotransferase and D-hydantoinase, respectively.

Reaction solution A for rat-phenol-sulfotransferase		Reaction solution B for D-hydantoinase	
PAP	40 μM	phthalimide	1mM
pNPS	20 mM	Bis-trispropane pH 7.0	100 mM
2-mercaptoethanol	5 mM		
Bis-trispropane pH 7.0	100 mM		

Table A2. Using eq (A14), the measurement of viscosity of reaction solutions A and B at 25 ^{o}C. Water is the standard liquid with known viscosity.

		Reaction solution A for rat-phenol-sulfotransferase	Reaction solution B for D-hydantoinase	Water, Standard Liquid (μ_o = 0.8937 cP at 25 ^{o}C)
Density, ρ (g/cm^3)		1.001	1.007	0.997
Time, t (s)	1	3.90	3.59	3.59
	2	3.95	3.68	3.52
	3	3.83	3.68	3.53
	4	3.92	3.66	3.56
	Ave.	3.90	3.65	3.55
Viscosity, μ (cP) (kg/m-s)		0.9858 9.858×10^{-4}	0.9281 9.281×10^{-4}	0.8937 8.937×10^{-4}

III. Prediction of Liquid Mass Diffusion Coefficient[123]

An equation for predicting diffusion coefficient that has been developed for nonelectrolytes in an infinitely dilute solution is Wilke-Chang equation,[124]

$$D_{AB} = \frac{7.4\times10^{-8} T(\Phi_B M_B)^{1/2}}{\mu_B V_A^{0.6}} \quad \text{(A15)}$$

where D_{AB} is the mass diffusion coefficient of A in dilute solution in B, in cm^2/s; T is the absolute temperature; Φ_B is the "association" parameter for solvent B, some values given in Table A4; M_B is the molecular weight of the solvent; μ_B is the solution viscosity, in cP; V_A is the molal volume of solute at normal boiling point, in cm^3/g.

Table A3 lists the contributions for each of the constituent atoms, of which can be added together and deducted specific ring corrections as per solute molecular formulae for predicting V_A.

Table A3. Atomic and structural diffusion volume increments[142, 143]

Element		Atomic volume, in cm^3/mol	Element		Atomic volume, in cm^3/mol
Antimony (Sb)		24.2	Oxygen (O)	double-bonded	7.4
Arsenic (As)		30.5		coupled to two other elements:	
Bismuth (Bi)		48.0		in aldehydes and ketones	7.4
Bromine (Br)		27.0		in methyl esters	9.1
Carbon (C)		14.8		in ethyl esters	9.9
Chlorine (Cl)	terminal, as in R-Cl	21.6		in higher esters and ethers	11.0
	medial, as in R-CHCl-R'	24.6		in acids	12.0
Chromium (Cr)		27.4		in union with S, P, N	8.3
Fluorine (F)		8.7	Phosphorus (P)		27.0
Germanium (Ge)		34.5	Silicon (Si)		32.0
Hydrogen (H)		3.7	Sulfur (S)		25.6
Iodine (I)		37.0	Tin (Sn)		42.3
Nitrogen (N)	double-bonded R-N=R'	15.6	Titanium (Ti)		35.7
	in primary amines R-NH_2	10.5	Vanadium (V)		32.0
	in secondary amines R-NH-R'	12.0	Zinc (Zn)		20.4

For a three-membered ring, as in ethylene oxide	deduct	6.0
For a four-membered ring, as in cyclobutane	deduct	8.5
For a five-membered ring, as in furane	deduct	11.5
For a six-membered ring, as in benzene, pyridine	deduct	15.0
For an anthracene ring formation	deduct	47.5
For a naphthalene ring formation	deduct	30.0

Table A4. The values of association parameter ϕ_B for a few common solvents[144] in Wilke-Chang equation.

Solvent	Φ_B
water	2.26
methanol	1.90
ethanol	1.50
benzene, ether, heptane, and other unassociated solvents	1.00

Example A1 Prediction of $D_{PAP\text{ - Solution A}}$

Estimate the diffusion coefficient of PAP, $C_{10}H_{15}N_5O_{10}P_2$, in the reaction solution A in Table A1 at 25°C. The molecular volume of PAP may be evaluated by using values from Table A3 as follows:

$$V_{PAP} = 10V_C + 15V_H + 5V_N + 10V_O + 2V_P - (Ring\ Factor)$$

$$V_{PAP} = 10(14.8) + 15(3.7) + (4\times 15.6 + 10.5) + (2\times 7.4 + 3\times 11.0 + 5\times 12.0) + 2\times 27.0 - (15.0 + 2\times 11.5)$$
$$= 400.2\ cm^3 / mol$$

At 25°C, the viscosity of reaction solution A is 0.9858 cP, from Table A2; the remaining parameters to be used are

T = 298K

Φ_B for water = 2.26

M_B for water =18

Substituting these values into eq (A15), we can obtain

$$D_{PAP-Solution\ A} = \frac{7.4\times 10^{-8}(298)(2.26\times 18)^{1/2}}{0.9858(400.2)^{0.6}} = 3.92\times 10^{-6}\ cm^2/s \quad (3.92\times 10^{-10}\ m^2/s)$$

Example A2 Prediction of $D_{phthalimide\text{ - Solution B}}$

Estimate the diffusion coefficient of phthalimide, $C_8H_5NO_2$, in the reaction solution B in Table A1 at 25°C. The molecular volume of phthalimide may be evaluated by using values from Table A3 as follows:

$$V_{Phthalimide} = 8V_C + 5V_H + V_N + 2V_O - (Ring\ Factor)$$

$$V_{Phthalimide} = 8(14.8) + 5(3.7) + 12.0 + 2(7.4) - (11.5 + 15.0) = 137.2\ cm^3 / mol$$

At 25°C, the viscosity of reaction solution B is 0.9281 cP, from Table A2; the remaining parameters to be used are

T = 298K

Φ_B for water = 2.26

M_B for water =18

Substituting these values into eq (A15), we can obtain

$$D_{Phthalimide-Solution\ B} = \frac{7.4\times10^{-8}(298)(2.26\times18)^{1/2}}{0.9281(137.2)^{0.6}} = 7.91\times10^{-6}\ cm^2/s \quad (7.91\times10^{-10}\ m^2/s)$$

IV. Apparent Michaelis Constants K^*_m and V^*_{max} for Immobilized Enzyme[145, 146]

Assume that enzymes are uniformly immobilized onto the surface of a nonporous support material, the activity of all enzymes are equal, and the support surface is surrounded by a stagnant boundary layer through which substrate has to diffuse in order to arrive at the reactive surface, as depicted in Figure A2.

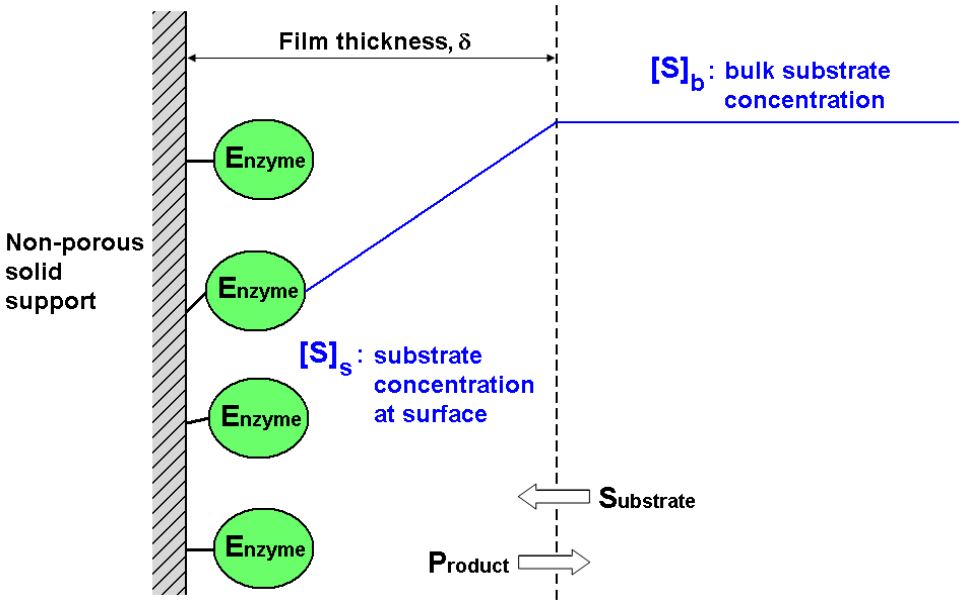

Figure A2. Schematic diagram of substrate concentration profile in a liquid film around immobilized enzymes. $[S]_s$ and $[S]_b$ are the substrate concentration at catalytic surface and the bulk substrate concentration, respectively. δ is the effective thickness of Nernst diffusion layer (boundary layer).

At the catalyst surface, the reaction rate is expressed by Michaelis-Menten equation:

$$r = r'A = -\frac{d[S]_s}{dt} = \frac{V_{\max}[S]_s}{K_m + [S]_s} \qquad \text{(A16)}$$

$$\text{or} \quad r' = \frac{r}{A} = \frac{V'_{\max}[S]_s}{K_m + [S]_s} \qquad \text{(A17)}$$

where r' is enzymatic reaction rate per unit of external surface area of catalyst (mmol cm^{-2} sec^{-1}); A is external surface area per unit catalytic volume (cm^2/cm^3); V'max is maximum enzymatic reaction rate per unit of external surface area (mmol cm^{-2} sec^{-1}).

There are two driving forces, electrical and diffusion effects, exert on substrate to move to the reactive surface.

Around each immobilized enzyme molecule there is assumed to prevail a gradient of electrical potential, $\frac{\partial \varphi}{\partial z}$, which is generated by charged groups on the support. In such a field, the molar flux of substrate from the boundary layer to the reactive surface, J_e, will be proportional to the negative gradient of the electrical potential, the concentration of substrate in the bulk solutions, $[S]_b$:

$$J_e = -u_s [S]_b \frac{\partial \varphi}{\partial z} \tag{A18}$$

where u_s is the electrical mobility of the substrate. This mobility is related to the diffusion coefficient, D, of the substrate by Nernst-Einstein equation:[147]

$$u_s = \frac{n_s DF}{RT} \tag{A19}$$

where n_s is the net charge number of the substrate, F is the Faraday constant, and R is the gas constant. Insert eq (A19) into eq (A18) gives

$$J_e = -\frac{n_s DF[S]_b}{RT} \frac{\partial \varphi}{\partial z} \tag{A20}$$

According to Fick's first law, the rate of thermal diffusion of substrate is

$$J_d = -D\frac{\partial [S]}{\partial z} = D\frac{[S]_b - [S]_s}{\delta} \tag{A21}$$

where $\frac{\partial [S]}{\partial z}$ is the substrate concentration gradient between the catalytic surface and the boundary of Nernst layer.

At steady-state, the reaction rate at catalyst surface, r', will equal the net flux of substrate from the boundary of Nernst layer to the catalyst surface, $J_e + J_d$, i.e.:

$$r' = J_e + J_d \tag{A22}$$

$$\text{or } \frac{V'_{max}[S]_s}{K_m + [S]_s} = D\frac{[S]_b - [S]_s}{\delta} - \frac{n_s DF[S]_b}{RT}\frac{\partial\varphi}{\partial z} \tag{A23}$$

Combining eq (A17) and eq (A23), it is possible to eliminate $[S]_s$ to get:

$$r'^2 - \frac{D}{\delta}(K_m + [S]_b + \frac{V'_{max}\delta}{D} - \frac{n_s F\delta}{RT}[S]_b\frac{\partial\varphi}{\partial z})r' + \frac{V'_{max}D}{\delta}[S]_b(1 - \frac{n_s F\delta}{RT}\frac{\partial\varphi}{\partial z}) = 0 \tag{A24}$$

Let $\begin{cases} \alpha = \frac{D}{\delta}(K_m + [S]_b + \frac{V'_{max}\delta}{D} - \frac{n_s F\delta}{RT}[S]_b\frac{\partial\varphi}{\partial z}) \\ \beta = \frac{V'_{max}D}{\delta}[S]_b(1 - \frac{n_s F\delta}{RT}\frac{\partial\varphi}{\partial z}) \end{cases}$, then eq (A24) has the form:

$$r'^2 - \alpha r' + \beta = 0 \tag{A25}$$

According to the binomial series, the roots of eq (A25) may be approximated to $\frac{\alpha}{\beta}$ or $\alpha - \frac{\alpha}{\beta}$. Therefore, at steady-state, the rate of conversion of substrate by enzyme is given by:

$$r' = \frac{\alpha}{\beta} \quad \text{or} \quad r' = \alpha - \frac{\alpha}{\beta} \tag{A26}$$

The second of these solutions need not be considered, since it demands that the reaction rate of the enzyme should be infinite when the thickness of the Nernst layer, δ, approaches zero. The first solution for the reaction rate of the immobilized enzyme is:

$$r' = \frac{V'_{max}[S]_b}{(K_m + \frac{V'_{max}\delta}{D})(\frac{RT}{RT - n_s F\delta\frac{\partial\varphi}{\partial z}}) + [S]_b} = \frac{V'_{max}[S]_b}{K'_m + [S]_b} \tag{A27}$$

This equation defines the apparent Michaelis constant as:

$$K_m^* = (K_m + \frac{\frac{V_{max}^*}{H}\delta}{D})(\frac{RT}{RT - n_s F\delta\frac{\partial\varphi}{\partial z}}) \qquad \text{(A28)}$$

The apparent Michaelis constant K'_m will approach Michaelis constant K_m as δ approaches zero in eq (A28); this means the reaction condition reduce to the case of homogeneous reaction with free enzyme from that of heterogeneous reaction with immobilized enzyme.

If n_s and $\frac{\partial\varphi}{\partial z}$ have the same sign, then the eq (A28) in parentheses on the right is >1; but it is <1 if the signs are opposite. If either n_s or $\frac{\partial\varphi}{\partial z}$ is zero, then the eq (A28) in parentheses on the right =1; so that only the diffusion term remains.

V. Prediction of Damkohler Nunber, *Da*

The analysis of Damkohler number (*Da*), a key factor for the proposed systematic analysis of immobilized enzyme, is described. *Da* is the ratio of the rate constants of chemical reaction to mass transfer factor. Appropriate values of *Da* can be used to respectively derive K^*_m, V^*_{max} and diffusion coefficient *D* of substrate under two extreme conditions.

Dimensionless Damkohler number, $Da \equiv k_s / (D/H)$, is defined as ratio of the rate constants of chemical reaction to mass transfer factor.[148] To simplify the equations derived in the text (3.2 Theoretical Considerations), two extreme conditions, $Da << 1$ and $Da >> 1$, were chosen. The $Da << 1$ condition can be used to obtain enzyme kinetic constants, K^*_m and V^*_{max}. The other condition, $Da >> 1$, can be used to obtain diffusion coefficient, *D* (Scheme 1). The calculation of *Da* is described as following.

Concerning *Da* in a plug-flow bioreactor with a catalytic plane surface, as shown in Figure 25, we start with the following set of simultaneous equations to solve eq (9) with boundary conditions eq (10).

$$\begin{cases} eq\,(12): \quad Da = \beta_n \tan \beta_n \\ eq\,(14): \ \alpha_\tau = 1 - \dfrac{[S]_{UV}}{[S]_o} = 1 - 4\sum_{n=1}^{\infty} \dfrac{\sin^2 \beta_n}{\beta_n[\sin(2\beta_n) + 2\beta_n]} \exp(-\dfrac{D\beta_n^2}{H^2}\tau) \end{cases} \tag{A29}$$

We use Newton-Raphson method to calculate the eigenvalues in eq (12), and we can set the function $f(\beta_n)$:

$$f(\beta_n) = \tan \beta_n - \frac{Da}{\beta_n} \tag{A30}$$

and then the iterative formula for $\beta_{n,m+1}$ is

$$\beta_{n,m+1} = \beta_{n,m} - \frac{f(\beta_{n,m})}{f'(\beta_{n,m})} = \frac{\tan \beta_{n,m} - \dfrac{Da}{\beta_{n,m}}}{\sec^2 \beta_{n,m} + \dfrac{Da}{\beta_{n,m}^2}}, \tag{A31}$$

where subscripts n and m represent the nth eigenvalue and the mth approximation in the iterative process, respectively.

Example A3 Determine the Da of the bioreactor shown in Figure 2 using the following parameters: height H = 1.67x10^{-4} m, the flow rate with space time τ = 480 s (or 8 min), the substrate diffusion coefficient, D = 3.92x10^{-10} m^2/s, the inlet and the outlet concentration of substrate, $[S]_o$ = 8.00 μM, and $[S]_{UV}$ = 6.76 μM (determined by UV-Vis spectrophotometer), respectively.

Sol: The detected reaction fraction is α_τ = 1-($[S]_{UV}$ / $[S]_o$) = 1-(6.76 / 8.00) = 0.155. We start to guess Da = 0.02 and make initial guesses for eigenvalues $\beta_{11} = \pi/4$, $\beta_{21} = 5\pi/4$, $\beta_{31} = 9\pi/4$, …, $\beta_{n1} = (4n\text{-}3)\pi/4$, and then use Newton-Raphson method and choose eq (A30) as the iterative equation to determine the corresponding eigenvalues. The following table shows the result for the first twenty eigenvalues of eq (A31) with the 8th approximation. In fact, if we have the eigenvalues to nine decimal places, then we only need seven iterations (m = 7), shown as the following table.

$\beta_{n,m}$	m = 1	m = 2	m = 3	m = 4	m = 5	m = 6	m = 7	m = 8
n = 1	0.785398163	0.305903828	0.115235347	0.138180132	0.140924588	0.140951674	0.140951676	0.140951676
n = 2	3.926990817	3.429859664	3.163075685	3.147949528	3.147945917	3.147945917	3.147945917	3.147945917
n = 3	7.068583471	6.570097948	6.301588401	6.286369852	6.286366784	6.286366784	6.286366784	6.286366784
n = 4	10.210176124	9.711203403	9.442135991	9.426902390	9.426899546	9.426899546	9.426899546	9.426899546
n = 5	13.351768778	12.852545746	12.583203249	12.567964688	12.567961961	12.567961961	12.567961961	12.567961961
n = 6	16.493361431	15.993986093	15.724479840	15.709239059	15.709236404	15.709236404	15.709236404	15.709236404
n = 7	19.634954085	19.135476336	18.865861465	18.850619502	18.850616894	18.850616894	18.850616894	18.850616894
n = 8	22.776546739	22.276995416	22.007303234	21.992060567	21.992057994	21.992057994	21.992057994	21.992057994
n = 9	25.918139392	25.418532660	25.148782646	25.133539525	25.133536978	25.133536978	25.133536978	25.133536978
n = 10	29.059732046	28.560082081	28.290287178	28.275043746	28.275041220	28.275041220	28.275041220	28.275041220
n = 11	32.201324699	31.701640064	31.431809306	31.416565653	31.416563143	31.416563143	31.416563143	31.416563143
n = 12	35.342917353	34.843204296	34.573344239	34.558100422	34.558097925	34.558097925	34.558097925	34.558097925
n = 13	38.484510006	37.984773225	37.714888780	37.699644838	37.699642352	37.699642352	37.699642352	37.699642352
n = 14	41.626102660	41.126345778	40.856440714	40.841196675	40.841194198	40.841194198	40.841194198	40.841194198
n = 15	44.767695314	44.267921183	43.997998459	43.982754342	43.982751874	43.982751874	43.982751874	43.982751874
n = 16	47.909287967	47.409498872	47.139560854	47.124316674	47.124314213	47.124314213	47.124314213	47.124314213
n = 17	51.050880621	50.551078422	50.281127028	50.265882797	50.265880342	50.265880342	50.265880342	50.265880342
n = 18	54.192473274	53.692659504	53.422696315	53.407452040	53.407449591	53.407449591	53.407449591	53.407449591
n = 19	57.334065928	56.834241865	56.564268196	56.549023885	56.549021440	56.549021440	56.549021440	56.549021440
n = 20	60.475658582	59.975825304	59.705842262	59.690597920	59.690595479	59.690595479	59.690595479	59.690595479

Taking the values of H, τ, D, $[S]_o$, $\beta_{1,8}$, $\beta_{2,8}$, $\beta_{3,8}$, …, $\beta_{20,8}$ into eq (24), we can predict the outlet concentration $[S]_{UV}$

$$[S]_{UV} = 4[S]_o \sum_{n=1}^{\infty} \frac{\sin^2 \beta_{n,8}}{\beta_{n,8}[\sin(2\beta_{n,8}) + 2\beta_{n,8}]} \exp(-\frac{D\beta_{n,8}^2}{H^2}\tau)$$

$$\approx 4(8.00\mu M) \sum_{n=1}^{20} \frac{\sin^2 \beta_{n,8}}{\beta_{n,8}[\sin(2\beta_{n,8}) + 2\beta_{n,8}]} \exp(-\frac{(3.92\times10^{-10} m^2/s)\beta_{n,8}^2}{(1.67\times10^{-4} m)^2}(480s))$$

$$= 32.00\mu M(2.1681\times10^{-1} + 2.8677\times10^{-37} + 1.1977\times10^{-130} + 5.5474\times10^{-285} + ...)$$

$$= 6.938\mu M > 6.76\mu M \text{ (detected value)}$$

Note that in most cases, such as this example, we can estimate the value of $[S]_{UV}$ by summing up only the first term of the series and use the set of simultaneous equations eqs (A29) to predict *Da* and $[S]_{UV}$.

Repeating the procedure for searching a more accurate value, we can continue to try other values of *Da* until the estimated value of $[S]_{UV}$ equals to or is near to that of the detected. The following table shows the result of finding *Da* to the desired degree of accuracy (three decimal places here). We have *Da* = 0.024 << 1, so this catalytic system is surface reaction limited.

Da	$\beta_{1,7}$	α_τ (predict value)	
0.0200	0.140951676	0.1328	
0.0210	0.144408517	0.1389	
0.0220	0.147782303	0.1449	
0.0230	0.151078600	0.1510	
0.0240	0.154302376	0.1569	0.1550 (detected value of α_τ)
0.0231	0.151404164	0.1515	
0.0232	0.151729008	0.1521	
0.0233	0.152053136	0.1528	
0.0234	0.152376553	0.1534	
0.0235	0.152699264	0.1539	
0.0236	0.153021272	0.1545	
0.0237	0.153342584	0.1551	0.1550 (detected value of α_τ)

Besides, there are two extreme cases for this reactor system to calculate approximate eigenvalues, β_n, the transfer limited condition and the surface reaction limited condition, as explained in the following:

Case 1. Mass transfer limited condition, *Da* >> 1. Figure A3(a) shows that we must find the intersections of *cot(β)* and *β/Da* to find the eigenvalues β_n. As shown in Figure A3(b), the curve of y_2 will be very close to *β*-axis, so the eigenvalues will get closer and closer to the points of *β*-intersection of the curve of y_1. According to Figure A3(b), these intersections, or the eigenvalues, are

$$\beta_1 = \frac{\pi}{2}, \quad \beta_2 = \frac{3\pi}{2}, \quad \beta_3 = \frac{5\pi}{2} \ldots, \quad \beta_n = \frac{(2n-1)\pi}{2} \qquad \text{for small and moderate } n\text{s} \qquad \text{(A32)}$$

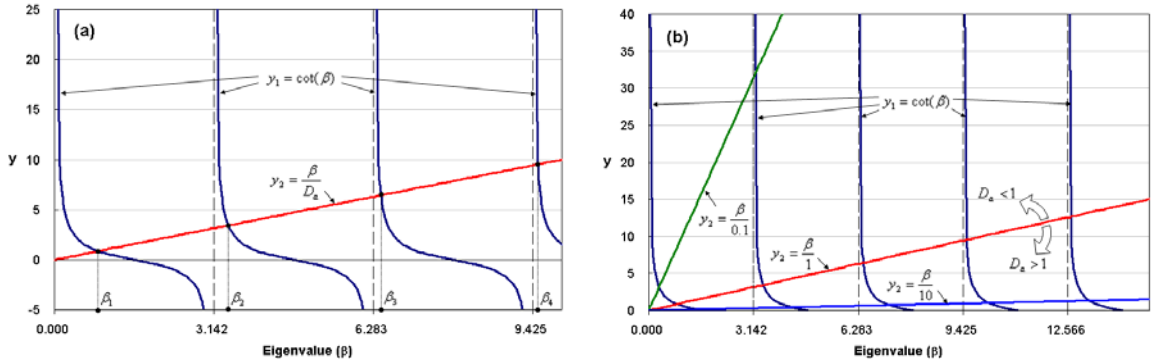

Figure A3 Curves of $y_1 = \cot(\beta)$ and $y_2 = \frac{\beta}{Da}$. The eigenvalues are the *β*-values of the points of intersection. (a) Eigenvalues, β_n, when *Da* = 1. (b) The points of intersection vary with *Da*.

Case 2. Surface reaction limited condition, *Da* << 1. For the first eigenvalue, the set of simultaneous equations (A29) can be estimated as

$$\lim_{\beta \to 0} \tan(\beta_1) \approx \beta_1 = \frac{Da}{\beta_1} \quad \text{or} \quad \beta_1 \approx \sqrt{Da} \qquad \text{(A33)}$$

Comparing $\sqrt{Da}$ with $\beta_{1,7}$ in example 1 as following table, $\beta_1 \approx \sqrt{Da}$ is a good approximation for *Da* <<1.

Da	$\sqrt{Da}$	$\beta_{1,7}$
0.0200	0.1414	0.140951676
0.0210	0.1449	0.144408517
0.0220	0.1483	0.147782303
0.0230	0.1517	0.151078600
0.0240	0.1549	0.154302376
0.0231	0.1520	0.151404164
0.0232	0.1523	0.151729008
0.0233	0.1526	0.152053136
0.0234	0.1530	0.152376553
0.0235	0.1533	0.152699264
0.0236	0.1536	0.153021272
0.0237	0.1539	0.153342584

For the $n \geq 2$ eigenvalues, from Figure A3(b) it seems clear that the eigenvalues get closer and closer to the vertical asymptotes of the curves of y_1; that is,

$$\beta_2 = \pi, \ \beta_3 = 2\pi, \ \ldots, \ \beta_n = (n-1)\pi \tag{A34}$$

Diffusion Coefficient, *D*, and Rate Constant of Surface Reaction, k_s. Approximations skillfully done as described above allows us to derive useful formula for the derivation of (a) the diffusion coefficient, *D*, of substrate in mass transfer limited condition and predict (b) the *Da* and surface rate constant, k_s, in surface reaction limited condition.

(a) Diffusion Coefficient of Substrate in Mass Transfer Limited Condition when *Da* >> 1

As shown in Example A3, only the first term of the series in eq (14) need to be concerned for a good approximation. Substituting eq (A32) $\beta_1 = \frac{\pi}{2}$ into eq (14) gives the diffusion coefficient of substrate

$$D \approx \frac{4H^2}{\pi^2 \tau} \ln\left(\frac{8[S]_o}{\pi(\pi-1)[S]_{UV}}\right) \tag{A35}$$

This is a good approximation to the diffusion coefficient of substrate as long as *Da* >> 1. Eq (A35) also indicates that this scheme can be designed to measure diffusion coefficient of substrate when the rate of reaction is much faster than the rate of mass transport of substrate

(perpendicular to the catalytic surface in this case) or in an efficiently enzyme-catalyzed reaction.

(b) Damkohler number, *Da*, and Surface Rate Constant, k_s, in Surface Reaction Limited Condition when *Da* << 1

We also concern only the first term of the series in eq (14) as Example A3. Substituting eq (A33) $\beta_1 \approx \sqrt{Da}$ into eq (14), then

$$\frac{[S]_{UV}}{4[S]_o} \approx \frac{\sin^2\sqrt{Da}}{\sqrt{Da}\left[\sin(2\sqrt{Da})+2\sqrt{Da}\right]}\exp(-\frac{DDa}{H^2}\tau)$$

$$= \frac{\sin\sqrt{Da}}{\sqrt{Da}}\frac{\sin\sqrt{Da}}{2(\sin\sqrt{Da}\cos\sqrt{Da}+\sqrt{Da})}\exp(-\frac{DDa}{H^2}\tau)$$

$$= \frac{\sin\sqrt{Da}}{\sqrt{Da}}\frac{1}{2(\cos\sqrt{Da}+\frac{\sqrt{Da}}{\sin\sqrt{Da}})}\exp(-\frac{DDa}{H^2}\tau) \quad \text{(A36)}$$

An appropriate approximation gives $(\frac{\sin\sqrt{Da}}{\sqrt{Da}})\Big|_{Da<<1} \approx 1$ and $\cos\sqrt{Da}\Big|_{Da<<1} \approx 1$, so eq (A36) can be rewritten as

$$Da \approx \frac{H^2}{D\tau}\ln(\frac{[S]_o}{[S]_{UV}}) \quad \text{(A37)}$$

or $$k_s \approx \frac{H}{\tau}\ln(\frac{[S]_o}{[S]_{UV}}) \quad \text{(A38)}$$

Using eq (A37) to estimate *Da* in the condition of Example A3,

$$Da \approx \frac{H^2}{D\tau}\ln(\frac{[S]_o}{[S]_{UV}}) = \frac{(1.67\times10^{-4}m)^2}{(3.92\times10^{-10}m^2/s)(480s)}\ln(\frac{8.00\mu M}{6.76\mu M}) = 0.0250$$

Consequently, this dimensionless *Da* is very close to the value of 0.024 evaluated in Example A3. Since *Da* is the ratio of the characteristic time scales for mixing and reaction, we need to concern the accuracy only in the scale of order rather than in what decimal places.

Therefore, eq (A38) allows us to predict the surface rate constant, k_s (m/s) when the rate of reaction is much slower than the rate of mass transport of substrate (perpendicular to the catalytic surface in this case) or in slow to moderately fast catalytic reactions.

References and Bibliography

[1] H.C. Lin, M.H. Lee, C.J. Su, T.Y. Huang, C.C. Lee, Y.S. Yang, A simple and low-cost method to fabricate TFTs with poly-Si nanowire channel. *IEEE Electron Device Letters* 26 (**2005**) 643-645.

[2] H.C. Lin, C.J. Su, C.Y. Hsiao, Y.S. Yang, T.Y. Huang, Water passivation effect on polycrystalline silicon nanowires. *Applied Physics Letters* 91 (**2007**) 202113-202115.

[3] C.H. Lin, C.Y. Hsiao, C.H. Hung, Y.R. Lo, C.C. Lee, C.J. Su, H.C. Lin, F.H. Ko, T.Y. Huang, Y.S. Yang, Ultrasensitive detection of dopamine using a polysilicon nanowire field-effect transistor. *Chemical Communications* (**2008**) 5749-5751.

[4] C.Y. Hsiao, C.H. Lin, C.H. Hung, C.J. Su, Y.R. Lo, C.C. Lee, H.C. Lin, F.H. Ko, T.Y. Huang, Y.S. Yang, Novel poly-silicon nanowire field effect transistor for biosensing application. *Biosensors & Bioelectronics* 24 (**2009**) 1223-1229.

[5] C.C. Lee, H.P. Chiang, K.L. Li, F.H. Ko, C.Y. Su, Y.S. Yang, Surface Reaction Limited Model for the Evaluation of Immobilized Enzyme on Planar Surfaces. *Analytical Chemistry* 81 (**2009**) 2737-2744.

[6] J.T. Hu, T.W. Odom, C.M. Lieber, Chemistry and physics in one dimension: Synthesis and properties of nanowires and nanotubes. *Accounts of Chemical Research* 32 (**1999**) 435-445.

[7] H.C. Lin, S.M. Sze, *Nanoelectronic technology: in search of the ultimate device structure*, Wiley, New York, 2004.

[8] B. Doyle, B. Boyanov, S. Datta, M. Doczy, S. Hareland, B. Jin, J. Kavalieros, T. Linton, R. Rios, R. Chau, *Tri-Gate Fully-Depleted CMOS Transistors: Fabrication, Design and Layout*, IEEE Symp. VLSI Technol. Dig. Tech., 2003, pp. 133-134.

[9] X.F. Duan, Y. Huang, C.M. Lieber, Nonvolatile memory and programmable logic from molecule-gated nanowires. *Nano Letters* 2 (**2002**) 487-490.

[10] X.F. Duan, C.M. Niu, V. Sahi, J. Chen, J.W. Parce, S. Empedocles, J.L. Goldman, High-performance thin-film transistors using semiconductor nanowires and nanoribbons. *Nature* 425 (**2003**) 274-278.

[11] Y. Cui, Q.Q. Wei, H.K. Park, C.M. Lieber, Nanowire nanosensors for highly sensitive and selective detection of biological and chemical species. *Science* 293 (**2001**) 1289-1292.

[12] F.-L. Yang, D.-H. Lee, H.-Y. Chen, C.-Y. Chang, S.-D. Liu, C.-C. Huang, T.-X. Chung, H.-W. Chen, C.-C. Huang, Y.-H. Liu, C.-C. Wu, C.-C. Chen, S.-C. Chen, Y.-T. Chen, Y.-H. Chen, C.-L. Chen, B.-W. Chan, P.-F. Hsu, J.-H. Shieh, H.-J. Tao, Y.-C. YEO, Y. Li, L.-W. Lee, P. Chen, M.-S. Liang, C. Hu, *5nm-Gate Nanowire FinFET*, IEEE Symp. VLSI Technol. Dig. Tech., 2004, pp. 196-197.

[13] H.C. Lin, M.F. Wang, F.J. Hou, H.N. Lin, C.Y. Lu, J.T. Liu, T.Y. Huang, High-performance p-channel Schottky-barrier SOI FinFET featuring self-aligned PtSi source/drain and electrical junctions. *IEEE Electron Device Letters* 24 (**2003**) 102-104.

[14] M.D. Austin, H.X. Ge, W. Wu, M.T. Li, Z.N. Yu, D. Wasserman, S.A. Lyon, S.Y. Chou, Fabrication of 5 nm linewidth and 14 nm pitch features by nanoimprint lithography. *Applied Physics Letters* 84 (**2004**) 5299-5301.

[15] Y.K. Choi, J. Zhu, J. Grunes, J. Bokor, G.A. Somorjai, Fabrication of sub-10-nm silicon nanowire arrays by size reduction lithography. *Journal of Physical Chemistry B* 107 (**2003**) 3340-3343.

[16] A.M. Morales, C.M. Lieber, A laser ablation method for the synthesis of crystalline semiconductor nanowires. *Science* 279 (**1998**) 208-211.

[17] D.W. Wang, Q. Wang, A. Javey, R. Tu, H.J. Dai, H. Kim, P.C. McIntyre, T. Krishnamohan, K.C. Saraswat, Germanium nanowire field-effect transistors with SiO2 and high-kappa HfO2 gate dielectrics. *Applied Physics Letters* 83 (**2003**) 2432-2434.

[18] N. Wang, Y.F. Zhang, Y.H. Tang, C.S. Lee, S.T. Lee, SiO2-enhanced synthesis of Si nanowires by laser ablation. *Applied Physics Letters* 73 (**1998**) 3902-3904.

[19] X.F. Duan, C.M. Lieber, General synthesis of compound semiconductor nanowires. *Advanced Materials* 12 (**2000**) 298-302.

[20] X.F. Duan, Y. Huang, Y. Cui, J.F. Wang, C.M. Lieber, Indium phosphide nanowires as building blocks for nanoscale electronic and optoelectronic devices. *Nature* 409 (**2001**) 66-69.

[21] Y. Huang, X.F. Duan, Q.Q. Wei, C.M. Lieber, Directed assembly of one-dimensional nanostructures into functional networks. *Science* 291 (**2001**) 630-633.

[22] E. Pavlovic, S. Oscarsson, A.P. Quist, Nanoscale site-specific immobilization of proteins through electroactivated disulfide exchange. *Nano Letters* 3 (**2003**) 779-781.

[23] C.J. Su, H.C. Lin, T.Y. Huang, High-performance TFTs with Si nanowire channels enhanced by metal-induced lateral crystallization. *IEEE Electron Device Letters* 27 (**2006**) 582-584.

[24] S.J. Park, T.A. Taton, C.A. Mirkin, Array-based electrical detection of DNA with nanoparticle probes. *Science* 295 (**2002**) 1503-1506.

[25] H.C. Lin, C.J. Su, High-performance poly-Si nanowire NMOS transistors. *IEEE Transactions on Nanotechnology* 6 (**2007**) 206-212.

[26] C.J. Su, H.C. Lin, H.H. Tsai, H.H. Hsu, T.M. Wang, T.Y. Huang, Operations of poly-Si nanowire thin-film transistors with a multiple-gated configuration. *Nanotechnology* 18 (**2007**).

[27] C.J. Su, H.C. Lin, H.H. Tsai, T.Y. Huang, W.X. Ni, *Fabrication and characterization of poly-Si nanowire devices with performance enhancement techniques*, IEEE, International Symposium on VLSI Technology, Systems and Applications, Hsinchu, TAIWAN, 2007, pp. 120-121.

[28] H.C. Lin, H.H. Hsu, C.J. Su, T.Y. Huang, A novel multiple-gate polycrystalline silicon nanowire transistor featuring an inverse-T gate. *IEEE Electron Device Letters* 29 (**2008**) 718-720.

[29] Z. Li, Y. Chen, X. Li, T.I. Kamins, K. Nauka, R.S. Williams, Sequence-specific label-free DNA sensors based on silicon nanowires. *Nano Letters* 4 (**2004**) 245-247.

[30] T.M. Su, Y.S. Yang, Mechanism of posttranslational regulation of phenol sulfotransferase: Expression of two enzyme forms through redox modification and nucleotide binding. *Biochemistry* 42 (**2003**) 6863-6870.

[31] T.G. Pai, K. Ohkimoto, Y. Sakakibara, M. Suiko, T. Sugahara, M.C. Liu, Manganese stimulation and stereospecificity of the dopa (3,4-dihydroxyphenylalanine)/tyrosine-sulfating activity of human monoamine-form phenol sulfotransferase - Kinetic studies

of the mechanism using wild-type and mutant enzymes. *Journal of Biological Chemistry* 277 (**2002**) 43813-43820.

[32] Y.S. Hsiao, Y.S. Yang, A single mutation converts the nucleotide specificity of phenol sulfotransferase from PAP to AMP. *Biochemistry* 41 (**2002**) 12959-12966.

[33] M. Suiko, Y. Sakakibara, H. Nakajima, H. Sakaida, M.C. Liu, Enzymic sulphation of dopa and tyrosine isomers by HepG2 human hepatoma cells: Stereoselectivity and stimulation by Mn2+. *Biochemical Journal* 314 (**1996**) 151-158.

[34] W.T. Chen, M.C. Liu, Y.S. Yang, Fluorometric assay for alcohol sulfotransferase. *Analytical Biochemistry* 339 (**2005**) 54-60.

[35] M. Seronferre, C.C. Lawrence, R.B. Jaffe, ROLE OF HCG IN REGULATION OF FETAL ZONE OF HUMAN FETAL ADRENAL-GLAND. *Journal of Clinical Endocrinology and Metabolism* 46 (**1978**) 834-837.

[36] C. Branden, J. Tooze, *Intoduction to protein structure*, Garland, New York, 1999.

[37] N.C. Price, L. Stevens, *Fundamentals of enzymology: the cell and molecular biology of catalytic proteins*, Oxford Univ. Press, New York, 1999.

[38] S.B. Lamb, D.C. Lamb, S.L. Kelly, D.C. Stuckey, Cytochrome P450 immobilisation as a route to bioremediation/biocatalysis. *FEBS Letters* 431 (**1998**) 343-346.

[39] D.R. Owens, New horizons - Alternative routes for insulin therapy. *Nature Reviews Drug Discovery* 1 (**2002**) 529-540.

[40] J. Krenkova, F. Foret, Immobilized microfluidic enzymatic reactors. *Electrophoresis* 25 (**2004**) 3550-3563.

[41] J.D. Newman, A.P.F. Turner, Home blood glucose biosensors: a commercial perspective. *Biosensors & Bioelectronics* 20 (**2005**) 2435-2453.

[42] L.Q. Cao, Immobilised enzymes: science or art? *Current Opinion in Chemical Biology* 9 (**2005**) 217-226.

[43] T. Cha, A. Guo, X.Y. Zhu, Enzymatic activity on a chip: The critical role of protein orientation. *Proteomics* 5 (**2005**) 416-419.

[44] A.H. Talasaz, M. Nemat-Gorgani, Y. Liu, P. Stahl, R.W. Dutton, M. Ronaghi, R.W.

Davis, Prediction of protein orientation upon immobilization on biological and nonbiological surfaces. *Proceedings of the National Academy of Sciences of the United States of America* 103 (**2006**) 14773-14778.

[45] G. Hardie, Kinetic-behavior of membrane-bound, irreversible enzyme-systems-experimental and theoretical considerations. *Journal of Histochemistry & Cytochemistry* 30 (**1982**) 1083-1085.

[46] Y. Takakuwa, H. Nishino, Y. Ishibe, T. Ishibashi, Properties and kinetics of membrane-bound enzymes when both the enzyme and substrate are components of the same microsomal membrane – Studies of lathosterol 5-desaturase. *Journal of Biological Chemistry* 269 (**1994**) 27889-27893.

[47] S.K.H. Fung, P.A. Grudowski, C.H. Wu, V. Kolagunta, N. Cave, C.T. Yang, S.J. Lian, V. Adams, O. Zia, B. Min, N. Grove, K.H. Chen, W.J. Liang, D.H. Lee, H.T. Huang, J. Cheek, H.C. Tuan, *65nm SOICMOS technology for high performance microprocessor application*, IEEE, International Symposium on VLSI Technology, Systems and Applications, Hsinchu, TAIWAN, 2006, pp. 58-59.

[48] S. Bentley, X. Li, D.A.J. Moran, I.G. Thayne, Fabrication of 22 nm T-gates for HEMT applications. *Microelectronic Engineering* 85 (**2008**) 1375-1378.

[49] M.T. Neves-Petersen, T. Snabe, S. Klitgaard, M. Duroux, S.B. Petersen, Photonic activation of disulfide bridges achieves oriented protein immobilization on biosensor surfaces. *Protein Science* 15 (**2006**) 343-351.

[50] G. Wang, N.M. Thai, S.T. Yau, Preserved enzymatic activity of glucose oxidase immobilized on unmodified electrodes for glucose detection. *Biosensors & Bioelectronics* 22 (**2007**) 2158-2164.

[51] E. Ruiz-Hitzky, K. Ariga, Y.M. Lvov, *Bio-inorganic hybrid nanomaterials - strategies, syntheses, characterization and applications*, Wiley-VCH: Weinheim, 2007.

[52] A. Le Nel, N. Minc, C. Smadja, M. Slovakova, Z. Bilkova, J.M. Peyrin, J.L. Viovy, M. Taverna, Controlled proteolysis of normal and pathological prion protein in a microfluidic chip. *Lab on a Chip* 8 (**2008**) 294-301.

[53] Y. Ishige, M. Shimoda, M. Kamahori, Extended-gate FET-based enzyme sensor with ferrocenyl-alkanethiol modified gold sensing electrode. *Biosensors & Bioelectronics*

24 (**2009**) 1096-1102.

[54] G. Maruccio, A. Biasco, P. Visconti, A. Bramanti, P.P. Pompa, F. Calabi, R. Cingolani, R. Rinaldi, S. Corni, R. Di Felice, E. Molinari, M.R. Verbeet, G.W. Canters, Towards protein field-effect transistors: Report and model of prototype. *Advanced Materials* 17 (**2005**) 816-822.

[55] S.V. Dzyadevych, A.P. Soldatkin, Y.I. Korpan, V.N. Arkhypova, A.V. El'skaya, J.M. Chovelon, C. Martelet, N. Jaffrezic-Renault, Biosensors based on enzyme field-effect transistors for determination of some substrates and inhibitors. *Analytical and Bioanalytical Chemistry* 377 (**2003**) 496-506.

[56] G.Y. Tseng, J.C. Ellenbogen, Nanotechnology - Toward nanocomputers. *Science* 294 (**2001**) 1293-1294.

[57] N.J. Gleason, J.D. Carbeck, Measurement of enzyme kinetics using microscale steady-state kinetic analysis. *Langmuir* 20 (**2004**) 6374-6381.

[58] S. Fang, H.J. Lee, A.W. Wark, H.M. Kim, R.M. Corn, Determination of ribonuclease H surface enzyme kinetics by surface plasmon resonance imaging and surface plasmon fluorescence spectroscopy. *Analytical Chemistry* 77 (**2005**) 6528-6534.

[59] C.L. Wa, R.L. Cerny, D.S. Hage, Identification and quantitative studies of protein immobilization sites by stable isotope labeling and mass spectrometry. *Analytical Chemistry* 78 (**2006**) 7967-7977.

[60] M. Bartolini, V. Cavrini, V. Andrisano, Characterization of reversible and pseudo-irreversible acetylcholine sterase inhibitors by means of an immobilized enzyme reactor. *Journal of Chromatography A* 1144 (**2007**) 102-110.

[61] R. Freeman, R. Gill, I. Willner, Following a protein kinase activity using a field-effect transistor device. *Chemical Communications* (**2007**) 3450-3452.

[62] M.B. Kerby, R.S. Legge, A. Tripathi, Measurements of kinetic parameters in a microfluidic reactor. *Analytical Chemistry* 78 (**2006**) 8273-8280.

[63] G.H. Seong, J. Heo, R.M. Crooks, Measurement of enzyme kinetics using a continuous-flow microfluidic system. *Analytical Chemistry* 75 (**2003**) 3161-3167.

[64] M.D. Lilly, W.E. Hornby, E.M. Crook, The kinetics of carboxymethylcellulose-ficin in

packed beds. *Biochemical Journal* 100 (**1966**) 718-723.

[65] L.A. DeLouise, B.L. Miller, Enzyme immobilization in porous silicon: Quantitative analysis of the kinetic parameters for glutathione-S-transferases. *Analytical Chemistry* 77 (**2005**) 1950-1956.

[66] C.J. Wong, *An embedding Method for Simulation of Immobilized Enzyme Kinetics and Transport in Sessile Hydrogel Drops*, Claremont Graduate University, 2005.

[67] F. Xu, H.S. Ding, A new kinetic model for heterogeneous (or spatially confined) enzymatic catalysis: Contributions from the fractal and jamming (overcrowding) effects. *Applied Catalysis A-General* 317 (**2007**) 70-81.

[68] H. Xiao, *Introduction to semiconductor manufacturing technology*, Prentice Hall, New Jersey, 2000.

[69] M.W. Duffel, A.D. Marshall, P. McPhie, V. Sharma, W.B. Jakoby, Enzymatic aspects of the phenol (aryl) sulfotransferases. *Drug Metabolism Reviews* 33 (**2001**) 369-395.

[70] R.M. Weinshilboum, D.M. Otterness, I.A. Aksoy, T.C. Wood, C. Her, R.B. Raftogianis, Sulfotransferase molecular biology: cDNAs and genes. *FASEB Journal* 11 (**1997**) 3-14.

[71] C. Clarke, P. Thorburn, D. McDonald, J.B. Adams, Enzymic-synthesis of steroid sulfates .XV. structural domains of estrogen sulfotransferase. *Biochimica Et Biophysica Acta* 707 (**1982**) 28-37.

[72] E. Chapman, M.D. Best, S.R. Hanson, C.H. Wong, Sulfotransferases: Structure, mechanism, biological activity, inhibition, and synthetic utility. *Angewandte Chemie-International Edition* 43 (**2004**) 3526-3548.

[73] B. Limoges, D. Marchal, F. Mavre, J.M. Saveant, Electrochemistry of immobilized redox enzymes: Kinetic characteristics of NADH oxidation catalysis at diaphorase monolayers affinity immobilized on electrodes. *Journal of the American Chemical Society* 128 (**2006**) 2084-2092.

[74] M.M. Orosco, C. Pacholski, M.J. Sailor, Real-time monitoring of enzyme activity in a mesoporous silicon double layer. *Nature Nanotechnology* 4 (**2009**) 255-258.

[75] J. Su, M.R. Bringer, R.F. Ismagilov, M. Mrksich, Combining microfluidic networks

and peptide arrays for multi-enzyme assays. *Journal of the American Chemical Society* 127 (**2005**) 7280-7281.

[76] R.A. Copeland, *Enzymes: a practical introduction to structure, mechanism, and data analysis*, Wiley-VCH, Inc., 2000.

[77] R. Eisenthal, M.J. Danson, *Enzyme Assays: A Practical approach*, Oxford Univ. Press, UK 2002.

[78] E. Ishikawa, M. Imagawa, S. Hashida, S. Yoshitake, Y. Hamaguchi, T. Ueno, Enzyme-labeling of antibodies and their fragments for enzyme-immunoassay and immunohistochemical staining. *Journal of Immunoassay* 4 (**1983**) 209-327.

[79] C.Y. Tsai, T.L. Chang, R. Uppala, C.C. Chen, F.H. Ko, P.H. Chen, Electrical detection of protein using gold nanoparticles and nanogap electrodes. *Japanese journal of applied physics* 44 (**2005**) 5711-5716.

[80] R.D. Schmid, R. Verger, Lipases: Interfacial enzymes with attractive applications. *Angewandte Chemie-International Edition* 37 (**1998**) 1609-1633.

[81] T. Sakata, Y. Miyahara, Detection of DNA recognition events using multi-well field effect devices. *Biosensors & Bioelectronics* 21 (**2005**) 827-832.

[82] F.H. Ko, Z.H. Yeh, C.C. Chen, T.F. Liu, Self-aligned platinum-silicide nanowires for biomolecule sensing. *Journal of Vacuum Science & Technology B* 23 (**2005**) 3000-3005.

[83] C.C. Chen, C.Y. Tsai, F.H. Ko, C.C. Pun, H.L. Chen, P.H. Chen, Room temperature operation of a coulomb blockade sensor fabricated by self-assembled gold nanoparticles using deoxyribonucleic acid hybridization. *Japanese journal of applied physics* 43 (**2004**) 3843-3848.

[84] S.X. Zhang, N. Wang, Y.M. Niu, C.Q. Sun, Immobilization of glucose oxidase on gold nanoparticles modified Au electrode for the construction of biosensor. *Sensors and Actuators B-Chemical* 109 (**2005**) 367-374.

[85] D. van der Voort, C.A. McNeil, R. Renneberg, J. Korf, W.T. Hermens, J.F.C. Glatz, Biosensors: basic features and application for fatty acid-binding protein, an early plasma marker of myocardial injury. *Sensors and Actuators B-Chemical* 105 (**2005**)

50-59.

[86] C. Lind, R. Gerdes, Y. Hamnell, I. Schuppe-Koistinen, H.B. von Lowenhielm, A. Holmgren, I.A. Cotgreave, Identification of S-glutathionylated cellular proteins during oxidative stress and constitutive metabolism by affinity purification and proteomic analysis. *Archives of Biochemistry and Biophysics* 406 (**2002**) 229-240.

[87] Y.B. Ji, V. Toader, B.M. Bennett, Regulation of microsomal and cytosolic glutathione S-transferase activities by S-nitrosylation. *Biochemical Pharmacology* 63 (**2002**) 1397-1404.

[88] R. Gopalakrishna, S. Jaken, Protein kinase C signaling and oxidative stress. *Free Radical Biology and Medicine* 28 (**2000**) 1349-1361.

[89] C.Y. Huang, Y.S. Yang, The role of metal on imide hydrolysis: metal content and pH profiles of metal ion-replaced mammalian imidase. *Biochemical and Biophysical Research Communications* 297 (**2002**) 1027-1032.

[90] K.P. Brooks, E.A. Jones, B.D. Kim, E.G. Sander, Bovine liver dihydropyrimidine amidohydrolase - purification, properties, and characterization as a zinc metalloenzyme. *Archives of Biochemistry and Biophysics* 226 (**1983**) 469-483.

[91] J. Kautz, K.D. Schnackerz, Purification and properties of 5,6-dihydropyrimidine amidohydrolase from calf liver. *European Journal of Biochemistry* 181 (**1989**) 431-435.

[92] M. Kikugawa, M. Kaneko, S. Fujimotosakata, M. Maeda, K. Kawasaki, T. Takagi, N. Tamaki, Purification, characterization and inhibition of dihydropyrimidinase from rat-liver. *European Journal of Biochemistry* 219 (**1994**) 393-399.

[93] O. May, M. Siemann, M.G. Siemann, C. Syldatk, Catalytic and structural function of zinc for the hydantoinase from Arthrobacter aurescens DSM 3745. *Journal of Molecular Catalysis B-Enzymatic* 4 (**1998**) 211-218.

[94] O. May, M. Siemann, M.G. Siemann, C. Syldatk, The hydantoin amidohydrolase from Arthrobacter aurescens DSM 3745 is a zinc metalloenzyme. *Journal of Molecular Catalysis B-Enzymatic* 5 (**1998**) 367-370.

[95] C.Y. Huang, Y.P. Chao, Y.S. Yang, Purification of industrial hydantoinase in one chromatographic step without affinity tag. *Protein Expression and Purification* 30

(**2003**) 134-139.

[96] T.M. Su, Y.S. Yang, Identification, purification, and characterization of a thermophilic imidase from pig liver. *Protein Expression and Purification* 19 (**2000**) 289-297.

[97] Y.S. Yang, S. Ramaswamy, W.B. Jakoby, RAT-LIVER IMIDASE. *Journal of Biological Chemistry* 268 (**1993**) 10870-10875.

[98] C. Syldatk, O. May, J. Altenbuchner, R. Mattes, M. Siemann, Microbial hydantoinases - industrial enzymes from the origin of life? *Applied Microbiology and Biotechnology* 51 (**1999**) 293-309.

[99] R. Olivieri, L. Angelini, L. Degen, E. Fascetti, Microbial transformation of racemic hydantoins to d-amino acids. *Biotechnology and Bioengineering* 23 (**1981**) 2173-2183.

[100] C. Syldatk, A. Laufer, R. Muller, H. Hoke, *Production of optically pure D- and L-a-amino acids by bioconversion of D,L-5-monosubstituted hydantoin derivatives*, Springer, Berlin, 1990.

[101] J. Ogawa, S. Shimizu, Microbial enzymes: new industrial applications from traditional screening methods. *Trends in Biotechnology* 17 (**1999**) 13-21.

[102] G. Carrea, S. Riva, Properties and synthetic applications of enzymes in organic solvents. *Angewandte Chemie-International Edition* 39 (**2000**) 2226-2254.

[103] A. Pandey, S. Benjamin, C.R. Soccol, P. Nigam, N. Krieger, V.T. Soccol, The realm of microbial lipases in biotechnology. *Biotechnology and Applied Biochemistry* 29 (**1999**) 119-131.

[104] M.J. Kim, M.Y. Choi, M.Y. Han, Y.K. Choi, J.K. Lee, J. Park, Asymmetric transformations of acyloxyphenyl ketones by enzyme-metal multicatalysis. *Journal of Organic Chemistry* 67 (**2002**) 9481-9483.

[105] A.B.L. Runmo, O. Pamies, K. Faber, J.E. Backvall, Dynamic kinetic resolution of gamma-hydroxy acid derivatives. *Tetrahedron Letters* 43 (**2002**) 2983-2986.

[106] O. Pamies, J.E. Backvall, Enzymatic kinetic resolution and chemoenzymatic dynamic kinetic resolution of delta-hydroxy esters. An efficient route to chiral delta-lactones. *Journal of Organic Chemistry* 67 (**2002**) 1261-1265.

[107] R.A. Gross, A. Kumar, B. Kalra, Polymer synthesis by in vitro enzyme catalysis. *Chemical Reviews* 101 (**2001**) 2097-2124.

[108] E. Katz, I. Willner, Integrated nanoparticle-biomolecule hybrid systems: Synthesis, properties, and applications. *Angewandte Chemie-International Edition* 43 (**2004**) 6042-6108.

[109] W.J. Parak, D. Gerion, T. Pellegrino, D. Zanchet, C. Micheel, S.C. Williams, R. Boudreau, M.A. Le Gros, C.A. Larabell, A.P. Alivisatos, Biological applications of colloidal nanocrystals. *Nanotechnology* 14 (**2003**) R15-R27.

[110] G.S. Huang, Y.S. Chen, H.W. Yeh, Measuring the flexibility of immunoglobulin by gold nanoparticles. *Nano Letters* 6 (**2006**) 2467-2471.

[111] X.H. Gao, Y.Y. Cui, R.M. Levenson, L.W.K. Chung, S.M. Nie, In vivo cancer targeting and imaging with semiconductor quantum dots. *Nature Biotechnology* 22 (**2004**) 969-976.

[112] N.L. Rosi, D.A. Giljohann, C.S. Thaxton, A.K.R. Lytton-Jean, M.S. Han, C.A. Mirkin, Oligonucleotide-modified gold nanoparticles for intracellular gene regulation. *Science* 312 (**2006**) 1027-1030.

[113] R. Baron, B. Willner, I. Willner, Biomolecule-nanoparticle hybrids as functional units for nanobiotechnology. *Chemical Communications* (**2007**) 323-332.

[114] S. Mann, W. Shenton, M. Li, S. Connolly, D. Fitzmaurice, Biologically programmed nanoparticle assembly. *Advanced Materials* 12 (**2000**) 147-150.

[115] C.M. Niemeyer, Nanoparticles, proteins, and nucleic acids: Biotechnology meets materials science. *Angewandte Chemie-International Edition* 40 (**2001**) 4128-4158.

[116] W. Beck, F.C. Brunner, P.U. Frasch, B. Ivancic, F.W. Schwerdt, T. Vogtmann, *Method for Stripping Layers of Organic Material*, U. S., 1975.

[117] P.C. Hiemenz, *Principles of Colloid and Surface Chemistry*, Marcel Dekker, New York, 1986.

[118] P.H. Rieger, *Electrochemistry*, Prentice-Hall, New Jersey, 1987.

[119] P. Vrabel, M. Polakovic, V. Stefuca, V. Bales, Analysis of mechanism and kinetics of

thermal inactivation of enzymes: evaluation of multi-temperature data applied to inactivation of yeast invertase. *Enzyme and Microbial Technology* 20 (**1977**) 348-354.

[120] S.M. Sze, *VLSI technology*, McGraw-Hill, New York, 1988.

[121] E.A. Amerasekera, F.N. Najm, *Failure mechanisms in semiconductor devices*, John Wiley & Sons, Chichester, 1997.

[122] O. Levenspiel, *Chemical reaction engineering*, Wiley, New York, 1999.

[123] J.R. Welly, C.E. Wicks, R.E. Wilson, *Fundamentals of momentum, heat, and mass transfer*, John Wiley & Sons, New York, 1984.

[124] C.R. Wilke, P. Chang, Correlation of diffusion coefficients in dilute solutions. *Aiche Journal* 1 (**1955**) 264-270.

[125] D.R. Lide, *CRC handbook of chemistry and physics*, CRC Press, Boca Raton, FL, 2004.

[126] T. Sato, D. Brown, B.F.G. Johnson, Nucleation and growth of nano-gold colloidal lattices. *Chemical Communications* (**1997**) 1007-1008.

[127] Y.S. Yang, S.W. Tsai, E.S. Lin, Effects of 3 '-phosphoadenosine 5 '-phosphate on the activity and folding of phenol sulfotransferase. *Chemico-Biological Interactions* 109 (**1998**) 129-135.

[128] E.S. Lin, Y.S. Yang, Colorimetric determination of the purity of 3 '-phospho adenosine 5'-phosphosulfate and natural abundance of 3 '-phospho adenosine 5 '-phosphate at picomole quantities. *Analytical Biochemistry* 264 (**1998**) 111-117.

[129] S.G. Burton, Development of bioreactors for application of biocatalysts in biotransformations and bioremediation. *Pure and Applied Chemistry* 73 (**2001**) 77-83.

[130] W.U. Wang, C. Chen, K.H. Lin, Y. Fang, C.M. Lieber, Label-free detection of small-molecule-protein interactions by using nanowire nanosensors. *Proceedings of the National Academy of Sciences of the United States of America* 102 (**2005**) 3208-3212.

[131] A.B. Kharitonov, M. Zayats, A. Lichtenstein, E. Katz, I. Willner, Enzyme monolayer-functionalized field-effect transistors for biosensor applications. *Sensors and Actuators B-Chemical* 70 (**2000**) 222-231.

[132] M.J. Schoning, M. Arzdorf, P. Mulchandani, W. Chen, A. Mulchandani, Towards a capacitive enzyme sensor for direct determination of organophosphorus pesticides: Fundamental studies and aspects of development. *Sensors* 3 (**2003**) 119-127.

[133] M.J. Schoning, M. Arzdorf, P. Mulchandani, W. Chen, A. Mulchandani, A capacitive field-effect sensor for the direct determination of organophosphorus pesticides. *Sensors and Actuators B-Chemical* 91 (**2003**) 92-97.

[134] G. Maruccio, P. Visconti, V. Arima, S. D'Amico, A. Blasco, E. D'Amone, R. Cingolani, R. Rinaldi, S. Masiero, T. Giorgi, G. Gottarelli, Field effect transistor based on a modified DNA base. *Nano Letters* 3 (**2003**) 479-483.

[135] R. Rinaldi, A. Biasco, G. Maruccio, V. Arima, P. Visconti, R. Cingolani, P. Facci, F. De Rienzo, R. Di Felice, E. Molinari, M.P. Verbeet, G.W. Canters, Electronic rectification in protein devices. *Applied Physics Letters* 82 (**2003**) 472-474.

[136] M.J. Matlosz, W. Ehrfeld, J.P. Baselt, *Microreaction Technology: IMRET 5: Proceedings of the Fifth International Conference on Microreaction Technology*, Springer-Verlag, Berlin, 2002.

[137] C.S. Wu, C.T. Wu, Y.S. Yang, F.H. Ko, An enzymatic kinetics investigation into the significantly enhanced activity of functionalized gold nanoparticles. *Chemical Communications* (**2008**) 5327-5329.

[138] S.J. Farlow, *Partial Differential Equations for Scientists and Engineers*, John Wiley & Sons, Inc., Singapore, 1982.

[139] S.I. Grossman, W.R. Derrick, *Advanced Engineering Mathematics*, Harper and Row, New York, 1988.

[140] D.P. Shoemaker, C.W. Garland, J.W. Nibler, *Experiments in physical chemistry*, McGraw-Hill, New York, 1996.

[141] P.J. Donlup, K.R. Harris, D.J. Young, *Experimental Methods for Studying Diffusion in Gases, Liquids, and Solids*, Wiley-Interscience, New York, 1922.

[142] G. Le Bas, *The Molecular Volumes of Liquid Chemical Compounds*, Longmans, Green & Co., London, 1915.

[143] T.K. Sherwood, R.L. Pigford, *Absorption and Extraction*, McGraw-Hill, New York,

1952.

[144] R.C. Reid, J.M. Praunsmitz, T.K. Sherwood, *The Properties of Gases and Liquids*, McGraw-Hill, New York, 1977.

[145] M.L. Shuler, F. Kargi, *Bioprocess Engineering: Basic Concepts*, Prentice Hall PTR, 2002.

[146] W.E. Hornby, M.D. Lilly, Some changes in the reactivity of enzymes resulting from their chemical attachment to water-insoluble derivatives of cellulose. *Biochemical Journal* 107 (**1968**) 669-674.

[147] K.J. Laidler, J.H. Meiser, *Physical Chemistry*, Benjamin-Cummings, 1982.

[148] M.J. Matlosz, W. Ehrfeld, J.P. Baselt, *Proceedings of the Fifth International Conference on Microreaction Technology*, Springer-Verlag, Berlin, 2002.

Curriculum Vitae

I. Education

PH.D. 7/2009 Doctor of Philosophy in Biological Science and Technology
National Chiao-Tung University
- Dissertation: A Systematic and Standardized Approach to Modeling and Measuring Immobilized Enzyme Kinetics
- Committee: Chang, Chun-Yen / 張俊彥 (Chair)
Huang, Tiao-Yuan / 黃調元
Yang, Yuh-Shyong / 楊裕雄 (Advisor)
Lyu, Ping-Chiang / 呂平江
Ko, Fu-Hsiang / 柯富祥
Hsu, Long / 徐 琅
Lu, Shiang-Cheng / 盧向成
Kao, Jiann-Shiun / 高健薰

(2008 全球金融風暴)

M.SC. 6/1995 Master of Science in Materials Science and Engineering
National Sun Yat-Sen University
- Thesis: Impurity Enhanced Intermixing in $Si_{1-x}Ge_x/Si$ Quantum Well Structure
- Readers: Wang, Dong-Po / 王東波
Hsieh, Kuang-Yeu / 謝光宇 (Advisor)
Chang, Ting-Chang / 張鼎張

(1994 交大生科所成立)

B.S. 6/1993 Bachelor of Science in Chemical Engineering
Chung Yuan Christian University

(賽保拾頭, 六輕延若十年, 1991 動工)

II. Employment History

3/1999-9/2003 Principal R&D Integration Engineer / Logic Technology Division
Senior R&D Integration Engineer / Mixed Mode / RF Division
Taiwan Semiconductor Manufacturing Co., Ltd.
(台積電 / 2000 股價 219)

6/1997-12/1998 Senior Etch Process Engineer / Fab II
United Microelectronics Corporation
(聯 電 / 1997 股價 187)

11/1995-6/1997 兵器連 副連長
八一迫擊砲 排長
陸軍步兵/168 師/504 旅/步 7 營/兵器連 (澎防部)
(1996 台海飛彈危機)

7/1995-11/1995 義務役預備軍官 45 期 - 八一迫擊砲少尉軍官訓 (陸軍步兵學校)

III. Publication

(1) Lee, C.-C.; Wu, C.-S.; Chiang, H.-P.; Su, C.-Y.; Li, K.-L.; Lo, Y.-R.; Ko, F.-H.; Yang, Y.-S. A New Approach to Measuring Immobilized Enzyme Kinetics Using Continuous-flow Assays, (in progress).

(2) Lee, C.-C.; Chiang, H.-P.; Li, K.-L.; Ko, F.-H.; Su, C.-Y.; Yang, Y.-S. (2009) Surface Reaction Limited Model for Evaluation of Immobilized Enzyme on Planar Surfaces, *Anal. Chem.* 81, 2737-2744. (IF = 5.712, 1/70 in CHEMISTRY, ANALYTICAL)

(3) Hsiao, C.-Y.; Lin, C.-H.; Hung, C.-H.; Su, C.-J.; Lo, Y.-R.; Lee, C.-C.; Lin, H.-C.; Ko, F.-H.; Huang, T.-Y.; Yang, Y.-S. (2009) Novel Poly-silicon Nanowire Field Effect Transistor for Biosensing Application, *Biosens. Bioelectron.*, 24, 1223-1229. (IF = 5.143, 3/70 in CHEMISTRY, ANALYTICAL)

(4) Lin, C.-H.; Hsiao, C.-Y.; Hung, C.-H.; Lo, Y.-R.; Lee, C.-C.; Su, C.-J.; Lin, H.-C.; Ko, F.-H.; Huang, T.-Y.; Yang, Y.-S. (2008) Ultrasensitive Detection of Dopamine Using a Polysilicon Nanowire Field-effect Transitor, *Chem. Comm.*, 5749-5751. (IF = 5.340, 13/125 in CHEMISTRY, MULTIDISCIPLINARY)

(5) Lin, H.-C.; Lee, M.-H.; Su, C.-J.; Huang, T.-Y.; Lee, C.-C.; and Yang, Y.-S. (2005) A Simple and Low-Cost Method to Fabreicate Thin Film Transistors with Poly-Si Nanowire Channel, *IEEE Electron Device Lett.*, 26, 643-645. (IF = 3.049, 23/229 in ENGINEERING, ELECTRICAL & ELECTRONIC)

(6) 李政哲,莊旻傑,林珮羽,楊裕雄 (2005) 微/奈米生物電子元件之發展現況與前瞻, 科儀新知, 第 148 期, 72-88 頁.

(7) 莊旻傑,蕭程允,李政哲,楊裕雄 (2005) 奈米碳管於生物檢測之應用, 微系統暨奈米科技協會會刊, 第 13 期, 24-36 頁.

(8) Li, C.-C.; Hsieh, K.-Y.; Wang, D.-P.; Tsai, W.-C.; Chang, C.-Y. "Observation of Impurity Enhanced Intermixing in $Si_{1-x}Ge_x$/Si Quantum Well Structure", Materials Research Society (MRS) Spring Meeting, April 8-12, 1996 (San Francisco, USA).

(9) Li, C.-C.; Hsieh, K.-Y.; Wang, D.-P.; Tsai, W.-C.; Chang, C.-Y. "Impurity Enhanced Intermixing in $Si_{1-x}Ge_x$/Si Quantum Well Structure", Electronic Devices and Material Symposium (EDMS) p. 185-190, July 6-7, 1995 (NSC 84-2215-E-110-003).

IV. Patent

(1) 李政哲, 林鴻志, 蘇俊榮, 楊裕雄, 黃調元 “矽奈米線場效電晶體裝置及作為奈米線生物感測與調控元件, 及其製造”, 公告日: 2008/03/01, 證書號: TW I294183.

(2) 李政哲, 吳集錫 “垂直型金屬-絕緣物-金屬電容器及其製造方法”, 公告日: 2007/07/11, 證書號: TW I283892.

(3) Lee, C.-C.; Wu, C.-H. “Vertical MIM Capacitors and Method of Fabricating the Same”, Patent Filed: 2005/10/31, No.: US 7,416,953.

(4) 李政哲, 吳集錫 “於低介電常數之介電層中嵌入金屬/絕緣體/金屬(MIM)電容之方法”, 公告日: 2004/01/21, 證書號: TW 196933.

(5) Lee, C.-C.; Wu, C.-H. “A MIM Device Structure Inserted into a Low *k* Material and the Method for Making Same”, Patent Filed: 2003/02/27, No.: US 6,713,840.

(6) 鄭隆一, 白源吉, 李政哲, 林維姜 “去除光阻的方法”, 公告日: 2001/08/11, 證書號: TW 139656.

(7) 白源吉, 鄭隆一, 李政哲, 林維姜 “去除光阻的方法”, 公告日: 2000/09/01, 證書號: TW 119958.

(8) 白源吉, 鄭隆一, 李政哲, 林維姜 “フォトレジスト材料の除去プロセス及び該除去プロセスを使用したCMOSフォトセンサ―の製造方法”, 公開日: 2000/08/04, 特許番號: JP 3,623,892.

(9) 鄭化仁, 李政哲 “避免氧化物/氮化物/氧化物蝕刻後產生缺陷的方法”, 公告日: 2000/05/11, 證書號: TW 114806.

(10) Cheng, L.-Y.; Pai, Y.-C.; Li, C.-C.; Lin, W.-C. “Method for In-Situ Removing Photoresist Material” Patent Filed: 1999/04/15, No.: US 6,194,324.

(11) Pai, Y.-C.; Cheng, L.-Y.; Li, C.-C.; Lin, W.-C. “Process for Removing Photoresist Material”, Patent Filed: 1999/01/14, No.: US 6,410,447.